CHAPTER 3

Future Ozone and Its Impact on Surface UV

Coordinating Lead Authors:
S. Bekki
G.E. Bodeker

Lead Authors:
A.F. Bais
N. Butchart
V. Eyring
D.W. Fahey
D.E. Kinnison
U. Langematz
B. Mayer
R.W. Portmann
E. Rozanov

Coauthors:
P. Braesicke
A.J. Charlton-Perez
N.E. Chubarova
I. Cionni
S.B. Diaz
N.P. Gillett
M.A. Giorgetta
N. Komala
F. Lefèvre
C. McLandress
J. Perlwitz
T. Peter
K. Shibata

Contributors:
H. Akiyoshi
J. Austin
M.P. Chipperfield
M. Dameris
S. Dhomse
S.M. Frith
R.R. Garcia
H. Garny
A. Gettelman
S.C. Hardiman
P. Jöckel
A.I. Jonsson
A. Kazantzidis
A. Kubin
J.-F. Lamarque
E. Mancini
M. Marchand
M. Michou
O. Morgenstern
L.D. Oman
S. Pawson
G. Pitari
D. Plummer
J.A. Pyle
D. Saint-Martin
J.F. Scinocca
T.G. Shepherd
D. Smale
R.S. Stolarski
H. Teyssèdre
S. Tilmes

CHAPTER 3

FUTURE OZONE AND ITS IMPACT ON SURFACE UV

Contents

SCIENTIFIC SUMMARY

Globally averaged total column ozone has declined over recent decades due to the release of ozone-depleting substances (ODSs) into the atmosphere. Now, as a result of the Montreal Protocol, ozone is expected to recover from the effects of ODSs as ODS abundances decline in the coming decades. However, a number of factors in addition to ODSs have led to and will continue to lead to changes in ozone. Discriminating between the causes of past and projected ozone changes is necessary, not only to identify the progress in ozone recovery from ODSs, but also to evaluate the effectiveness of climate and ozone protection policy options.

Factors Affecting Future Ozone and Surface Ultraviolet Radiation

- **At least for the next few decades, the decline of ODSs is expected to be the major factor affecting the anticipated increase in global total column ozone. However, several factors other than ODS will affect the future evolution of ozone in the stratosphere.** These include changes in (i) stratospheric circulation and temperature due to changes in long-lived greenhouse gas (GHG) abundances, (ii) stratospheric aerosol loading, and (iii) source gases of highly reactive stratospheric hydrogen and nitrogen compounds. Factors that amplify the effects of ODSs on ozone (e.g., stratospheric aerosols) will likely decline in importance as ODSs are gradually eliminated from the atmosphere.

- **Increases in GHG emissions can both positively and negatively affect ozone.** Carbon dioxide (CO_2)-induced stratospheric cooling elevates middle and upper stratospheric ozone and decreases the time taken for ozone to return to 1980 levels, while projected GHG-induced increases in tropical upwelling decrease ozone in the tropical lower stratosphere and increase ozone in the extratropics. Increases in nitrous oxide (N_2O) and methane (CH_4) concentrations also directly impact ozone chemistry but the effects are different in different regions.

- **The Brewer-Dobson circulation (BDC) is projected to strengthen over the 21st century and thereby affect ozone amounts.** Climate models consistently predict an acceleration of the BDC or, more specifically, of the upwelling mass flux in the tropical lower stratosphere of around 2% per decade as a consequence of GHG abundance increases. A stronger BDC would decrease the abundance of tropical lower stratospheric ozone, increase poleward transport of ozone, and could reduce the atmospheric lifetimes of long-lived ODSs and other trace gases. While simulations showing faster ascent in the tropical lower stratosphere to date are a robust feature of chemistry-climate models (CCMs), this has not been confirmed by observations and the responsible mechanisms remain unclear.

- **Substantial ozone losses could occur if stratospheric aerosol loading were to increase in the next few decades, while halogen levels are high.** Stratospheric aerosol increases may be caused by sulfur contained in volcanic plumes entering the stratosphere or from human activities. The latter might include attempts to geoengineer the climate system by enhancing the stratospheric aerosol layer. The ozone losses mostly result from enhanced heterogeneous chemistry on stratospheric aerosols. Enhanced aerosol heating within the stratosphere also leads to changes in temperature and circulation that affect ozone.

- **Surface ultraviolet (UV) levels will not be affected solely by ozone changes but also by the effects of climate change and by air quality change in the troposphere.** These tropospheric effects include changes in clouds, tropospheric aerosols, surface reflectivity, and tropospheric sulfur dioxide (SO_2) and nitrogen dioxide (NO_2). The uncertainties in projections of these factors are large. Projected increases in tropospheric ozone are more certain and may lead to reductions in surface erythemal ("sunburning") irradiance of up to 10% by 2100. Changes in clouds may lead to decreases or increases in surface erythemal irradiance of up to 15% depending on latitude.

Expected Future Changes in Ozone

Full ozone recovery from the effects of ODSs and return of ozone to historical levels are not synonymous. In this chapter a key target date is chosen to be 1980, in part to retain the connection to previous Ozone Assessments. Noting, however, that decreases in ozone may have occurred in some regions of the atmosphere prior to 1980, 1960 return dates are also reported.

The projections reported on in this chapter are taken from a recent compilation of CCM simulations. The ozone projections, which also form the basis for the UV projections, are limited in their representativeness of possible futures since they mostly come from CCM simulations based on a single GHG emissions scenario (scenario A1B of *Emissions Scenarios. A Special Report of Working Group III of the Intergovernmental Panel on Climate Change*, Cambridge University Press, 2000) and a single ODS emissions scenario (adjusted A1 of the previous (2006) Ozone Assessment).

Throughout this century, the vertical, latitudinal, and seasonal structure of the ozone distribution will be different from what it was in 1980. For this reason, ozone changes in different regions of the atmosphere are considered separately.

- **The projections of changes in ozone and surface clear-sky UV are broadly consistent with those reported on in the 2006 Assessment.**

- **The capability of making projections and attribution of future ozone changes has been improved since the 2006 Assessment.** Use of CCM simulations from an increased number of models extending through the entire period of ozone depletion and recovery from ODSs (1960–2100) as well as sensitivity simulations have allowed more robust projections of long-term changes in the stratosphere and of the relative contributions of ODSs and GHGs to those changes.

- **Global annually averaged total column ozone is projected to return to 1980 levels before the middle of the century and earlier than when stratospheric halogen loading returns to 1980 levels.** CCM projections suggest that this early return is primarily a result of GHG-induced cooling of the upper stratosphere because the effects of circulation changes on tropical and extratropical ozone largely cancel. Global (90°S–90°N) annually averaged total column ozone will likely return to 1980 levels between 2025 and 2040, well before the return of stratospheric halogens to 1980 levels between 2045 and 2060.

- **Simulated changes in tropical total column ozone from 1960 to 2100 are generally small.** The evolution of tropical total column ozone in models depends on the balance between upper stratospheric increases and lower stratospheric decreases. The upper stratospheric increases result from declining ODSs and a slowing of ozone destruction resulting from GHG-induced cooling. Ozone decreases in the lower stratosphere mainly result from an increase in tropical upwelling. From 1960 until around 2000, a general decline is simulated, followed by a gradual increase to values typical of 1980 by midcentury. Thereafter, although total column ozone amounts decline slightly again toward the end of the century, by 2080 they are no longer expected to be affected by ODSs. Confidence in tropical ozone projections is compromised by the fact that simulated decreases in column ozone to date are not supported by observations, suggesting that significant uncertainties remain.

- **Midlatitude total column ozone is simulated to evolve differently in the two hemispheres**. Over northern midlatitudes, annually averaged total column ozone is projected to return to 1980 values between 2015 and 2030, while for southern midlatitudes the return to 1980 values is projected to occur between 2030 and 2040. The more rapid return to 1980 values in northern midlatitudes is linked to a more pronounced strengthening of the poleward transport of ozone due to the effects of increased GHG levels, and effects of Antarctic ozone depletion on southern midlatitudes. By 2100, midlatitude total column ozone is projected to be above 1980 values in both hemispheres.

- **October-mean Antarctic total column ozone is projected to return to 1980 levels after midcentury, later than in any other region, and yet earlier than when stratospheric halogen loading is projected to return to 1980 levels.** The slightly earlier return of ozone to 1980 levels (2045–2060) results primarily from upper stratospheric cooling and resultant increases in ozone. The return of polar halogen loading to 1980 levels (2050–2070)

in CCMs is earlier than in empirical models that exclude the effects of GHG-induced changes in circulation. Our confidence in the drivers of changes in Antarctic ozone is higher than for other regions because (i) ODSs exert a strong influence on Antarctic ozone, (ii) the effects of changes in GHG abundances are comparatively small, and (iii) projections of ODS emissions are more certain than those for GHGs. Small Antarctic ozone holes (areas of ozone <220 Dobson units, DU) could persist to the end of the 21st century.

- **March-mean Arctic total column ozone is projected to return to 1980 levels two to three decades before polar halogen loading returns to 1980 levels, and to exceed 1980 levels thereafter.** While CCM simulations project a return to 1980 levels between 2020 and 2035, most models tend not to capture observed low temperatures and thus underestimate present-day Arctic ozone loss such that it is possible that this return date is biased early. Since the strengthening of the Brewer-Dobson circulation through the 21st century leads to increases in springtime Arctic column ozone, by 2100 Arctic ozone is projected to lie well above 1960 levels.

Uncertainties in Projections

- **Conclusions dependent on future GHG levels are less certain than those dependent on future ODS levels since ODS emissions are controlled by the Montreal Protocol.** For the six GHG scenarios considered by a few CCMs, the simulated differences in stratospheric column ozone over the second half of the 21st century are largest in the northern midlatitudes and the Arctic, with maximum differences of 20–40 DU between the six scenarios in 2100.

- **There remain sources of uncertainty in the CCM simulations.** These include the use of prescribed ODS mixing ratios instead of emission fluxes as lower boundary conditions, the range of sea surface temperatures and sea ice concentrations, missing tropospheric chemistry, model parameterizations, and model climate sensitivity.

- **Geoengineering schemes for mitigating climate change by continuous injections of sulfur-containing compounds into the stratosphere, if implemented, would substantially affect stratospheric ozone, particularly in polar regions.** Ozone losses observed following large volcanic eruptions support this prediction. However, sporadic volcanic eruptions provide limited analogs to the effects of continuous sulfur emissions. Preliminary model simulations reveal large uncertainties in assessing the effects of continuous sulfur injections.

Expected Future Changes in Surface UV

While a number of factors, in addition to ozone, affect surface UV irradiance, the focus in this chapter is on the effects of changes in stratospheric ozone on surface UV. For this reason, clear-sky surface UV irradiance is calculated from ozone projections from CCMs.

- **Projected increases in midlatitude ozone abundances during the 21st century, in the absence of changes in other factors, in particular clouds, tropospheric aerosols, and air pollutants, will result in decreases in surface UV irradiance.** Clear-sky erythemal irradiance is projected to return to 1980 levels on average in 2025 for the northern midlatitudes, and in 2035 for the southern midlatitudes, and to fall well below 1980 values by the second half of the century. However, actual changes in surface UV will be affected by a number of factors other than ozone.

- **In the absence of changes in other factors, changes in tropical surface UV will be small because changes in tropical total column ozone are projected to be small.** By the middle of the 21st century, the model projections suggest surface UV to be slightly higher than in the 1960s, very close to values in 1980, and slightly lower than in 2000. The projected decrease in tropical total column ozone through the latter half of the century will likely result in clear-sky surface UV remaining above 1960 levels. Average UV irradiance is already high in the tropics due to naturally occurring low total ozone columns and high solar elevations.

- **The magnitude of UV changes in the polar regions is larger than elsewhere because ozone changes in polar regions are larger.** For the next decades, surface clear-sky UV irradiance, particularly in the Antarctic, will continue to be higher than in 1980. Future increases in ozone and decreases in clear-sky UV will occur at slower rates than those associated with the ozone decreases and UV increases that occurred before 2000. In Antarctica, surface clear-sky UV is projected to return to 1980 levels between 2040 and 2060, while in the Arctic this is projected to occur between 2020 and 2030. By 2100, October surface clear-sky erythemal irradiance in Antarctica is likely to be between 5% below to 25% above 1960 levels, with considerable uncertainty. This is consistent with multi-model-mean October Antarctic total column ozone not returning to 1960 levels by 2100. In contrast, by 2100, surface clear-sky UV in the Arctic is projected to be 0–10% below 1960 levels.

3.1 INTRODUCTION

The primary goal of the Montreal Protocol and its Amendments and Adjustments is to avoid depletion of the ozone layer. Ozone depletion elevates surface ultraviolet (UV) radiation, thereby posing a threat to Earth's biosphere. The mechanism used to achieve this goal is the control of the production and consumption of anthropogenic ozone-depleting substances (ODSs: see Box 3-1). Chapter 5 in this Assessment describes the Montreal Protocol mechanism in more detail while Chapters 1, 2 and 5 summarize the success of the Montreal Protocol to date. At present, throughout most of the stratosphere, equivalent stratospheric chlorine (ESC; see Box 3-1) is significantly elevated above natural levels due to the cumulative effect of historical emissions of ODSs. Elevated ESC remains the most important anthropogenic perturbation to stratospheric ozone. However, as halogen loading declines in the future, other factors are expected to displace ODSs as the dominant influence on ozone. Perhaps the most important of these are continued and increasing emissions of long-lived greenhouse gases (GHGs). For example, GHGs affect ozone directly because they act as stratospheric source gases for ozone-destroying radicals (e.g., methane (CH_4) and nitrous oxide (N_2O)) and indirectly because they change temperatures (predominantly carbon dioxide (CO_2)).

This chapter builds on and extends Chapter 5 of the 2006 Ozone Assessment ("Climate-Ozone Connections," Baldwin and Dameris et al., 2007) by assessing the most

Box 3-1. Measures of Atmospheric Halogens

In this chapter, as in the 2006 Ozone Assessment (hereafter also cited as WMO (2007)), ozone-depleting substances (ODSs) are defined as those gases of anthropogenic origin controlled under the Montreal Protocol. Principal ODSs are chlorofluorocarbons (CFCs), hydrochlorofluorocarbons (HCFCs), halons, carbon tetrachloride, 1,1,1-trichloroethane (methyl chloroform), and methyl bromide. These gases are useful in meeting global application demands, for example, in refrigeration, air conditioning, insulating foams, and fumigation, but contain the halogens (chlorine and/or bromine atoms) which, when released, react to destroy stratospheric ozone. Other gases emitted in human activities (e.g., methane (CH_4) and nitrous oxide (N_2O)) also influence ozone (Section 3.2.2), but have not been considered ODSs under the Montreal Protocol.

When chlorine and bromine atoms are released from the degradation of ODSs in the stratosphere, they combine to form the inorganic chlorine- and bromine-containing compounds that belong to the chemical groups called total inorganic chlorine (Cl_y) and inorganic bromine (Br_y). The combination of Cl_y and Br_y amounts represents the potential for halogens to destroy ozone in a stratospheric air mass. A measure of this potential is defined as equivalent stratospheric chlorine (ESC; Eyring et al., 2007), "equivalent" since it weights Br_y with respect to Cl_y, according to

$$ESC = Cl_y + \alpha \times Br_y \quad (1)$$

where the units are stratospheric mixing ratio and α is the weighting factor that accounts for the greater effectiveness of bromine in ozone destruction compared to the effectiveness of chlorine on a per-atom basis. In general, α varies with altitude, latitude, and time, following changes in Cl_y and Br_y which in turn follow total emissions of organic halogen gases at Earth's surface. In 2010, α is estimated to be ~60 in the lower stratosphere and ~5 in the upper stratosphere (Sinnhuber et al., 2009). ESC can be calculated as a function of latitude, longitude, altitude, and time from distributions of Cl_y and Br_y simulated with a chemistry-climate model (CCM). Some ODSs, such as methyl chloride and methyl bromide, and a number of other halogen-containing gases, have natural sources. These natural emissions are responsible for the low background level of ESC.

Deriving ESC directly from observations is hindered by the lack of direct measurements of Cl_y and Br_y. As an alternative, the spatial and temporal distributions of Cl_y and Br_y can be approximated from time series measurements of ODS surface concentrations combined with estimated rates at which individual gases release their halogens into the stratosphere (so-called fractional release rates) and estimates of the age of air parcels (i.e., the time elapsed since air parcels entered the stratosphere at the tropical tropopause; see Box 8-1 of WMO (2007)). Using these estimates in equation (1) yields equivalent effective stratospheric chlorine (EESC; see Section 1.4.4), which has been widely used before the availability of ESC from CCM outputs. ESC and EESC are similar in that they both represent aggregate quantities that quantify the combined potential of Cl_y and Br_y in a particular air mass to destroy ozone. They differ in the way in which the Cl_y and Br_y inputs are obtained. For CCMs, ESC is calculated directly from the simulated fields of chlorine- and bromine-containing species. In contrast, EESC is estimated from measured source gas surface concentrations and assumptions about their transport and conversion to Cl_y and Br_y in the stratosphere.

recent literature on the likely effects of increasing GHG emissions on future ozone amounts and resultant changes in climate parameters. This chapter also builds on and extends Chapter 6 of the 2006 Ozone Assessment ("The Ozone Layer in the 21st Century," Bodeker and Waugh et al., 2007) by assessing chemistry-climate model (CCM) projections of the evolution of ozone through the 21st century. The number of available CCMs and CCM sensitivity simulations has significantly increased since the previous Assessment. In contrast to WMO (2007), which assessed two- and three-dimensional model simulations of future ozone, this chapter assesses ozone projections from the current generation of three-dimensional CCMs. The simulations used in this chapter are based on those from 17 CCMs that participated in the second round of a coordinated model intercomparison organized by the Chemistry-Climate Model Validation (CCMVal) Activity (Eyring et al., 2005) of WCRP's (World Climate Research Programme) SPARC (Stratospheric Processes And their Role in Climate) project (hereafter referred to as CCMVal-2). The participating CCMs are listed in Table 3-1 (see Section 3.3.1) and described in detail in the cited literature, in Chapter 2 of SPARC CCMVal (2010), and in Morgenstern et al. (2010). An extensive assessment of these CCMs was made in the SPARC CCMVal Report (2010), which provides a strong foundation for this chapter. Results presented in that report are augmented here by including additional reference model simulations, as well as sensitivity simulations in which either greenhouse gas (GHG) or ODS levels are kept fixed at 1960 values or in which alternative GHG scenarios are used. The reference simulations include the most important forcings of the long-term evolution of ozone and provide the primary data set of ozone projections used here. The sensitivity simulations, by fixing a single forcing at a constant baseline level, permit a quantitative separation of the effects of different factors on future ozone. Thus details of the full recovery of ozone from the effects of ODSs (see Box 3-2) were determined by quantifying the contribution of ESC to future ozone changes and contrasting it with that from climate change.

Although interest in the factors affecting surface UV has focused primarily on ozone to date, other factors, some related to changes in climate, will play an increasingly important role in modulating future surface UV levels as the ozone layer recovers. This chapter builds on and extends the prognostic aspects of Chapter 7 of the 2006 Ozone Assessment ("Surface Ultraviolet Radiation: Past, Present, and Future," Bais and Lubin et al., 2007), with a primary focus on the role of ozone in affecting the future evolution of UV. While a brief discussion of the non-ozone factors affecting surface UV is included in this chapter, it primarily serves as a link to the UNEP (United Nations Environment Programme) Environmental Effects Assessment Panel report (UNEP, 2010).

While ESC is projected to return close to historical levels during the 21st century, global ozone amounts are not necessarily expected to return close to their respective historical levels over the same period because factors other than ESC will increasingly affect future ozone amounts. Therefore, this chapter reports both the dates when ESC, ozone, and UV return to some respective historical values, and the dates when ozone is no longer expected to be influenced by ODSs (Box 3-2). Annual mean total column ozone and surface UV may not necessarily return to historical levels at the same time. Summertime ozone exerts a greater influence on annual mean surface UV than ozone in other seasons, and so it is the return of summertime ozone to historical levels that is more relevant for surface UV.

The scope of this chapter includes providing a discussion framework that accommodates a wide variety of factors beyond ODSs that affect ozone. In some regions of the atmosphere, for example in the Antarctic lower stratosphere, the steep decline in springtime ozone until ~2000 is projected to be followed by a slow increase back to 1980 levels during the latter half of the 21st century, mirroring what is expected from changes in ESC over that period. In the tropical upper stratosphere, where the effects of GHG-induced cooling are significant, ozone concentrations could significantly exceed 1960 or 1980 values by the end of the 21st century. These changes are necessarily larger than what would be expected from ESC declines alone. In contrast, in the tropical lower stratosphere, ozone shows little sensitivity to stratospheric halogen loading and is more strongly influenced by long-term changes in atmospheric circulation. This chapter, in addition to addressing the full recovery of ozone from ODSs, explores a suite of scenarios for future ozone in different regions of the atmosphere, and the impact of projected ozone changes on surface UV.

Section 3.2 details how future changes in stratospheric halogen loading will affect the future evolution of ozone (the primary focus in this chapter), describes other factors that will affect future ozone, and discusses how ozone and other factors will affect future surface UV. Section 3.3 begins by noting the recent improvements in ozone projections compared to those presented in WMO (2007) and by describing the CCMs, the emissions scenarios to which they were applied, and their evaluation. Section 3.3 focuses mainly on long-term CCM projections of stratospheric ozone based primarily on a common reference scenario. In addition to this reference scenario, a number of sensitivity simulations allow the two most important factors affecting future ozone (i.e., ODSs and GHGs) to be quantitatively disentangled. These results form the basis for statements regarding the milestones of

Box 3-2. Ozone Return Dates and Full Ozone Recovery

The context for the discussion of future ozone in this chapter is provided by defining two distinct milestones in the future evolution of ozone. These quantitative milestones are motivated by the need to answer questions often put forth by policymakers and the public, viz.:

1. When do we expect ozone to return to levels typical of some earlier time?
2. When do we expect ozone to no longer be significantly affected by ozone-depleting substances (ODSs)?

Identifying the first milestone requires *no attribution* to the separate factors affecting ozone and, hence, can be evaluated directly from time series of observed or simulated ozone. If ozone has already returned to levels typical of some target year, measurements alone can be used to address this milestone and answer the related question. Since this is not the case for the target years considered here (i.e., 1960 and 1980), the expected return of ozone to these historical levels is evaluated here instead from multi-model mean chemistry-climate model (CCM) projections. The selection of a target year, and its associated ozone level, should not be interpreted as selecting past states defined by the absence of significant ozone depletion from ODSs.

In this chapter a key target date is chosen to be 1980 in order to retain a connection to previous Ozone Assessments. Noting, however, that decreases in ozone may have occurred in some regions of the atmosphere prior to 1980, 1960 return dates are also presented and discussed. Evaluating return dates is relevant for gauging when the adverse impacts of enhanced surface ultraviolet radiation on human health and ecosystems caused by ozone depletion are likely to become negligible. In addition, the return dates of ozone to historical levels in some regions are also valuable in demonstrating the effectiveness of policies that have abated anthropogenic ODS emissions if ODSs have been the dominant driver of ozone changes in those regions.

Identifying the second milestone is equivalent to assessing when the third stage of ozone recovery, so-called "full ozone recovery from ODSs" as defined in WMO (2007), has or is expected to occur. This, by definition, requires an *attribution* of projected changes in ozone to different factors, since ozone is not affected by ODSs alone. The required attribution can be obtained using idealized CCM simulations that hold certain model forcings fixed in conjunction with reference simulations that include the most important forcings for the long-term evolution of ozone. The reference and idealized simulations also provide a method, based on a subjective statistical test, for quantifying what is meant by "no longer significantly affected by ODSs" (Section 3.3.6). When analyzing CCM simulations for full ozone recovery from ODSs as defined here, the choice of 1960 as the start date implicitly assumes that the contribution of anthropogenic emissions of ODSs to equivalent stratospheric chlorine (ESC) prior to 1960 was negligible. However, ESC in 1960 was not zero because of the contribution of natural sources of halogens (see Box 3-1). If the sensitivity of ozone destruction to stratospheric halogen loading does not change with time, this milestone is equivalent to a return of ESC to 1960 levels. This definition has the advantage that it directly assesses the effectiveness of the Montreal Protocol in model projections of ozone but requires the additional step of attributing observed or modeled changes in ozone to ODS and other factors.

Both milestones defined above can be evaluated for total column ozone or vertically resolved ozone, averaged globally or averaged over some region of the atmosphere.

full ozone recovery from the effects of ODSs. Section 3.4 builds on the ozone projections in Section 3.3 to detail how future surface UV radiation will be affected by changes in ozone and provides a point of connection between this Ozone Assessment and the UNEP Environmental Effects Assessment Panel report (UNEP, 2010).

3.2 FACTORS AFFECTING FUTURE OZONE AND SURFACE UV

This section discusses the factors that will affect the future evolution of stratospheric ozone and consequently UV reaching the surface. While the primary focus remains on ODS emissions and the associated increase in stratospheric halogen loading (Section 3.2.1), developments since WMO (2007) have highlighted the potentially important roles of nitrous oxide (N_2O) emissions (Section 3.2.2) and anthropogenic enhancements of the stratospheric sulfate aerosol layer, from both increased surface sulfur emissions (Section 3.2.5) and possible geoengineering actions (Section 3.2.6). New research has also advanced our understanding of how the Brewer-Dobson circulation (BDC) is likely to change (Section 4.2.2 of Chapter 4 of this Assessment) and affect future ozone (Section 3.2.4.1). The increase in GHG emissions and subsequent changes in climate, including cooling of the stratosphere (Section 3.2.3), is an overarching theme linking many of the factors likely to affect ozone in the future. Evaluating the recovery of ozone from ODSs involves all of these factors, in addition to ODSs. As ESC levels decline in the future, the factors that act to amplify the effects of ESC on ozone

(e.g., stratospheric aerosols) will decline in importance, while other factors, especially those related to GHGs and climate change, will emerge to dominate the long-term evolution of ozone. Attributing past and future changes in ozone to these different factors is essential to identify the stages of ozone recovery. Furthermore, because ozone protection policy governs only ESC (by limiting emissions of ODSs), evaluating the effectiveness of such policy requires attributing observed and projected ozone changes to ESC and other factors. While the discussion of UV in this section is primarily focused on the effects of future changes in stratospheric ozone on surface UV (Section 3.2.7), research since WMO (2007) has mostly dealt with other factors affecting surface UV, which are summarized briefly in Section 3.2.8.

3.2.1 Stratospheric Halogen Loading

At present, and for much of the 21st century, elevated stratospheric halogen loading is expected to remain the most important factor affecting stratospheric ozone. In the model simulations of 21st century ozone made in support of WMO (2007), ODSs were prescribed at the surface according to the Ab "best guess" scenario of WMO (2003) (Eyring et al., 2007). This scenario was superseded by the "baseline" halogen scenario A1 defined in WMO (2007), which prescribes halogen loadings higher than in Ab. There are notable differences between the two scenarios. The A1 scenario includes larger emissions of chlorofluorocarbon-11 (CFC-11) and CFC-12 after 2010 due to their larger estimated banks. Increases in projected hydrochlorofluorocarbon-22 (HCFC-22) emissions, due to expectations of greater future use in A1 than in the Ab scenario, are also important. However, at the 2007 Meeting of the Parties to the Montreal Protocol, the Parties agreed to an earlier phase-out of HCFCs, with nearly a full phase-out in developing countries (Article 5) by 2030. Scenario A1 does not include this phase-out. Hence, a new scenario has been developed that includes this phase-out. This adjusted A1 scenario has been used in the model simulations performed in support of the present Assessment. In this new scenario, only HCFCs have been adjusted, while emissions of CFCs, halons, and other non-HCFC species remain identical to the original A1 scenario.

Due to the uncertainty in their future trends, brominated very short-lived substances (VSLS, atmospheric lifetime <0.5 year) are not considered in the standard scenarios. As a result, the bromine loading in most CCMs used in support of the previous and current Assessments is only determined by the projected evolution of long-lived organic source gases methyl bromide (CH_3Br) and halons (halon-1211, halon-1202, halon-1301, and halon-2402). However, observations suggest that the stratospheric bromine loading is 5^{+3}_{-2} parts per trillion (ppt) higher than can be explained by tropospheric levels of CH_3Br and the halons. This additional bromine (~5 ppt out of the current total of ~20 ppt) may likely come from short-lived bromine-containing compounds (see Chapter 1; WMO, 2007). The degradation of those species could release a substantial amount of bromine into the tropical tropopause layer (TTL) and lowermost stratosphere. The average photochemical lifetime of VSLS is comparable with, or shorter than, the average transport time scales in the TTL, which vary from rapid in deep convection to slow outside of regions of deep convection. This may lead to a highly variable distribution of bromine injections in the form of VSLS into the tropical lower stratosphere, as some surface and balloon observations suggest (see Section 1.3.1 and references therein). There is also uncertainty in how dehydration and wet removal of degradation products of VSLS occur (Sinnhuber and Folkins, 2006). Current and future trends in brominated VSLS are difficult to determine. VSLS, and their rapid vertical transport through the troposphere, are also very difficult to describe in global models and are not explicitly treated in the CCMs used here. Together, these gaps in our understanding of the stratospheric bromine budget are a source of uncertainty in long-term projections of stratospheric halogen loading and hence ozone.

3.2.2 Stratospheric Reactive Nitrogen and Hydrogen Levels

Natural ozone loss in the absence of chlorine is primarily due to the chemical effects of nitrogen (NO_x) and hydrogen (HO_x) radicals. NO_x and HO_x levels are controlled by the amount of the long-lived source gases N_2O, H_2O, and CH_4 which are also GHGs. Since the levels of these source gases are affected by anthropogenic emissions and/or climate change, their future evolution will influence ozone through changes in NO_x and HO_x.

The amount of NO_x in the stratosphere is largely controlled by the amount of N_2O entering at the tropical tropopause (of which approximately 10% is converted to NO_x). The preindustrial level of N_2O was ~270 parts per billion (ppb) and the present level is ~320 ppb. Future changes in ozone due to NO_x increases have been evaluated using model simulations based on scenarios for the 21st century that include projected N_2O emissions (Randeniya et al., 2002; Chipperfield and Feng, 2003; Portmann and Solomon, 2007). It was shown that several percent of global total ozone loss is possible by 2100 due to increases in anthropogenic N_2O. The effects of increasing N_2O levels on ozone depend on altitude. The resulting NO_x increase causes ozone losses in the middle stratosphere, centered just above the ozone concentration maximum, while chlorine and hydrogen radicals destroy ozone predominately

in both the lower and upper stratosphere (see Figure 3-1). Interactions between halogen and nitrogen species cause nitrogen species to be less effective at destroying ozone in the lower stratosphere while halogen levels remain elevated. In contrast, temperature decreases cause a faster chemical loss of total reactive nitrogen (NO_y) and hence NO_x (nitrogen oxides, NO + NO_2) in the upper stratosphere (Rosenfield and Douglass, 1998). Because of these effects, the changes in active nitrogen species levels and in the amount of ozone destroyed by those species are not expected to follow the change in N_2O levels.

The efficiency of N_2O emissions in destroying stratospheric ozone can also be compared to that of ODSs. Ravishankara et al. (2009) computed the Ozone Depletion Potential (ODP, see Chapter 5) of N_2O in the same way that it is computed for halogen source gases. Surprisingly, they found that the ODP-weighted anthropogenic emissions of N_2O were larger than those of any chlorine-containing source gas emitted in 2008. Moreover, they also found that the ODP-weighted anthropogenic emissions of N_2O were already significant in 1987 when CFC emissions were peaking. This result is partly due to the long lifetime of N_2O (approximately 125 years) since the ODP is weighted by the ozone depletion over the lifetime of the gas. Further study is needed to characterize the effects of N_2O emissions and carefully examine the tradeoffs with ODSs (see also Section 5.4.2.2).

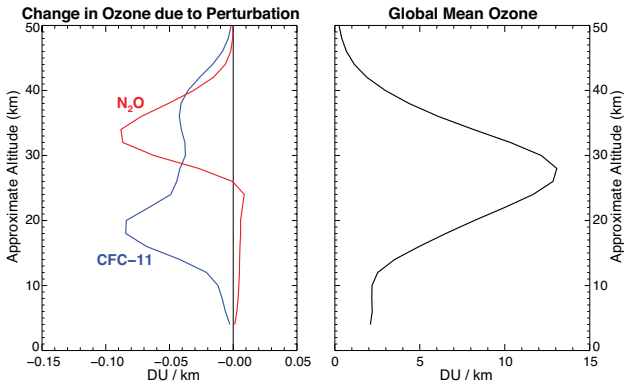

Figure 3-1. The change in global average ozone concentrations (Dobson units per kilometer) due to a 100 ppt increase in CFC-11 and a 20 ppb increase in N_2O for year 2000 levels of source gases and background aerosol conditions computed with the NOCAR 2-D model (Portmann et al., 1999). The global average ozone profile for the same conditions is also shown. Note that in order to illustrate differences in the ozone loss profiles, the relative sizes of the CFC-11 and N_2O perturbations were chosen to achieve ozone loss peaks of the same magnitude. Adapted from Figure S1 of the supplementary material from Ravishankara et al. (2009).

Future levels of HO_x will be mostly determined by changes in CH_4 emissions and by the amount of H_2O entering the tropical stratosphere. In terms of ozone depletion, these two sources of HO_x have differing effects on ozone. Increasing H_2O tends to enhance the chemical ozone loss in the upper stratosphere where H_2O is converted to HO_x (HO_x is the dominant ozone loss cycle in the upper stratosphere and mesosphere), whereas increasing H_2O leads to a reduction in ozone loss in the middle stratosphere because H_2O enhances conversion of nitrogen dioxide (NO_2), the ozone-destroying nitrogen radical, into HNO_3. However, when all the radiative and dynamical feedbacks associated with the H_2O increase are accounted for in a CCM, the effects on column ozone exhibit a strong hemispheric asymmetry, especially at high latitudes (Tian et al., 2009). Changes in the abundance of H_2O also have the potential to affect the sulfuric acid aerosol size distribution. However, these H_2O-driven aerosol changes have been estimated to be negligible (SPARC, 2006). Polar stratospheric cloud (PSC) formation and the heterogeneous reaction rates on liquid ternary aerosol are more sensitive to H_2O changes. H_2O increases may be expected to enhance PSC formation and hence accelerate chemical polar ozone destruction as long as chlorine levels are high enough. CH_4 increases also enhance H_2O in the stratosphere but additionally cause ozone increases in the troposphere and lowermost stratosphere due to direct ozone production from methane oxidation. The net effect of increases in CH_4 levels on global ozone is expected to be ozone production (Randeniya et al., 2002). Thus it is important to assess the sources of H_2O changes in the stratosphere to predict the net effect on ozone.

H_2O increased in the stratosphere in the latter part of the 20th century but showed a sustained decrease after 2000 (Randel et al., 2006). Increases in CH_4 levels have caused part of this H_2O increase in the middle and upper stratosphere but not in the lower stratosphere (Rohs et al., 2006). In addition, the separation of the climate change signal from natural variability has proved difficult (Garcia et al., 2007; Austin et al., 2007; Oman et al., 2008).

3.2.3 Stratospheric Temperatures

Because of the temperature dependence of gas-phase chemical reaction rates and the formation of PSCs, stratospheric temperatures have a large impact on ozone abundances. A cooling of the middle and upper stratosphere increases ozone by slowing gas-phase destruction rates. In contrast, a cooling of the polar lower stratosphere is expected to enhance PSC formation which, when halogen levels are elevated, favors ozone destruction. In the Antarctic, where temperatures are already well below the

thresholds of PSC formation, additional cooling is likely to have less of an effect than in the Arctic, where stratospheric temperatures are closer to the thresholds of PSC formation. Predictions of future changes in ozone must therefore account for future changes in temperature.

Stratospheric temperatures are controlled by a combination of radiative and dynamical processes (see also Section 4.3.1). Since regional heating and cooling by dynamical processes tend to cancel out in the global mean, the global mean temperature is in radiative equilibrium to a good approximation (e.g., Fomichev et al., 2002). Dynamical processes, on the other hand, lead to latitudinal variations in heating and cooling. For example, the projected strengthening of the BDC in response to increasing GHG levels (Section 4.3.2) causes adiabatic cooling of the tropical lower and middle stratosphere, and adiabatic warming at high latitudes (Section 3.2.4).

Current CCMs are reasonably good at reproducing the Stratospheric Sounding Unit/Mesospheric Sounding Unit (SSU/MSU) record of observed changes in stratospheric temperature since 1979 (Figure 4-10, and Section 4.3; Gillett et al., 2010). The multi-model ensemble approximately captures the magnitude of observed global mean cooling in the upper and lower stratosphere, as well as the volcanic warming and the recent leveling off of lower stratospheric temperatures (Section 4.3.1). Nonetheless, discrepancies between individual models and the observations may still be significant, and there are some clear areas of disagreement between the models and observations, such as in SSU channel 26 after 1995. However, the uncertainties in the observations remain poorly quantified (Randel et al., 2009). Thus it is possible that this discrepancy results from observational errors rather than from a common bias in the CCMVal models. Over the 21st century CCMVal-2 models simulate a continued strong cooling of the middle to upper stratosphere of 4–10 K in the tropics, due to increasing GHG concentrations (Figure 3-2(e)). Weaker cooling is simulated lower down in the stratosphere, and little change in temperature is simulated in the lowermost stratosphere due to the competing effects of ozone recovery and continued GHG increases.

3.2.4 Transport and Dynamics

3.2.4.1 Brewer-Dobson Circulation

As described in Section 4.2.2, the BDC is the stratospheric overturning circulation that transports air upward in the tropics, poleward at midlatitudes, and downward at middle and high latitudes, and so plays a crucial role in determining the meridional distribution of ozone and long-lived trace gases. Climate models and CCMs consistently predict an acceleration of the BDC in response to climate change, producing a trend of ~2% per decade in net upward mass flux in the tropical lower stratosphere in the multi-model mean (Section 4.3.2). An acceleration of the BDC would increase the rate at which ODSs are removed from the stratosphere (Butchart and Scaife, 2001), thus advancing ozone recovery. However, this removal mechanism is not represented in current CCMs as a consequence of the lower boundary condition for ODSs where mixing ratios, not fluxes, are specified (Section 3.3.7). An accelerated BDC would also increase the rate at which other gases such as N_2O and CH_4 get into the stratosphere, which would in turn affect the lifetimes of these gases and the evolution of ozone. In addition, the projected increase in the strength of the BDC would decrease ozone in the tropical lower stratosphere where ozone-poor air of tropospheric origin enters and rises slowly in relative isolation within this region. During the transit through the tropical lower stratosphere, ozone is continuously produced by molecular oxygen (O_2) photolysis within the rising air. As a result, tropical lower stratospheric ozone content is mostly determined by a balance between the rate of ozone production (i.e., from photolysis of O_2) and the rate at which the air is transported through and out of the tropical lower stratosphere (essentially the rate of ascent and, to a lesser extent, mixing with the subtropics) (Avallone and Prather, 1996). A faster transit of air through the tropical lower stratosphere from an enhanced BDC would ultimately lead to less time for production of ozone and hence lower ozone levels in this region. In contrast, ozone levels would increase in the extratropical lower stratosphere due to increased downward transport of ozone-rich air from above. This latitudinal dependence is illustrated in Figure 3-3, which shows 1970 to 2090 changes in the residual vertical velocity $\bar{w}^*$ at 70 hPa and the corresponding changes in total column ozone from an ensemble of simulations using one CCM, the Canadian Middle Atmosphere Model (CMAM) (McLandress and Shepherd, 2009a). The close correspondence between changes in $\bar{w}^*$ and ozone (a negative correlation) highlights the potential importance of future changes in the strength of the BDC on ozone. However, the fact that the modest modeled increases in the strength of the BDC to date are difficult to detect in the currently available measurements (Section 4.2.2) suggests that some caution should be exercised when diagnosing projected future changes in ozone in the light of expected changes in the BDC.

3.2.4.2 Vortex Integrity and Mixing

Future changes in the shape and strength of the polar vortex and in the frequency and strength of sudden stratospheric warmings (SSWs) will likely alter meridional transport which will in turn affect polar ozone. Charlton-Perez et al. (2008) diagnose a significant increase in major SSW

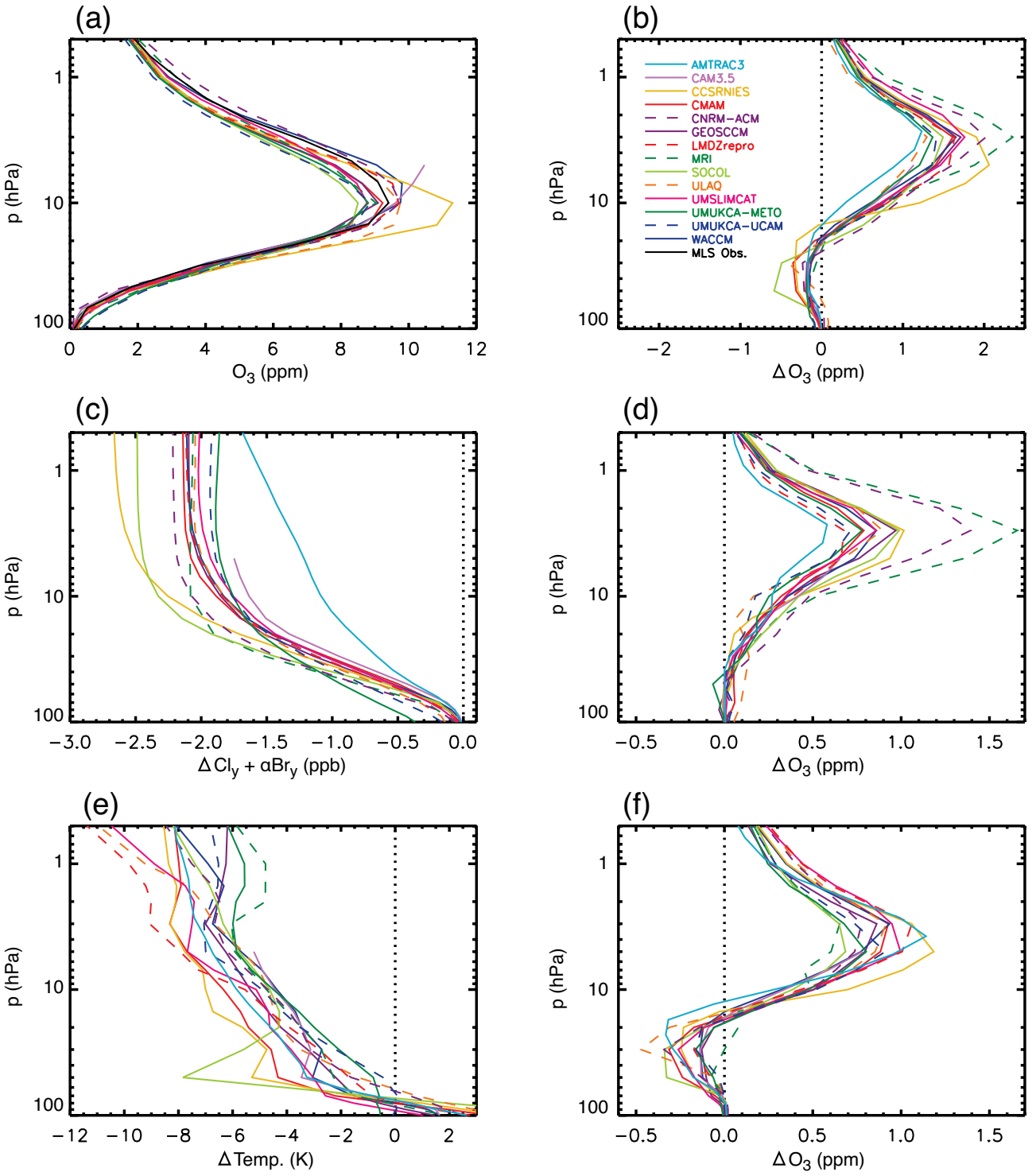

Figure 3-2. Vertical profile results of the Multiple Linear Regression (MLR) analysis for the CCMVal-2 models (described in Table 3-1) in the latitude band 10°S–10°N. (a) Ozone in the year 2000 (parts per million) versus pressure (hectoPascals), (b) Ozone change from 2000 to 2100, (c) ESC change (parts per billion) from 2000 to 2100, (d) ESC-congruent ozone change. (e) and (f) are the same as (c) and (d), except for temperature. From Chapter 9 of SPARC CCMVal (2010), their Figure 9.4.

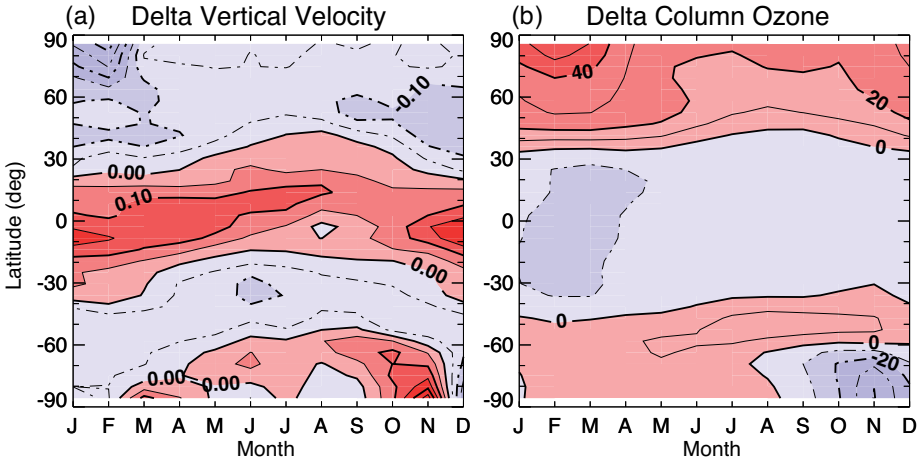

Figure 3-3. Difference between future and past (a) residual vertical velocity at 70 hPa and (b) total column ozone (deviation about global mean). Contour intervals are 0.05 mm/s and 10 DU. Future and past time periods are computed using 20-year means centered about 2090 and 1970, respectively. From McLandress and Shepherd (2009a), adapted from panels (b) and (f) of their Figure 6.

frequency of 1 event per decade between 1960 and 2099 in the Atmospheric Model with TRansport and Chemistry (AMTRAC) using a crossing method based on transition from westerlies to easterlies to detect major SSWs. However, using a criterion for major SSW occurrence based on the amplitude of the Northern Annular Mode and simulations from the CMAM, McLandress and Shepherd (2009b) showed that the future increase in the frequency of major SSWs in that model was a consequence of changes in the underlying climatology (i.e., mean vortex strength) and did not mean an increase in stratospheric variability. A recent study by Bell et al. (2010), however, found an increase in both stratospheric variability and major SSW frequency in simulations using enhanced GHG concentrations. Clearly, a consensus on the impact of stratospheric climate changes on vortex variability has not yet been reached, and cleanly separating changes in vortex variability from changes in the mean vortex strength remains a challenge.

The isolation of the polar vortex in conjunction with mixing across the vortex edge is an important dynamical regulator for ozone amounts at high latitudes (e.g., Strahan and Polansky, 2006) and midlatitudes (Braesicke and Pyle, 2003; Hadjinicolaou and Pyle, 2004; Wohltmann et al., 2007). Assessments of observed and modeled changes in stratospheric mixing are sparse. Garny et al. (2007) diagnosed recent trends in stratospheric mixing on selected isentropic surfaces in the lower stratosphere and found substantial differences for different heights, horizontal regions and seasons, with, for example, long-term positive trends in mixing in southern midlatitudes at 450K nearly year-round and negative trends in southern high latitudes at 650K from May to August. In models, the choice of vertical resolution (Rind et al., 2007) and advection algorithm (Stenke et al., 2008) plays an important role. Modeling the 2002 major warming in the Southern Hemisphere, Konopka et al. (2005) diagnosed a larger degree of isolation than for similar events in the Northern Hemisphere. Changes in Antarctic vortex isolation at the end of the 21st century have been examined for a subset of CCMs (Chapter 5 of the SPARC CCMVal Report, 2010). Some of the models analyzed indicate increased mixing between the vortex and midlatitudes above 1000K (~35 km) in the future, suggesting that winter planetary wave activity may have increased in the models. In this model intercomparison, no consensus could be found as to how the Antarctic vortex size and depth may change toward 2100. Note that the link between the modeled strengthening of the BDC and changes in mixing is not straightforward. Therefore, based on current knowledge, we cannot judge with high confidence how mixing across vortex barriers will change in the future and how this will affect ozone.

3.2.5 Background and Volcanic Stratospheric Aerosols

A layer of sulfuric acid aerosol is present at all latitudes in the lower stratosphere. During volcanically quiescent periods (also called "background" conditions), the dominant source of this aerosol layer is thought to be carbonyl sulfide photolysis and, possibly, sulfur entering the stratosphere in the form of sulfur dioxide (SO_2) (SPARC, 2006). The other major source of sulfur to the stratosphere is volcanoes. Chapters 3 and 6 of WMO (2007) (Chipperfield and Fioletov et al., 2007; Bodeker and Waugh et al., 2007) contain an in-depth discussion of volcanic aerosols and their effects on ozone. Chapter 8 of the CCMVal report (SPARC CCMVal, 2010) contains recent modeling intercomparisons of volcanic effects on ozone.

Volcanic eruptions can inject large amounts of sulfur directly into the stratosphere. This can considerably enhance the stratospheric aerosol layer (or Junge layer) for several years. Such an effect was observed after the eruptions of El Chichón in 1982 and Mt.

Pinatubo in 1991. The enhanced stratospheric aerosol loading can lead to very significant ozone depletion on a global scale, as was both observed and modeled after these eruptions. The ozone depletion is mostly due to heterogeneous reactions on sulfuric acid aerosol particles that convert halogen reservoir species into more reactive forms. The overall chemical changes include an increase in halogen radicals at the expense of nitrogen radicals. Thus, the net effect on ozone depends primarily on the stratospheric halogen loading, changing for instance from ozone decreases when chlorine loading is high to small ozone increases when chlorine loading is low (Tie and Brasseur, 1995). As a result, the potential for ozone depletion from enhanced aerosol loading is expected to decline as ESC decays toward natural levels late in the 21st century. The future recovery of ozone would be temporarily interrupted by large volcanic eruptions, especially during the first half of the 21st century. Small volcanic eruptions can also influence ozone, as was found in aircraft measurements that probed the Hekla, Iceland, volcanic plume in the lowermost stratosphere (Millard et al., 2006). The volcanic plume contained high SO_2 levels and very low ozone levels, near zero in places, and was still 30% depleted two weeks after. Simulations using a three-dimensional (3-D) chemistry-transport model (Chipperfield, 2006) showed that increased heterogeneous activation of chlorine due to elevated H_2O and HNO_3 from the volcanic plume was the likely cause of the ozone loss. Events such as these would not be expected to cause widespread ozone loss because of both the small size of the eruption and the short residence time of volcanic aerosols in the lowermost stratosphere. The analyses of these events do, however, confirm the link between aerosols and ozone depletion.

By virtue of their optical properties, aerosols also impact the radiative balance of the atmosphere and, hence, can affect stratospheric temperatures and dynamics substantially. Since the previous Assessment, several studies have attempted to separate the chemical and dynamical signals in the ozone response following the Mt. Pinatubo eruption. Using a two-dimensional model forced with meteorological analyses, Fleming et al. (2007) showed that, while the chemical ozone destruction due to halogen chemistry on volcanic aerosols took place in the lower stratosphere in both hemispheres, dynamical effects acted to decrease (increase) total column ozone in the Northern (Southern) Hemisphere. This result was confirmed by Telford et al. (2009) using a CCM nudged toward meteorological analyses. They found that, in addition to the ~10 Dobson unit (DU) chemical ozone loss in both hemispheres following the Mt. Pinatubo eruption, the quasi-biennial oscillation (QBO) (see Chapter 2) increased ozone by ~10 DU in the Southern Hemisphere and decreased ozone by ~10 DU in the Northern Hemisphere. These two modeling studies confirm the earlier work of Hadjinicolaou et al. (1997) that demonstrated the existence of a large dynamical effect on ozone following the eruption.

From long-term aerosol measurements, it has been suggested that background stratospheric aerosol levels have been increasing in the last decade possibly due to enhanced tropospheric SO_2 background (see Sections 2.4.3.3 and 4.1.4 in Chapters 2 and 4 of this Assessment). There are a few reasons why a change in background aerosol levels could significantly affect ozone while chlorine levels remain elevated. First, halogen radical levels (and thus ozone loss) increase more strongly with aerosol loading when the aerosol loading is small, because the halogen activation saturates at high aerosol loadings due to the reduction of dinitrogen pentoxide (N_2O_5). Second, depending on the cause of this observed aerosol increase, it is possible that the increases may be larger at lower altitudes, where halogen radicals impact ozone most strongly. Thus, the potential for significant changes in background aerosol levels remains an uncertainty in predicting ozone changes in the coming decades.

3.2.6 Geoengineering by Sulfate Aerosol Injection

Doubts regarding the effectiveness of current international agreements to restrict emissions of GHGs to the atmosphere to mitigate climate change have led to a debate about the possibility of intentionally modifying climate through large-scale geoengineering actions; see Crutzen (2006) and a series of replies in a special issue of *Climatic Change* (vol. 77, no. 3-4, 2006). Such climate engineering schemes, if ever applied, might impact stratospheric ozone (Royal Society, 2009). Proposed schemes and uncertainties in their implementation are discussed in Chapter 5 of this Assessment (Section 5.4.2.4). Present knowledge strongly suggests that the addition of sunlight-reflecting sulfuric acid aerosols into the stratosphere would have large impacts on the future evolution of stratospheric ozone and as such should be considered alongside the other factors discussed in this chapter.

As discussed in the previous section, observations show a marked decrease in global ozone following the explosive volcanic eruptions of El Chichón in 1982 and Mt. Pinatubo in 1991. The primary reason for this enhanced ozone loss is the enhanced activation of stratospheric chlorine on volcanic aerosol particles (Kinnison et al., 1994; Solomon et al., 1996; Portmann et al., 1996; Tilmes et al., 2008b). Similar effects are expected for geoengineered stratospheric aerosol enhancements. An

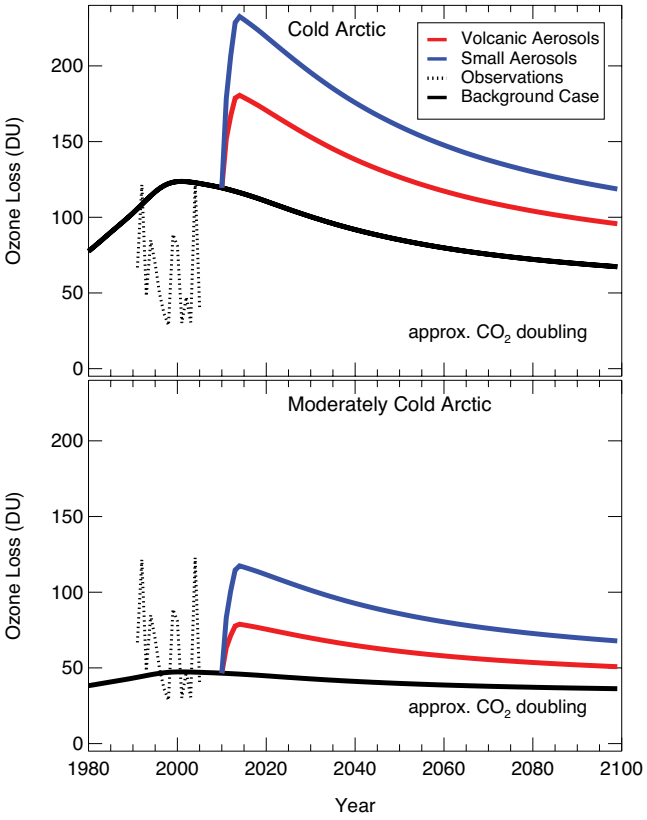

Figure 3-4. An illustration of the possible impact of geoengineering by stratospheric injection of sulfate aerosols on Arctic chemical ozone loss. The panels show estimates of the potential ozone loss (Dobson units) from chlorine activation as a function of time for different stratospheric aerosol loadings and for two types of Arctic winters. The top panel corresponds to cold Arctic winters, conditions that are expected to lead to the maximum impact of geoengineering on ozone depletion. The bottom panel is for moderately cold Arctic winters, representative of about half of the past 15 Arctic winters. In each panel, the solid and dotted black lines represent the ozone loss for a background stratospheric aerosol loading and observed stratospheric aerosol loading respectively. The red line shows the ozone loss estimated when 2 teragrams per year (Tg/yr) of stratospheric sulfur are added to the stratosphere, starting in 2010 and reaching a saturation value of 5.3 Tg of sulfur in the form of large volcanic-sized aerosol particles. The blue line corresponds to an alternative geoengineering scenario assuming the formation of smaller aerosol particles. In this scenario, a smaller injection of 1.5 Tg of sulfur per year would achieve the same radiative effect necessary to counteract the impact of a doubling of atmospheric carbon dioxide concentrations. Adapted from Tilmes et al. (2008a).

illustration of the impact of an enhanced stratospheric aerosol layer on chemical ozone loss is shown in Figure 3-4 (Tilmes et al., 2008a). For large, geoengineered, stratospheric aerosol loadings that appear to be required for significant climate change mitigation, model estimates suggest that chlorine activation could be more than doubled in the Arctic if it is implemented in the next 20 years, resulting in Arctic ozone depletion of 200–230 DU during very cold winters (comparable to the total amount of available ozone in the Arctic lower stratosphere). As stratospheric halogen levels decline over the 21st century, the impact of an enhanced aerosol layer on chlorine activation would be reduced but would still be significant. The expected recovery of the Antarctic ozone hole could be delayed by between 30 to 70 years depending on the assumed geoengineered aerosol size distribution (Tilmes et al., 2008a).

Further understanding of the consequences of geoengineering for stratospheric ozone and climate has been gained from numerical model simulations initially using global climate models (Matthews and Caldeira, 2007; Caldeira and Wood, 2008; Rasch et al., 2008; Robock et al., 2009) and, more recently, CCMs (Tilmes et al., 2009; Heckendorn et al., 2009). The CCM investigations confirm the empirical results of Tilmes et al. (2008a) that stratospheric sulfate injection could enhance stratospheric ozone depletion in both the Arctic and Antarctic while the levels of halogens remain elevated. Tilmes et al. (2009) quantified the impact of an enhanced burden of stratospheric sulfur on the ozone layer including the impacts on stratospheric dynamics and transport during the period when the stratospheric halogen loading is projected to slowly decline (Newman et al., 2007). Model calculations with a fixed enhanced sulfate aerosol loading (large enough to counteract the forcing generated by a doubling of CO_2 abundance with respect to preindustrial values) predict a one- to two-fold increase in Arctic ozone depletion due to a stronger polar vortex and lower temperatures (Rasch et al., 2008). The impact on midlatitude ozone was calculated to be smaller for 2050 chlorine levels (Tilmes et al., 2009). An additional risk is the possible occurrence of a large volcanic eruption, further increasing the amount of sulfur in the stratosphere (Tilmes et al., 2009).

Significant uncertainty remains regarding the behavior of artificially injected stratospheric aerosol, since the coagulation and settling of aerosol is strongly dependent on the injection scenario. Aerosol heating, in particular at the tropical tropopause, could also result in enhanced amounts of water vapor entering the stratosphere (Heckendorn et al., 2009), which would cause stratospheric ozone loss. According to CCM simulations of predicted 2050 conditions (Tilmes et al., 2009; Heckendorn et al., 2009), a geoengineered enhanced aerosol loading would lead to substantial and coupled changes in stratospheric dynam-

ics and ozone chemistry, especially in halogen heterogeneous chemistry. To date there have been no investigations of the impact on ozone caused by a gradual ramp-up of the amount of SO_2 injected, with the purpose of keeping global average temperature nearly constant (Wigley, 2006). Overall, we caution that these ozone projections are based on simple scenarios, idealized conditions, and on only two CCMs, including one without any aerosol microphysics. Because the ozone response depends on complex and competing interactions between chemical, aerosol microphysical, radiative, and dynamical processes that are represented differently in different models, more reliable ozone projections in a hypothetical geoengineered climate state require more realistic simulations with a range of models.

3.2.7 Effects of Ozone on Future Surface UV

In the 1980s and 1990s, a number of theoretical and experimental studies were devoted to quantifying ozone effects on UV spectral irradiance reaching the ground (e.g., Brühl and Crutzen, 1989; Schwander et al., 1997; Tsay and Stamnes, 1992; Madronich et al., 1998; Lapeta et al., 2000). Figure 3-5 shows the dependence of erythemal irradiance (CIE, 1993) on total ozone and other atmospheric parameters (cloud optical thickness, surface albedo, and aerosol optical thickness) within the range of values that can be observed in real atmospheric conditions. To quantify UV radiation, we use here the "erythemally weighted irradiance," or simply "erythemal irradiance," which is a measure of the biological effectiveness of solar UV radiation incident per unit area of human skin and is commonly used for public information and awareness. The effective wavelengths of erythemal irradiance lie between 307 and 325 nm, depending mainly on solar zenith angle and total ozone. Other effects on humans and ecosystems are more sensitive to shorter or longer wavelengths of UV radiation, hence ozone-induced changes in the corresponding weighted irradiances would be either larger (e.g., for DNA damage) or smaller (e.g., for phytoplankton damage) compared to erythemal irradiance.

To estimate the response of UV radiation to ozone variations, the radiation amplification factor (RAF) approach proposed by Booth and Madronich (1994) is widely used. It provides simple but useful estimates of different biological weightings of UV irradiance response to ozone changes. For erythemal irradiance, the RAF was shown to be about −1.1 (WMO, 1999). At the same time, the influence of ozone on UV irradiance depends on solar elevation. Recently, a simple equation was proposed by Madronich (2007) enabling the calculation of erythemal irradiance (or the UV Index) under cloud-free skies and low surface-albedo conditions as a function of total ozone (in the range 200–400 DU), taking into account also the effect of solar zenith angle. The uncertainty of these estimates increases for solar zenith angles larger than ~60°. However, the application of these approaches can lead to random and/or systematic uncertainties in calculating the UV response to future total ozone changes because they do not account for possible changes in ozone and temperature profiles. The influence of aerosols, clouds, and surface albedo are also neglected.

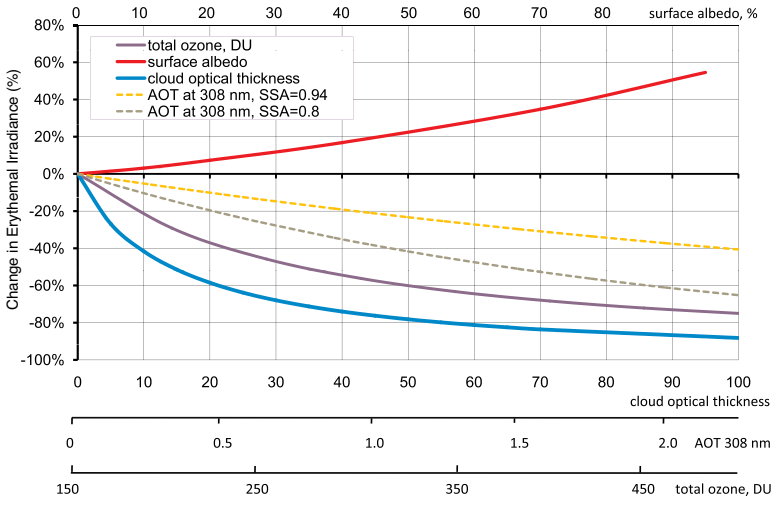

Figure 3-5. Relative changes (percent) in erythemal irradiance due to total ozone, cloud optical thickness, surface albedo and aerosol optical thickness (AOT) at 308 nm for two values of single scattering albedo (SSA), calculated for 50° solar zenith angle with the Tropospheric Ultraviolet-Visible (TUV) v.2 model (Madronich and Flocke, 1999). All parameters vary within the range observed in real atmospheric conditions. Except for the effect of cloud optical thickness, all calculations refer to cloud-free skies. For the calculation of erythemal irradiance changes due to ozone, typical values were used for the aerosol optical thickness, AOT = 0.31, (Kinne et al., 2006) and the single scattering albedo, SSA = 0.94 (Chubarova, 2009). For estimating the effects from aerosols, surface albedo, and cloud optical thickness, an ozone column of 300 DU was used in the model simulations.

The effects of the vertical distribution of ozone in the troposphere and the stratosphere, as well as the temperature profiles (which affect the ozone cross-sections) should be taken into account when calculating the UV response to ozone changes (Brühl and Crutzen, 1989; Schwander et al., 1997; McKenzie et al., 2003). As discussed in Tsay and Stamnes (1992) and Brühl and Crutzen (1989), transport of ozone from the stratosphere to the troposphere tends to decrease UV at the surface, but for low solar elevation angles an increase may occur. Changes in ozone vertical distribution and temperature profile can modify erythemal irradiance by as much as 14%, according to Lapeta et al. (2000). In Kazantzidis et al. (2005) it was emphasized that the most significant effects of changes in vertical ozone distribution on surface erythemal irradiance are observed at large solar zenith angles (up to 20% at 85° solar zenith angle). However, UV levels are usually very small for these conditions.

The future evolution of ozone will determine to a great extent future levels of surface UV radiation and the date of return to the UV levels in the 1980s or 1960s. However, in some regions UV radiation levels in the future may not return to historical levels due to influences from factors related to climate change (e.g., cloudiness, surface albedo, aerosols, UV-absorbing tropospheric gases; see Section 3.2.8). A detailed analysis of future UV levels due to ozone in different geographical areas is given in Section 3.4.

3.2.8 Factors Other Than Stratospheric Ozone Affecting Surface UV

In addition to ozone, UV radiation is affected by other atmospheric parameters, for example, changes in cloudiness, aerosols, surface albedo, and, to some extent, by other mineral and organic gas species. Since WMO (2007) a number of publications have discussed and quantified the factors other than ozone that affect surface UV irradiance (e.g., Kazadzis et al., 2007; Tanskanen and Manninen, 2007; Lindfors and Arola, 2008; Staiger et al., 2008; Badosa et al., 2007; Chubarova, 2008; Rieder et al., 2008; McKenzie et al., 2008; Chubarova et al., 2009). A comparison of the relative effects of changes in ozone and in other atmospheric parameters on surface erythemal irradiance is shown in Figure 3-5. Changes in cloud optical thickness, typically between 0 and 40, are the most important driver of day-to-day and long-term changes in surface UV irradiance, generally dominating the effect of changes in total column ozone. Aerosols, and in particular highly absorbing aerosols, also affect surface UV irradiance. However, for typical values of aerosol optical thickness (~0.3), the effect is small compared to clouds. Increases in surface albedo, for example due to changes in snow or ice cover, can significantly enhance surface UV. The sensitivity of surface UV to the changes in atmospheric parameters shown in Figure 3-5 does not account for more complicated, nonlinear interactions in their effects (for example, the interaction of clouds and inhomogeneous surface albedo, or cloud and aerosol interactions) or for spatial inhomogeneities in the atmosphere.

Since surface UV is appreciably sensitive to a number of factors other than ozone, projections of these factors, in addition to ozone, are required to make reliable and robust projections of surface UV irradiance. However, at present, projections of atmospheric factors other than ozone have large uncertainties, making accurate projections of surface UV elusive.

3.2.8.1 Clouds

Because climate change is likely to affect future cloudiness, and given the sensitivity of surface UV to changes in cloudiness (Figure 3-5), understanding potential future changes in cloud cover is essential to quantifying future changes in UV. To this end, projections of changes in cloudiness obtained from the Third Coupled Model Intercomparison Project (IPCC, 2007) and indirectly from Chapter 10 of SPARC CCMVal (2010) have been used. Climate models forced according to the Special Report on Emissions Scenarios (SRES) A1B scenario from IPCC (2000) (which is the standard scenario of the stratospheric ozone projections discussed here; see Section 3.3.1) predict with some consistency that by the end of the 21st century cloud cover would have decreased over most of the low and middle latitudes, and substantially increased at high latitudes. Trenberth and Fasullo (2009) examined top-of-atmosphere radiation changes in climate model projections and also found decreases in cloudiness through the 21st century predominantly after 2040. Coverage of optically thick low-level clouds is projected to also decrease over low and middle latitudes (Trenberth and Fasullo, 2009), in agreement with the tendency for low-level clouds to dissipate as the ocean warms (Clement et al., 2009). In Chapter 10 of SPARC CCMVal (2010), cloud projections were used to estimate future changes in surface erythemal irradiance by converting shortwave cloud transmittance to erythemal UV cloud transmittance. Shortwave cloud transmittances evaluated from the IPCC (2007) climate models and from Chapter 10 of SPARC CCMVal (2010) CCMs agree reasonably well. However, these projections are highly uncertain as the cloud response to climate change appears to be the primary source of spread between climate model simulations (Dufresne and Bony, 2008).

Projections of surface UV irradiance that include the effects of cloud changes result in more complex patterns in projected UV compared to clear-sky UV projections. Increases in erythemal irradiance of 10–15% by the

end of 21st century due to changes in cloudiness are projected for the tropical regions of South-East Asia and Central America, with more moderate increases over Southern Europe in summer (Chapter 10 of SPARC CCMVal, 2010). A UV reduction of 10–15% is projected by 2100 due to increases in cloudiness over some northern high-latitude regions and over Antarctica.

3.2.8.2 Aerosols

The effect of atmospheric aerosols on surface UV radiation depends on their optical and microphysical properties and total atmospheric loading. While the tropospheric burden of sulfate aerosols is generally projected to decrease in the future, projections for black carbon (soot) are less certain (IPCC, 2007). Projections of aerosol properties have been aided by recent modeling studies (Kinne et al., 2006, Schulz et al., 2006). However, at present, despite general agreement on projections of annual mean aerosol optical thickness, the disparity of aerosol absorption in various models leads to large uncertainties in surface UV, precluding robust assessments of future aerosol effects on UV irradiance. There are also large uncertainties in the methods used to generate emissions scenarios as well as in assessing the present-day emissions, especially for black carbon and organic carbon (IPCC, 2007). Furthermore, it remains unresolved whether emissions of soil dust aerosols will increase or decrease in response to changes in the atmospheric state and circulation (Tegen et al., 2004). Differences in emission regulation strategies between countries result in large spatial variability in aerosol trends.

Climate model simulations project increases in aerosol optical thickness of ~1.4% by 2030 for the A1B scenario but decreases of ~5% for the SRES B1 scenario, a lower emission scenario (IPCC, 2000; Jacobson and Streets, 2009). Resultant changes in surface UV radiation are estimated to be smaller than −0.5% for the A1B scenario, and about 0.1–1.5% for the B1 scenario, depending on the aerosol properties and solar elevation.

3.2.8.3 Surface Albedo and Sea Ice Cover

The effects of surface albedo on UV irradiance are well documented (WMO, 1999; WMO, 2003; WMO, 2007). Under clear-sky conditions, the presence of snow/ice may increase UV by up to 50%, while in overcast or close to overcast conditions with optically thick clouds, the UV increase due to high snow/ice surface albedo can reach several hundred percent because of effective multiple scattering. On the other hand, sea ice cover significantly reduces penetration of harmful UV-B irradiance in the underwater environment. As a result, possible climate warming-induced changes in snow and sea ice cover may affect both terrestrial and aquatic ecosystems.

Reductions in sea ice extent through the 21st century in both the Arctic and Antarctic have been projected by a number of models, albeit with a rather large range of model responses in the Northern Hemisphere sea ice extent, ranging from very little change to a strong and accelerating reduction over the 21st century (Zhang and Walsh, 2006). According to Overland and Wang (2007), the projected summer loss in sea ice extent would be greater than 40% by 2050 for the marginal seas of the Arctic basin. Stroeve et al. (2007) reported that sea ice in the Arctic is melting faster than projected in IPCC (2007) under all SRES emissions scenarios. The accelerated decrease in Arctic sea ice extent has also been documented in satellite data (Comiso et al., 2008). This sea ice melting is projected to decrease the surface albedo and increase UV irradiance in the underwater environment. In the 20th- and 21st-century simulations, Antarctic sea ice cover is projected to decrease more slowly than in the Arctic (Stroeve et al., 2007), particularly in the vicinity of the Ross Sea, where most models predict a local minimum in surface warming (Meehl, et al., 2007).

It is well established that mountain glaciers and snow cover have declined on average in both hemispheres (IPCC, 2007). They are expected to continue declining in the future (Bradley et al., 2004). This would result in considerable local reductions in surface albedo and UV in the corresponding regions.

3.2.8.4 Tropospheric Gases

Several tropospheric gases, such as SO_2, NO_2, and ozone, can efficiently absorb UV-B radiation. Their influence depends mainly on their total column amount, which can be especially high over industrial areas and over areas influenced by forest fires. Their impact is also determined by the effectiveness of UV absorption discussed in Chapter 7 of WMO (2007) (Bais and Lubin et al., 2007). The average effect of increasing NO_2 on erythemal irradiance has been shown to be about −2% in industrial areas (Chubarova, 2008). However, on some days the influence can be much stronger. For example, in Tokyo the amount of NO_2 can be 20 times higher than the average, decreasing UV-B irradiance by about 15% (McKenzie et al., 2008). Similar effects from NO_2 have been observed during intense forest fires, when erythemal irradiance has been attenuated by 10–15% (Chubarova et al., 2009). SO_2 column amounts can easily reach 2 DU over areas affected by high volcanic activity or over regions close to coal burning industries, resulting in ~2% attenuation of erythemal irradiance. At some UV wavelengths, the reduction by SO_2 can exceed 20% (McKenzie et al., 2008).

The amounts of these gases in the troposphere depend strongly on their emissions. In industrialized regions, such as North America and Europe, emissions

of NO_x and volatile organic compounds are decreasing, while in regions dominated by developing countries, significant growth in emissions is observed (IPCC, 2007). Since 1980, SO_2 emissions in 25 countries in Europe have been reduced by more than a factor of 4, while in the USA they have been halved (IPCC, 2007). However, over the same period, SO_2 emissions from Asia and from developing countries in other regions have been increasing. There is a clear positive trend in tropospheric ozone concentrations projected by models under the A2p scenario, with increases between 11.4 and 20.5 DU by 2100 (Gauss et al., 2003). Taking into account that ozone absorbs UV radiation more effectively in the lower troposphere due to enhanced scattering, these increases in tropospheric ozone may result in approximately a 5–10% reduction in surface erythemal irradiance. The modeling study of Jacobson and Streets (2009) also projects by 2030 an increase in surface ozone of ~14% under the A1B scenario and ~4% under the B1 scenario.

3.3 PROJECTIONS OF OZONE THROUGH THE 21ST CENTURY

Since the 2006 Assessment (WMO, 2007), a new suite of 17 chemistry-climate model (CCM) simulations coordinated through the SPARC CCMVal activity has become available. These simulations, from the second phase of CCMVal (referred to as CCMVal-2), form the basis for this section and improve on the CCMVal-1 simulations reported in WMO (2007) by:

- Starting in 1960 rather than in 1980. In most regions of the atmosphere, ozone depletion occurs prior to 1980 in nearly all of the CCMs assessed here. By starting the simulations in 1960 at a time when ozone was not expected to be significantly affected by ODSs, and including sensitivity simulations, the CCMs can now be used to project the timing of the third stage of ozone recovery, i.e., the full recovery of ozone from the effects of ODSs. Stage-three ozone recovery was not reported on in WMO (2007). Furthermore, the availability of pre-1980 model data permits a more robust calculation of the 1980 ozone threshold and hence a more accurate determination of when ozone returns to 1980 levels.

- Having available almost all simulations from 1960 to 2100. In WMO (2007) only one CCM provided simulations beyond 2050. The extension to 2100 now permits more robust conclusions to be drawn regarding the expected evolution of ozone through the latter half of the 21st century.

- Applying a more rigorous statistical analysis. The larger number of models, the availability of continuous simulations from 1960 to 2100 by nearly all CCMs, and a new method for calculating and analyzing multi-model time series (described in Section 3.3.2.2) have allowed a more robust analysis than was presented in WMO (2007).

- Having available a number of sensitivity simulations with fixed forcings. In addition to the reference simulations as reported in WMO (2007), simulations where either surface concentrations of ODSs or GHGs are held fixed at their 1960 levels (Section 3.3.1) permit a more in-depth analysis of the factors affecting ozone through the 21st century than previously possible and allow the assessment of full ozone recovery from ODSs.

- Having available simulations based on different GHG emissions scenarios. WMO (2007) reported only on simulations based on the SRES A1B scenario.

3.3.1 Model Descriptions and Scenarios

In this chapter the focus is on "future" simulations to 2100, whereas the "past" simulations (from 1960 up to 2006) are discussed in Chapter 2. Ozone projections and the attribution of ozone changes to ODSs and GHGs are based on the recently completed CCMVal-2 multi-model ensemble. These simulations have been extensively analyzed in SPARC CCMVal (2010), as well as in a variety of individual model studies. In addition to this large ensemble of future reference simulations from 17 CCMs, in which realistic scenarios of ODSs and GHGs are used, several more specialized sensitivity simulations by a subset of CCMs (Waugh et al., 2009; Eyring et al., 2010a; Eyring et al., 2010b; Charlton-Perez et al., 2010; Oman et al., 2010) are assessed here.

The CCM simulations are all transient simulations in which ozone responds interactively to the secular trends in GHGs, ODSs, and in other boundary conditions. They are commonly separated into "past" (or "historical") transient reference simulations that are driven by observed forcing and "future" transient reference simulations that are forced by trace gas projections and generally use modeled sea surface temperatures (SSTs) and sea ice concentrations (SICs). The CCMVal-2 "past" reference simulation (REF-B1) is designed to reproduce ozone changes from 1960 to the recent past (2006) when global ozone observations are available. It includes solar and volcanic forcings, and SSTs/SICs from observations. It allows a detailed investigation of the role of natural variability and other atmospheric changes important for

ozone trends (see Chapter 2). The CCMVal-2 "future" reference simulation (REF-B2) is a self-consistent simulation from the past into the future. In this simulation the surface time series of halocarbons is based on the adjusted A1 halogen scenario (WMO, 2007, see also Section 3.2.1). The long-lived GHG concentrations are taken from the SRES A1B scenario (IPCC, 2000). SSTs and SICs are generally prescribed from coupled ocean model simulations. Of the 17 CCMs that provided ozone projections analyzed in this chapter, only CMAM was coupled to an interactive ocean model (see Table 3-1). Some CCMs generated an ensemble of future simulations with the same boundary conditions but different initial conditions (see Table 3-1). In general, the ozone variability between ensemble members from a single model is much smaller than the inter-model differences (Chapter 6, WMO, 2007; Austin et al., 2008).

Additional sensitivity simulations based on different emissions scenarios were also performed by some CCM groups to attribute the future evolution of stratospheric ozone to ODS and GHG forcings and to study the coupled chemistry-climate system under a variety of GHG scenarios (see Tables 3-1 and 3-2). These include sensitivity simulations with ODSs fixed at 1960 levels (fODS) to assess the milestone of full ozone recovery (Waugh et al., 2009; Eyring et al., 2010a) (see Section 3.3.6). In addition, sensitivity simulations with GHGs fixed at 1960 levels (fGHG) were performed, for example, to address the issue of the linear additivity of the effects of GHGs and ODSs on ozone. By comparing the sum of the ozone responses in the fixed GHG and ODS simulations (each relative to the 1960 baseline) with the ozone response in the REF-B2 reference simulation, the linear additivity of the responses can be assessed (McLandress et al., 2010; Eyring et al., 2010a). A subset of four CCMs also provided future projections under GHG scenarios different to SRES A1B (Oman et al., 2010; Eyring et al., 2010b). These GHG sensitivity simulations (GHG-x) include simulations forced with the SRES A2 and B1 GHG scenario from IPCC (2000) and with the new Representative Concentration Pathways (RCPs; Moss et al., 2008) that form the basis for the climate simulations of the Coupled Model Intercomparison Project, Phase 5 (CMIP5, Taylor et al., 2009), in support of the Fifth IPCC Assessment Report. They are generated by integrated assessment models and harmonized with the historical emissions from Lamarque et al. (2010) in both amplitude and geographical distribution. The RCP simulations performed by CAM3.5 are RCP 8.5 (Riahi et al., 2007), RCP 4.5 (Clarke et al., 2007), and RCP 2.6 (van Vuuren et al., 2007), where the number after "RCP" indicates the radiative forcing in W/m^2 reached by 2100 in each scenario. By 2100, for example, CO_2 in the RCP 8.5 and SRES A2 scenarios is ~200 ppm and ~100 ppm higher than in SRES A1B, while in the SRES B1/RCP 4.5 and RCP 2.6 scenario it is ~150 ppm and ~250 ppm lower, respectively. The different levels of GHGs lead to differences in ozone projections (see Section 3.2 on factors affecting future ozone).

3.3.2 Model Evaluation and Multi-Model Mean Analysis

3.3.2.1 Model Evaluation

Confidence and guidance in interpreting CCM projections of future changes in atmospheric composition can be gained by first ensuring that the CCMs are able to reproduce key processes for stratospheric ozone (e.g., Eyring et al., 2005; SPARC CCMVal, 2010). Limitations and deficiencies in the models can be revealed through inter-model comparisons and through comparisons with observations. An improvement over the approach used in CCMVal-1 and WMO (2007) is that for the current Assessment, a more extensive set of ozone-related processes was evaluated in the CCMs (SPARC CCMVal, 2010). In this chapter the evolution of ozone and inorganic chlorine (Cl_y) is shown for individual CCMs in several figures to portray the full distribution of model simulations. However, the discussion and conclusions are based on the time series of the multi-model mean and associated statistical confidence and prediction intervals (see Section 3.3.2.2).

A detailed summary of the key findings of SPARC CCMVal (2010) on the evaluation of CCMs against observations is presented for chemical composition in Chapter 2, and for the Brewer-Dobson circulation (BDC) and temperature in Chapter 4. This section briefly summarizes relevant conclusions from these chapters, with a focus on processes and results that are important for long-term ozone projections.

- *BDC and Temperature*. Both are important drivers of the evolution of ozone. Most CCMs are capable of reproducing the amplitude and vertical structure of the observed trends in global-mean stratospheric temperatures, although the model spread is high in some regions. Tropical upwelling is well simulated in the lower stratosphere compared to meteorological analyses. Models consistently predict a strengthening of the BDC and hence a decrease in mean age of air as a result of climate change, but they disagree on the relative role of resolved and parameterized wave drag. This strengthening of the BDC is partly supported by several lines of observational evidence (see Section 4.2.2) but not by recent estimates of the age of air inferred from tracers observations in the northern midlatitude lower stratosphere, which indicate a statistically insignificant trend (Engel et al., 2009). However, the small model-simulated trends in the

BDC lie within the large uncertainties of the stratospheric age-of-air measurements.

- *Tropical and Midlatitude Ozone.* In the tropics, climate change and halogen loading influence total column ozone through dynamical processes in the lower stratosphere and chemical processes in the upper stratosphere. Over the historical period, the CCMs simulate negative trends in tropical upper stratospheric ozone, in agreement with observations (see Section 2.4.5.3). The

Table 3-1. A summary of the CCMs and the simulations used in this chapter. REF-B2 is the future reference simulation, fODS is a simulation with fixed ODSs, fGHG a simulation with fixed GHGs, and GHG-x are simulations with a GHG scenario different to SRES A1B; see details in Section 3.3.1 and Table 3-2. *N* × REF means that the group provided *N* realizations of this simulation. Further details on the models can be found in Morgenstern et al. (2010) and in Chapter 2 of SPARC CCMVal (2010) as well as in the references given below. EMAC-FUB and NIWA-SOCOL did not contribute a REF-B2 simulation for SPARC CCMVal (2010), but provided simulations later (Austin et al., 2010b; Eyring et al., 2010a).

CCM *	Group and Location **	Horizontal Resolution	Upper Level	Reference Simulation	fODS	fGHG	GHG-x	References
AMTRAC3	GFDL, USA	~200 km	0.017 hPa	REF-B2	---	---	---	Austin and Wilson (2010)
CAM3.5	NCAR, USA	1.9° × 2.5°	3.5 hPa	REF-B2	---	---	RCP2.6 RCP4.5 RCP8.5	Lamarque et al. (2008)
CCSRNIES	NIES, Tokyo, Japan	T42	0.012 hPa	REF-B2	fODS	fGHG	SRESB1 SRESA2	Akiyoshi et al. (2009)
CMAM	MSC, Univ. of Toronto, York Univ., Canada	T31	0.00081 hPa	3 × REF-B2	3 × fODS	3 × fGHG	---	Scinocca et al. (2008); de Grandpré et al. (2000)
CNRM-ACM	Meteo-France, France	T63	0.07 hPa	REF-B2	---	---	---	Déqué (2007); Teyssèdre et al. (2007)
E39CA	DLR, Germany	T30	10 hPa	REF-B2 (with solar cycle and QBO)	---	fGHG	---	Stenke et al. (2009); Garny et al. (2009)
EMAC-FUB	FU Berlin, Germany	T42	0.01 hPa	REF-B2 (with solar cycle and QBO)	---	fGHG	---	Jöckel et al. (2006); Nissen et al. (2007)
GEOSCCM	NASA/GSFC, USA	2° × 2.5°	0.015 hPa	REF-B2	fODS	---	SRESA2	Pawson et al. (2008)
LMDZrepro	IPSL, France	2.5° × 3.75°	0.07 hPa	REF-B2	fODS	---	---	Jourdain et al. (2008)
MRI	MRI, Japan	T42	0.01 hPa	2 × REF-B2	fODS	fGHG	---	Shibata and Deushi (2008a; 2008b)
NIWA-SOCOL	NIWA, New Zealand	T30	0.01 hPa	REF-B2	---	---	---	Schraner et al. (2008); Egorova et al. (2005)

Table 3-1, continued.

SOCOL	PMOD/WRC; ETHZ, Switzerland	T30	0.01 hPa	3 × REF-B2	fODS	fGHG	---	Schraner et al. (2008); Egorova et al. (2005)
ULAQ	Univ. of L'Aquila, Italy	R6 / 11.5° × 22.5°	0.04 hPa	REF-B2	fODS	fGHG	---	Pitari et al. (2002); Eyring et al. (2006; 2007)
UMSLIMCAT	Univ. of Leeds, UK	2.5° × 3.75°	0.01 hPa	REF-B2	fODS	---		Tian and Chipperfield (2005); Tian et al. (2006)
UMUKCA-METO	MetOffice, UK	2.5° × 3.75°	84 km	REF-B2	---	---	---	Morgenstern et al. (2008; 2009)
UMUKCA-UCAM	Univ. of Cambridge, UK	2.5° × 3.75°	84 km	REF-B2	---	---	---	Morgenstern et al. (2008; 2009)
WACCM	NCAR, USA	1.9° × 2.5°	5.9603 × 10^{-6} hPa	3 × REF-B2	fODS	fGHG	SRESB1	Garcia et al. (2007)

* CCM acronyms are defined in Appendix B of this Assessment.

** GFDL, Geophysical Fluid Dynamics Laboratory (NOAA); NCAR, National Center for Atmospheric Research; NIES, National Institute for Environmental Studies; MSC, Meteorological Service of Canada; DLR, Deutschen Zentrum für Luft- und Raumfahrt; FU, Freie University; NASA, National Aeronautics and Space Administration; GSFC, Goddard Space Flight Center; IPSL, Institut Pierre-Simon Laplace; MRI, Meteorological Research Institute; NIWA, National Institute of Water and Atmospheric Research; PMOD, Physical-Meteorological Observatory-Davos; WRC, World Radiation Center; ETHZ, Swiss Federal Institute of Technology-Zürich.

Table 3-2. Summary of CCMVal-2 reference and sensitivity simulations used in this chapter.

Simulation Name	Period	GHGs	ODSs	SSTs/SICs	Background & Volcanic Aerosol	Solar Variability	QBO
REF-B2	Transient simulation 1960–2100	SRES A1B (medium) (from IPCC, 2000)	OBS + adjusted A1 scenario (WMO 2007, Table 8-5)	Modeled SSTs and SICs	OBS Background surface area density from 2000	No	Only internally generated
fODS Fixed ODSs	1960–2100	Same as in REF-B2	ODSs fixed at 1960 levels	Same as in REF-B2	Same as in REF-B2	Same as in REF-B2	Same as in REF-B2
fGHG Fixed GHGs	1960–2100	GHG fixed at 1960 levels	Same as in REF-B2	1955–1964 average of REF-B2, repeating each year	Same as in REF-B2	Same as in REF-B2	Same as in REF-B2
GHG-x (SRES A2 and B1, RCP 2.6, 4.5, and 8.5	2000–2100	GHG scenario different from SRES A1B	Same as in REF-B2	SSTs/SICs distribution consistent with GHG scenario	Same as in REF-B2	Same as in REF-B2	Same as in REF-B2

multi-model mean over the historical period indicates a small negative trend in tropical total column ozone, with a rather large model range. This small negative modeled trend is difficult to verify against observations since their length is limited and natural variability is high. Over midlatitudes, the multi-model mean adequately reproduces the negative trends in total column ozone although there is significant model spread.

- *Polar Ozone*. Both models and observations indicate that Antarctic stratospheric ozone loss, together with increasing GHG concentrations, has led to a poleward shift and strengthening of the Southern Hemisphere westerly tropospheric jet during summer. Most CCMs adequately represent lower stratospheric Antarctic vortex isolation, although some have deficiencies with respect to specific chemical or dynamical polar processes. Overall, they tend to reproduce well the Antarctic ozone losses inferred from observations; however it should be noted that many models show a late final warming in the Southern Hemisphere. This will extend chemical ozone loss later into the Antarctic spring. In the Arctic, while a few models represent the chemical ozone loss observed over the past three decades, most underestimate the loss, mainly because they tend not to capture the low temperatures observed in the Arctic lower stratosphere.

The multi-model mean estimates of past ozone changes simulated by CCMs under the REF-B1 scenario are generally consistent with the observed changes (see Chapter 2 of SPARC CCMVal, 2010). Overall, there is sufficient agreement among the CCMs, and between CCMs and observations, on the underlying causes of the ozone changes so that general conclusions can be drawn and some confidence placed in the CCM projections.

3.3.2.2 Analysis Method for Multi-Model Time Series

Chapter 9 of SPARC CCMVal (2010) introduced a time series additive model (TSAM) to analyze the CCMVal-2 multi-model projections. This method is used to calculate baseline-adjusted anomaly time series relative to the values at a particular reference year (here 1960 and 1980) for ozone and other species for each model simulation. The values at the reference year are obtained from a smooth fit to the model time series calculated with the TSAM method. This smooth fit is referred to as the individual model trend estimate. Note that the term "trend" does not denote the result of a linear regression analysis but rather refers to a smooth trajectory passing through the data. The multi-model trend estimate is the average of the individual model trend estimates. By definition, both the individual model trends and the multi-model trends pass through zero at the specified reference year. Two types of uncertainty intervals are constructed. The first is the point-wise 95% confidence interval. This interval has a 95% chance of overlapping the true trend and represents the local uncertainty in the trend at each year. The second interval is the 95% prediction interval which, by construction, is larger than the confidence interval. The 95% prediction interval is a combination of the local uncertainty in the trend and uncertainty due to natural interannual variability about the trend; it gives a sense of where an ozone value for a given year might reasonably lie. Both the confidence and prediction intervals are time varying.

The credibility of simulated ozone projections is linked to a realistic representation of processes that drive stratospheric ozone. Process-based performance metrics have been used to assess the ability of CCMs to reproduce key processes for stratospheric ozone and its impact on climate (SPARC CCMVal, 2010). While it could be preferable to use metric-based weightings when calculating multi-model means, SPARC CCMVal (2010) concluded that more analysis is needed to assess the robustness and interpretation of performance metrics, and their possible use in assigning relative weights to ozone projections. For this reason, and to remain consistent with the multi-model mean time series presented in SPARC CCMVal (2010), the multi-model mean ozone projections from the CCMVal-2 simulations are shown here without applying weights. The robustness of the CCMVal-2 multi-model mean ozone projections and uncertainties is demonstrated by the fact that it is generally insensitive to whether outliers are included or not (Waugh and Eyring, 2008; Chapter 9 of SPARC CCMVal, 2010). Indeed, the multi-model means of total column ozone calculated from simulations of the 4 CCMs selected in Chapter 2 as the highest-scoring models are found to be very close to the multi-model means calculated from all 17 CCMs.

3.3.3 Tropical Ozone

3.3.3.1 Long-Term Projections of Tropical Ozone

The 1960 to 2100 annual mean tropical (25°S–25°N) total column ozone time series are shown in Figure 3-6(a) for the REF-B2 simulations (Table 3-2). The simulated decrease in annual mean total column ozone of 8 DU from 1960 to 2000 is larger than observed. Following the simulated minimum in tropical ozone around 2000, by 2025 about 70% of the ozone lost since 1980 is projected to have been replenished and by 2050 ozone levels are projected to be at or very slightly above 1980 values (see Table 3-3). In the latter half of the 21st century, the annual mean tropical column ozone is projected to decline despite the projected

Table 3-3. Summary of the extent to which total column ozone is projected to have returned to 1960 and 1980 levels from its absolute minimum. A value of 0% denotes that ozone has not increased above the minimum, 50% denotes that ozone at this date is halfway between the simulated minimum and the 1960 or 1980 level, 100% denotes that ozone has returned to the 1960 or 1980 level, and >100% denotes that ozone exceeds the 1960 or 1980 level at this date. The reference year and the total column ozone in that year are listed in the second column. The year in which the minimum ozone occurred and the total column ozone at the minimum are listed in the 3rd column. In each of the cells in subsequent columns, the value obtained from the multi-model trend estimate is listed in boldface on the center line, with the 95% confidence intervals extracted from the TSAM statistics listed on the lines above and below. All ozone values have been rounded to the nearest DU and all percentage values to the nearest 5%.

Region	Reference Year; Total Column Ozone (DU)	Year When Minimum Occurs; Total Column Ozone (DU)	Difference to Reference Year, in 2025		Difference to Reference Year, in 2050		Difference to Reference Year, in 2075		Difference to Reference Year, in 2100	
Unit			(DU)	(%)	(DU)	(%)	(DU)	(%)	(DU)	(%)
Global annual mean	1960 (312 DU)	2001 (296 DU)	−10 **−8** −6	40% **50%** 65%	−2 **−1** 1	90% **95%** 105%	1 **3** 5	105% **115%** 130%	2 **4** 6	115% **125%** 140%
	1980 (306 DU)		−4 **−2** 0	60% **80%** 100%	3 **5** 7	130% **150%** 170%	7 **8** 10	170% **180%** 200%	8 **10** 11	180% **190%** 210%
Tropics annual mean	1960 (272 DU)	2000 (265 DU)	−5 **−4** −3	30% **45%** 55%	−3 **−2** −1	55% **70%** 85%	−4 **−3** −2	45% **60%** 70%	−7 **−6** −4	0% **25%** 45%
	1980 (270 DU)		−3 **−1** 0	40% **70%** 100%	−1 **0** 2	80% **110%** 140%	−2 **−1** 1	60% **90%** 120%	−4 **−3** −2	20% **40%** 60%
Northern midlatitude annual mean	1960 (357 DU)	2000 (344 DU)	−4 **−2** −1	70% **85%** 90%	5 **7** 10	140% **155%** 175%	11 **14** 16	185% **205%** 225%	15 **18** 21	215% **240%** 260%
	1980 (353 DU)		0 **3** 5	100% **130%** 155%	9 **11** 14	200% **230%** 255%	15 **18** 21	265% **300%** 335%	19 **22** 25	310% **355%** 380%
Southern midlatitude annual mean	1960 (349 DU)	2002 (322 DU)	−18 **−15** −12	35% **45%** 55%	−5 **−2** 1	80% **90%** 105%	3 **6** 9	110% **120%** 135%	6 **9** 12	120% **130%** 145%
	1980 (339 DU)		−8 **−5** −2	55% **70%** 90%	5 **7** 11	130% **145%** 165%	13 **16** 19	175% **190%** 210%	16 **19** 22	195% **210%** 230%
Antarctic October mean	1960 (374 DU)	2003 (244 DU)	−100 **−95** −85	20% **30%** 35%	−61 **−53** −44	55% **60%** 65%	−35 **−26** −18	75% **80%** 85%	−18 **−9** 1	85% **95%** 100%
	1980 (322 DU)		−50 **−42** −34	35% **45%** 55%	−10 **−1** 8	85% **100%** 110%	17 **25** 34	120% **130%** 145%	33 **43** 52	140% **155%** 165%
Arctic March mean	1960 (459 DU)	2002 (422 DU)	−19 **−15** −10	50% **60%** 75%	2 **6** 11	105% **115%** 130%	18 **22** 27	150% **160%** 175%	27 **33** 38	175% **190%** 205%
	1980 (445 DU)		−6 **−1** 3	75% **95%** 115%	15 **20** 24	165% **185%** 205%	31 **36** 40	235% **255%** 275%	41 **46** 52	290% **300%** 325%

monotonic decline in 50 hPa tropical Cl_y through the 21st century (Figure 3-6(b)), with 1980 Cl_y values reached around 2040. Over the entire 1960 to 2100 period, secular variations in tropical column ozone are only ~10 DU.

Austin et al. (2010a, see also Chapter 9 of SPARC CCMVal, 2010) compared these future projections with those assessed in WMO (2007) and noted that there was little change, at least up to 2050. However, they found

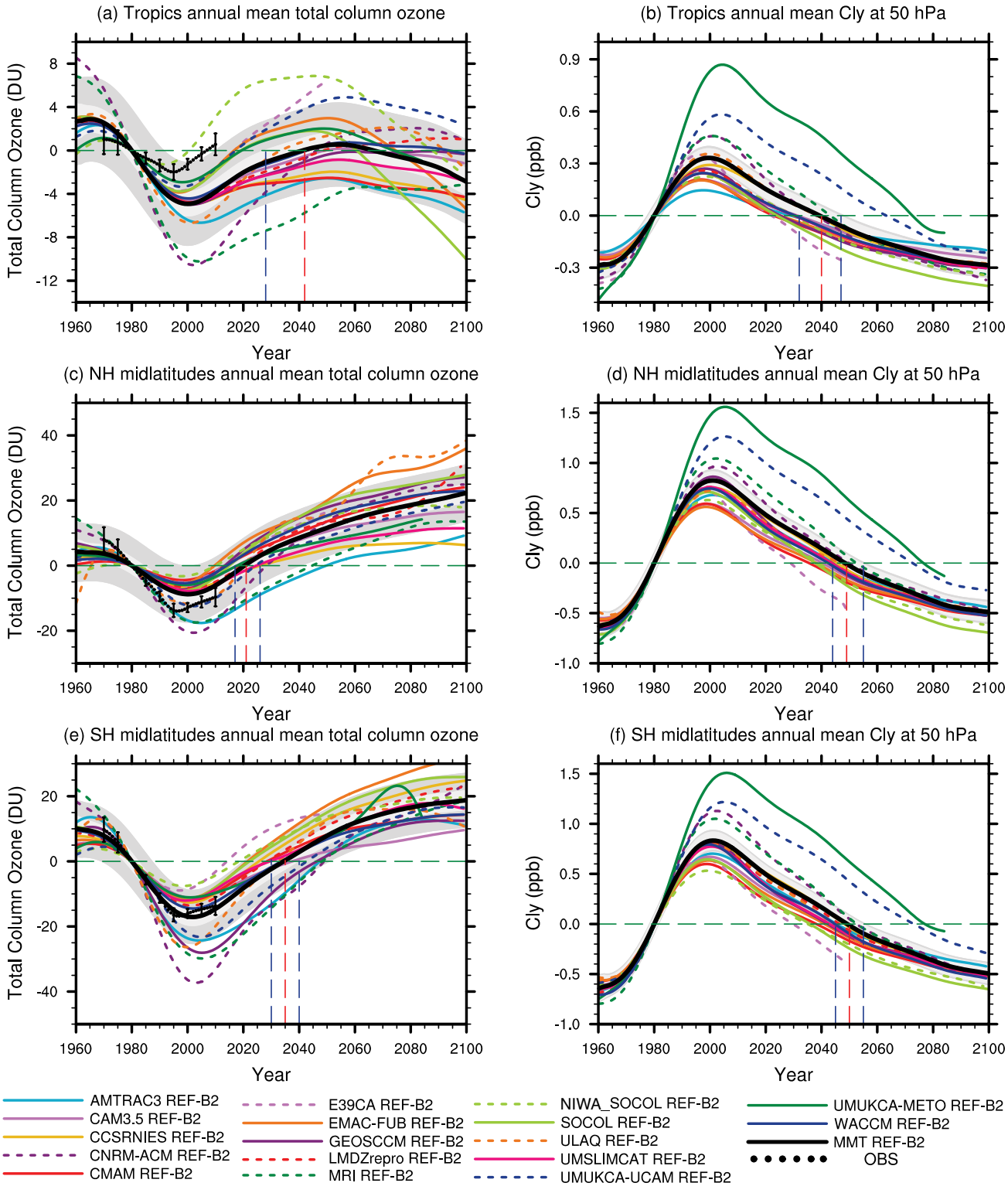

reduced uncertainty in the projections, mainly because of a greater number of simulations covering the whole period from 1960 to 2100. Nonetheless, as with the CCM projections considered in WMO (2007), there was a wide spread among the tropical ozone amounts simulated by the individual models and these extended significantly above and below the observed values. Apart from two models, there were no notable changes in the model total column ozone biases in this region (Chapter 9 of SPARC CCMVal, 2010). WMO (2007) did not report on the projected behavior of tropical total column ozone after 2050, as only one CCM simulated that period (Bodeker and Waugh et al., 2007). On the other hand, the projections from that single model, shown in Figure 6-10 of WMO (2007), do not show the late 21st century decline in total column ozone found in the latest multi-model projections.

Oman et al. (2010) found that using the SRES A2 scenario rather than the SRES A1B in the GEOSCCM significantly increased the abundance of reactive nitrogen and hydrogen in the upper stratosphere. However, any increased chemical ozone destruction from the additional NO_y and HO_x was largely mitigated by the additional GHG cooling in the SRES A2 scenario, which slows gas phase ozone destruction. As a result, the ozone evolution in the upper stratosphere was similar for both scenarios. Results from the CCSRNIES model confirm this finding (Eyring et al., 2010b). In general, Eyring et al. (2010b) found that the projected behavior of tropical total column ozone was not very sensitive to the range of different GHG scenarios (SRES A1B, A2, and B1; RCP 2.6, 4.5 and 8.5; see Section 3.3.1). By 2100 the differences among scenarios was only ~4 DU, which is small compared to the differences found in the extratropics (see Section 3.3.4).

3.3.3.2 Processes Determining Future Tropical Ozone

Chapter 9 of SPARC CCMVal (2010) performed a multiple linear regression on the time series of tropical ozone in the current CCMs and found that between 2000 and 2100 the change in ozone was quite different above and below ~20 hPa (see Figure 3-2(b)). In the upper stratosphere ozone is projected to increase, with the largest increase of around 1.5 ppm occurring near 3 hPa for the multi-model mean. In contrast, lower stratospheric ozone is projected to decrease, consistent with earlier studies (WMO, 2007; Eyring et al., 2007). In both regions the rate of change in ozone is fairly constant through the 21st century (see for example Figure 9.4 of SPARC CCMVal, 2010). The projected increase in upper stratospheric ozone was found to be related mainly to a decrease in halogen concentrations (see Figures 3-2(c) and (d)) and GHG-induced cooling (see Figures 3-2(e) and (f)). These two mechanisms made roughly equal contributions to the ozone increase over the 21st century under the SRES A1B GHG and A1 adjusted halogen scenarios (Chapter 9 of SPARC CCMVal, 2010). In WMO (2007) and in the studies of Shepherd and Jonsson (2008), Jonsson et al. (2009), and Waugh et al. (2009), similar conclusions were reached based on single models. Figure 3-7 shows the results of a regression of global mean ozone concentration onto changes in ODS and CO_2 heating rates in simulations of the CMAM (Jonsson et al., 2009). Note that the change in ozone associated with future changes in GHG amounts is expected to be somewhat larger than that associated with future temperature changes, since some future GHG-induced cooling is balanced by ozone-induced warming (Shepherd and Jonsson, 2008). In the tropical lower stratosphere, the primary mechanism causing long-term changes in ozone is the increase in tropical upwelling through the 21st century, which is a robust feature in the CCM simulations (Chapters

Figure 3-6 (at left). 1980 baseline-adjusted multi-model trend estimates of annually averaged total column ozone (DU; left) and Cl_y at 50 hPa (ppb; right) for the tropics (25°S–25°N, upper row) and midlatitudes (middle row: 35°N–60°N, lower row: 35°S–60°S) (thick dark gray line) with 95% confidence and 95% prediction intervals appearing as light- and dark-gray shaded regions, respectively, about the trend (note the different vertical scale among the panels). The baseline-adjusted individual model trends are also plotted (colored lines). The red vertical dashed line indicates the year when the multi-model trend in total column ozone (left) and Cl_y at 50 hPa (right) returns to 1980 values and the blue vertical dashed lines indicate the uncertainty in these return dates. The black dotted lines in the left panels show observed total column ozone, where a linear least squares regression model was used to remove the effects of the quasi-biennial oscillation, solar cycle, El Niño-Southern Oscillation, and volcanoes from four observational data sets. 2σ uncertainties on the observations were derived by applying the regression model to 10,000 statistically equivalent time series obtained from Monte Carlo resampling of the regression model residuals. The observations include ground-based measurements (updated from Fioletov et al., 2002), merged satellite data (Stolarski and Frith, 2006), the National Institute of Water and Atmospheric Research (NIWA) combined total column ozone database (Bodeker et al., 2005), and Solar Backscatter Ultraviolet (SBUV, SBUV/2) retrievals (updated from Miller et al., 2002). The observational time series is shifted vertically so that it equals 0 in 1980. See Table 3-1 for model descriptions. Redrawn from Figures 9.2, 9.7, 9.8, and 9.9 of SPARC CCMVal (2010) and updated with two new CCM simulations.

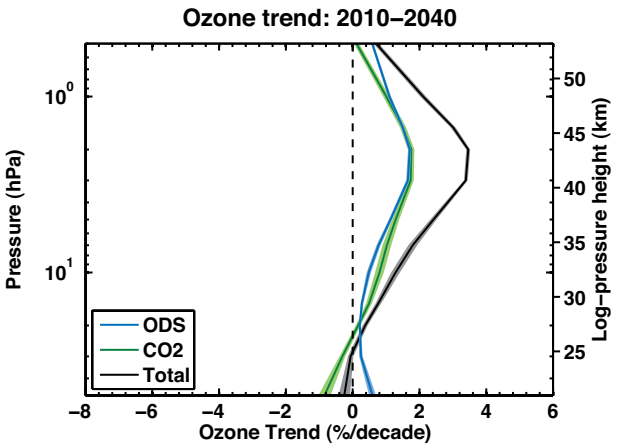

Figure 3-7. Attribution of future (2010–2040) global mean ozone changes over 50–0.5 hPa using simulations from the Canadian Middle Atmosphere Model (CMAM). The simulated ozone mixing ratio trend (%/decade) is shown in black while the contributions from CO_2 and ODSs changes to the ozone trend are shown in green and blue, respectively (note the ODS contribution is estimated from the upper stratospheric Cl_y). The gray shaded areas indicate the 99% confidence intervals for the linear fits to the ensemble average time series. The green and blue shaded regions indicate the uncertainty in the CO_2 and ODS attribution estimates, derived from the 99% confidence intervals for the fitted CO_2, ODS, ozone and temperature linear trends. Adapted from Jonsson et al. (2009).

4 and 9 of SPARC CCMVal 2010; Eyring et al., 2010a). This increase in upwelling in the tropics ultimately leads to a decrease in ozone levels in the tropical lower stratosphere, where ozone levels are mostly determined by a balance between the rate of ozone production and the ascent rate (see Section 3.2.4.1). Because GHG increases are projected to increase ozone in the tropical upper stratosphere, but decrease ozone in the tropical lower stratosphere, if or when ozone returns to historical levels (e.g., to the amounts of ozone observed in 1960 or 1980) will vary between these altitudes (see Section 3.3.6).

The attribution of ozone changes in the tropical upper and lower stratosphere, as well as in the total column, to changes in ODSs and GHGs from four CCMs analyzed by Eyring et al. (2010a) is shown in the correlative time series plots (i.e., plots showing the temporal evolution of the correlation between ozone and ESC) in Figure 3-8. The construction and evaluation methods for this figure and Figure 3-10 are described in Appendix 3A. The reference simulations show ozone decreasing from 1960 to 2000 in the upper stratosphere in response to increasing ESC. However, as ESC decreases from 2000 to 2100 ozone does not simply retrace the 1960 to 2000 path but is systematically elevated through the 21st century such that ozone returns to 1980 values in the late 2020s, well before ESC returns to its 1980 value in the mid-2050s. The elevated ozone through the 21st century results from GHG-induced stratospheric cooling (see Section 3.2.3) indicated by the red to blue transition from 1960 to 2100 in the reference trace in Figure 3-8(a), with a possible contribution from GHG-induced changes in transport. The fixed ODS simulation shows ozone in the upper stratosphere slowly increasing with time under the influence of GHG-induced stratospheric cooling. In contrast to the reference simulation, the fixed GHG simulation shows that the response of ozone to ESC through the 21st century is almost identical to that through the 20th century. In this simulation, because GHGs are fixed, temperatures show almost no

Figure 3-8 (at right). Correlative time series plots for 5 hPa, 50 hPa, and column ozone amounts (parts per million or Dobson units, left axis; ppm or DU change with respect to 1960, right axis) averaged between 25°S and 25°N as extracted from the CCM multi-model trend time series (see Appendix 3A-1). (a) Annual mean tropical ozone as a function of ESC = $Cl_y + 5\times Br_y$ (in parts per billion) at 5 hPa. (b) As in panel (a) but at 50 hPa and with ESC = $Cl_y + 60\times Br_y$. In panels (a) and (b) the REF, fixed ODSs (fODS), and fixed GHGs (fGHG) simulations (see Table 3-2) are shown using traces colored according to the multi-model-mean temperature using the scale shown in the bottom left of each panel. The gray traces in these two panels show the additive effects of the fODS and fGHG simulations calculated from: $Gray_{ESC}(t) = fGHG_{ESC}(t) + fODS_{ESC}(t) - fODS_{ESC}(1960)$ and $Gray_{ozone}(t) = fGHG_{ozone}(t) + fODS_{ozone}(t) - fODS_{ozone}(1960)$. Differences between the gray and REF traces indicate a lack of linear additivity in the system. Panel (c), as in (b) but for total column ozone and without color coding by temperature. In this panel the linear additivity test trace is shown in yellow (yellow = blue + green). In all three panels, on each trace, reference years are shown every 10th data point with year labels shown for the REF and fODS simulations. The multi-model mean is derived from three CCMs in panel (a) (CCSRNIES, CMAM, and MRI) and four CCMs in panel (b) and (c) (CCSRNIES, CMAM, MRI, and WACCM). See Table 3-1 for model descriptions. From Eyring et al. (2010a), their Figure 4.

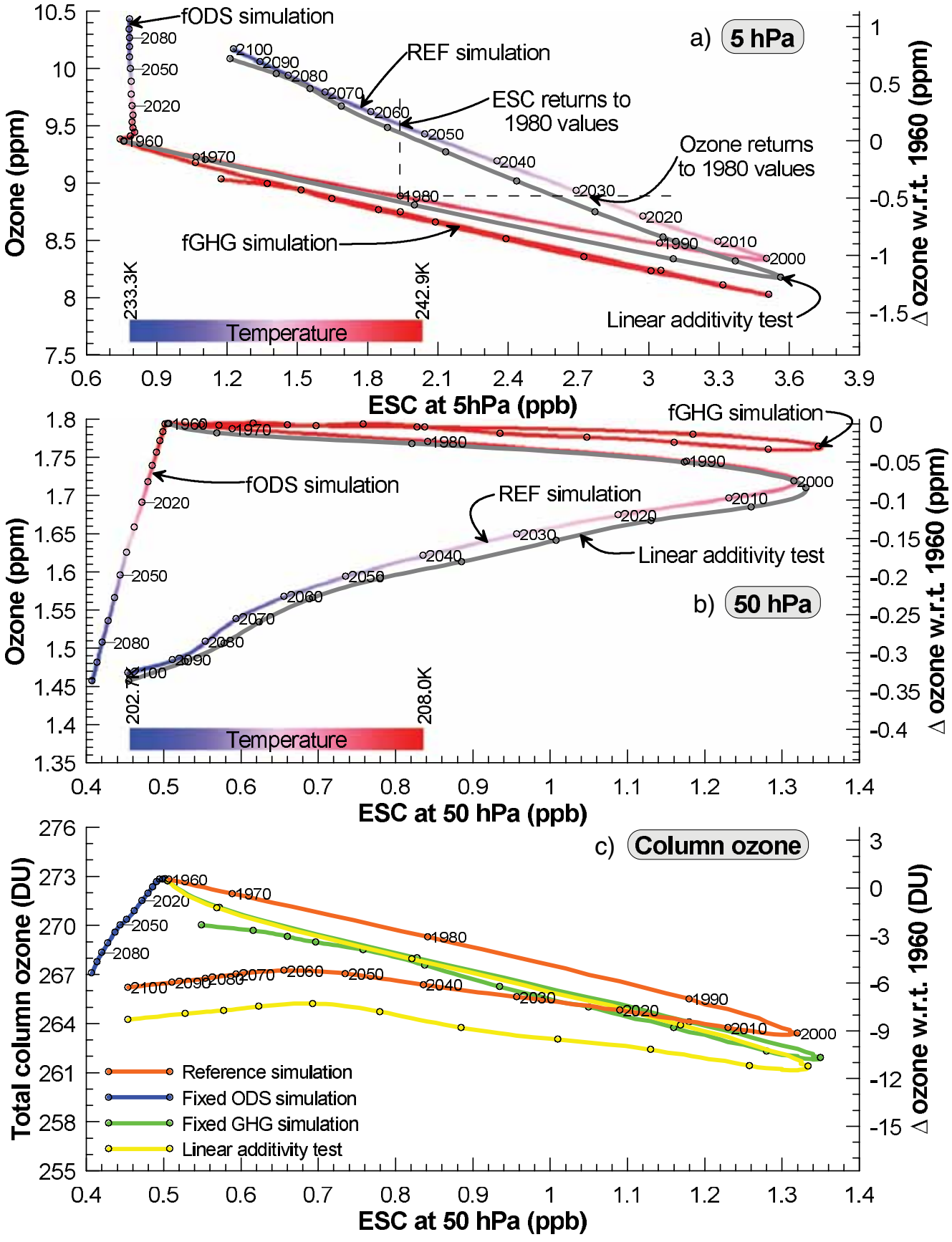
a) 5 hPa
fODS simulation
REF simulation
ESC returns to 1980 values
Ozone returns to 1980 values
fGHG simulation
Linear additivity test
Temperature
233.3K
242.9K
Ozone (ppm)
Δ ozone w.r.t. 1960 (ppm)
ESC at 5hPa (ppb)
b) 50 hPa
fGHG simulation
fODS simulation
REF simulation
Linear additivity test
Temperature
202.7K
208.0K
Ozone (ppm)
Δ ozone w.r.t. 1960 (ppm)
ESC at 50 hPa (ppb)
c) Column ozone
Reference simulation
Fixed ODS simulation
Fixed GHG simulation
Linear additivity test
Total column ozone (DU)
Δ ozone w.r.t. 1960 (DU)
ESC at 50 hPa (ppb)

trend from 1960 to 2100. The close agreement between the REF and gray traces (the sum of the ozone changes due to only the effect of ODSs (fGHG) and due to only the effects of GHGs (fODS)) in Figure 3-8(a) indicates that the system is close to being linearly additive (i.e., the two effects can be considered separately). The system deviates most from linear additivity around the turn of the century when ODS abundances and ozone depletion are close to their maximum. This may result from the fact that the fODS simulations are forced by SSTs taken from coupled climate model simulations where the radiative forcing effects of the varying ODS levels were included. As a result, even though ODS levels are kept fixed at 1960 values in the fODS simulations, the radiative effects of the varying ODSs could be partly felt through the SSTs.

Eyring et al. (2010a) found that in the tropical lower stratosphere (Figure 3-8(b)), ozone shows little response to ESC through the 20th and 21st centuries, as seen from the fGHG trace. The ~25% decrease in ozone from 1960 to 2100 in the reference simulation results from GHG-induced changes to stratospheric dynamics as discussed above and confirmed by the fixed ODS simulation. Note also that in the fixed ODS simulation, ESC decreases with time in response to these circulation changes. As in the upper stratosphere, the response of ozone to ODSs and GHGs is again almost linearly additive as shown by the close agreement between the REF and gray traces in Figure 3-8(b). The ozone decreases simulated in the tropical lower stratosphere dominate the increases in the tropical upper stratosphere such that tropical total column ozone (Figure 3-8(c)) remains suppressed below what would be expected from changes in ESC from 2000 onwards. Interestingly, unlike ozone at 5 and 50 hPa in the tropics, total column ozone shows deviations away from linear additivity demonstrated by the lack of coincidence of the orange and yellow traces in Figure 3-8(c).

3.3.4 Midlatitude Ozone

3.3.4.1 Long-Term Projections of Midlatitude Ozone

Figure 3-6 panels (c) to (f) show projections of 21st century midlatitude (35°N–60°N and 60°S–35°S) column ozone and Cl_y at 50 hPa (Austin et al., 2010a; Eyring et al., 2010a; Chapter 9 of SPARC CCMVal, 2010). The 50 hPa level was chosen as a representative level of future ozone changes in the lower stratosphere in the tropics, midlatitudes, and polar regions (see for example Figure 3-2(b) and Figure 3-9(b)). In the multi-model trend, in both hemispheres, minimum total column ozone is reached around the turn of the century, followed by a steady and significant increase. By 2025, northern (southern) midlatitude total column ozone is projected to have regained 130% (70%) of the amount lost between 1980 and 2000 (2002) and 230% (145%) of this loss regained by 2050 (see Table 3-3). In other words, by 2050, midlatitude total column ozone in both hemispheres is projected to lie above 1980 levels. By 2100, the column ozone in the northern (southern) midlatitudes is projected to have increased by 22 DU (19 DU) compared to 1980 amounts (Table 3-3).

As noted by Austin et al. (2010a), the midlatitude column ozone broadly follows the behavior of Cl_y at 50 hPa (compare left and right panels of Figure 3-6) but with the ozone returning, on average, to 1980 levels 28^{+5}_{-4} and 15 ± 5 years in advance of the chlorine for the northern and southern midlatitudes, respectively. For chlorine, there is, on average, no significant interhemispheric differences in the timing of the return to 1980 levels. Austin et al. (2010a) concluded that the earlier return of ozone to 1980 amounts in the Northern Hemisphere was mainly due to stronger transport from low latitudes, which was also noted in the independent studies of Shepherd (2008) and Li et al. (2009).

3.3.4.2 Processes Determining Future Midlatitude Ozone

Chapter 9 of SPARC CCMVal (2010) found in all simulations analyzed that the increase in the midlatitude total column ozone resulted from ozone increases throughout the stratosphere. The increase in the upper stratosphere peaks in volume mixing ratio at ~3 hPa in both hemispheres (see Figures 3-9(a) and (b)). This in turn was the result of the combined effects of (i) a decline in Cl_y (Figures 3-9(c) and (d); see also Figures 3-6(d) and (f)) and Br_y and, (ii) the GHG-induced cooling of the middle and upper stratosphere (Figures 3-9(e) and (f)). The relative importance of the factors affecting ozone can be different under a different GHG scenario (see Section 3.3.6). In a separate single model study, Waugh et al. (2009) also found that GHG-induced cooling of the middle and upper stratosphere was an important process for midlatitude ozone evolution in the 21st century under the SRES A1B scenario. For the northern midlatitudes, Li et al. (2009) estimated that by the 2060s stratospheric cooling, together with increased poleward transport by the BDC, increased the extratropical column ozone in the model analyzed by Waugh et al. (2009) by up to 6% compared to 1980 amounts. A smaller increase of 3% in the southern midlatitudes resulted from the smaller increase in transport in that hemisphere, consistent with the findings of Austin et al. (2010a). In both hemispheres the largest increase occurred at 60°. Chapter 9 of SPARC CCMVal (2010) found that the projected evolution of midlatitude middle and upper stratospheric ozone was very similar to that in the tropics in terms of the magnitude of the changes (compare Figures 3-2(b) and

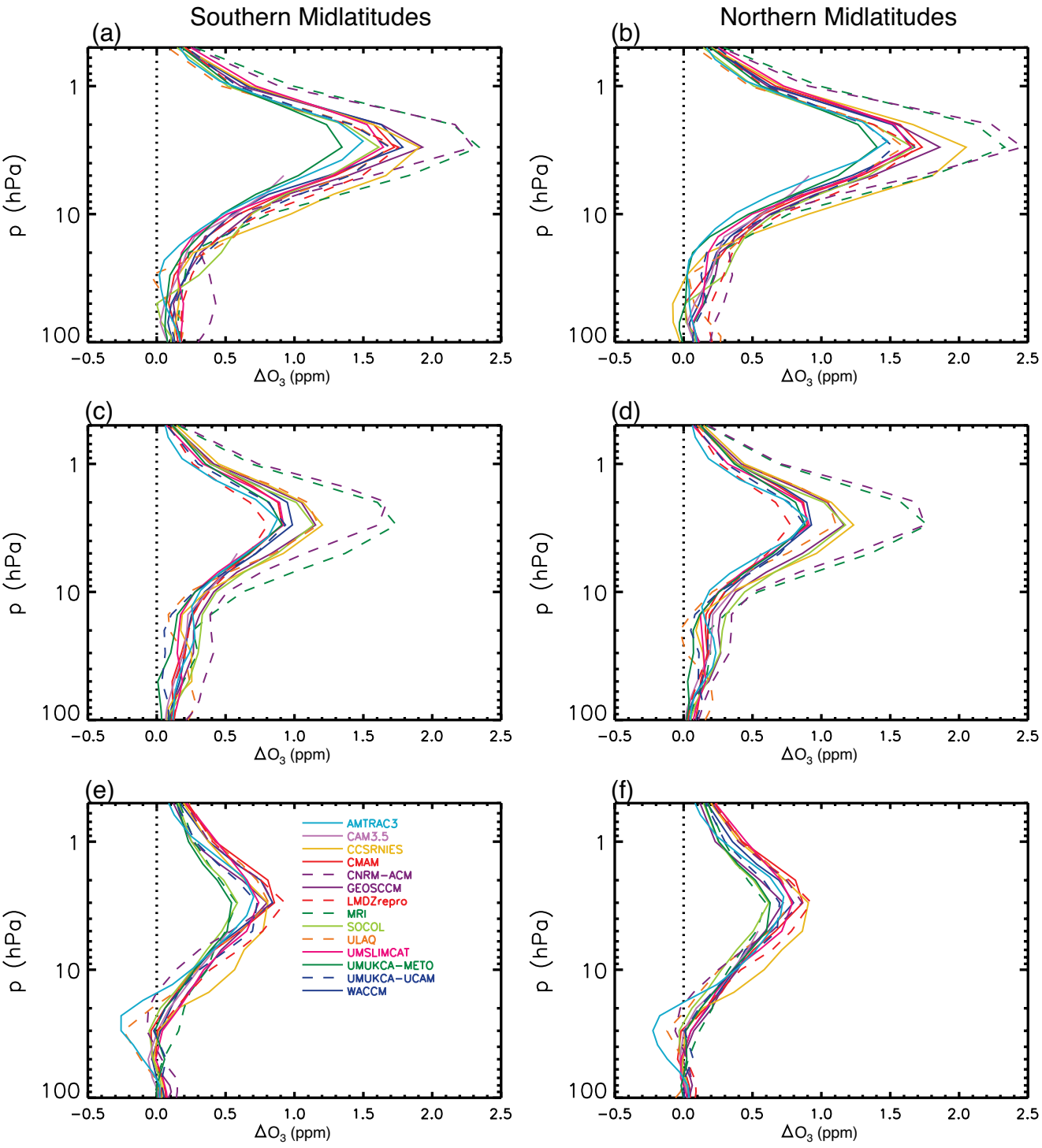

Figure 3-9. Vertical profiles of differences in midlatitude (30°–50°) ozone (parts per million) over the 21st century based on a Multiple Linear Regression (MLR). Leftmost panels are for southern midlatitudes and rightmost panels for northern midlatitudes. (a) and (b) net change in the ozone profile from 2000 to 2100. (c) and (d) ozone changes congruent with changes in ESC. (e) and (f) ozone changes congruent with changes in temperature. See Table 3-1 for model descriptions. From Chapter 9 of SPARC CCMVal (2010), their Figure 9.10 (a)-(f).

3-9). In the lower stratosphere the evolution of midlatitude ozone differed from that in the tropics. However, in midlatitudes the increase in the residual meridional circulation leads to an increase in ozone rather than a decrease (Shepherd, 2008; Li et al., 2009).

An attribution of total column ozone changes in the northern and southern midlatitudes to changes in ODSs and GHGs from five CCMs analyzed by Eyring et al. (2010a) is shown in the correlative time series plot in panels (b) and (c) of Figure 3-10. The reference simulations show that total column ozone decreases from 1960 to 2000, but at a greater rate over southern midlatitudes than over northern midlatitudes. Over northern midlatitudes, ozone shows a −7 DU/ppb sensitivity to ESC over the 1960 to 2000 period, in general agreement with the results reported in Guillas et al. (2004). Over southern midlatitudes the sensitivity is −16 DU/ppb. The heightened sensitivity of total column ozone to ESC in the Southern Hemisphere most likely does not result from differences in the in situ contribution of ESC to southern midlatitude ozone destruction, but rather from the effects of export of ozone-depleted air from the Antarctic ozone hole. Because the multi-model trends shown in Figure 3-10 include fewer models than the multi-model trends displayed elsewhere, the quantitative values listed above are less certain than would be the case otherwise. A comparison of the reference and fixed GHG simulations for the midlatitudes shows that increasing GHGs have elevated ozone throughout the period. In both hemispheres, as ESC decreases, total column ozone does not simply retrace the 1960–2000 path, but shows systematically elevated ozone through the 21st century. As a result, over northern midlatitudes, total column ozone returns to 1980 values in the mid-2020s, well before ESC returns to its 1980 value around 2050. Similarly, over southern midlatitudes total column ozone returns to 1980 values in the mid-2030s (a decade later than in the northern midlatitudes), and well before ESC returns to its 1980 value around 2050. From the fixed ODS simulation (blue traces in Figure 3-10), it is clear that the elevated ozone through the 21st century results from GHG-induced stratospheric cooling and changes in transport, in particular changes in the strength of the BDC (see Figure 3-3). These simulations also show ESC decreasing with time even though ODSs are fixed at 1960 values. This likely results from the increasing strength of the BDC through the 21st century (Section 3.2.4.1) and a resultant decrease in the time available to photolyze ODSs. It is also clear from the reference and fixed ODS simulation traces in Figure 3-10 that by 2100, total column ozone over midlatitudes is still influenced by ESC. In both the northern and southern midlatitudes the effects of ODSs and GHGs on ozone are approximately additive (agreement of black and yellow traces in Figures 3-10(b) and (c)) in the multi-model trend.

3.3.5 Polar Ozone

3.3.5.1 Long-Term Projections of Polar Ozone

The largest ozone depletion seen in CCM simulations based on the SRES A1B GHG and A1 adjusted halogen scenarios occurs in the polar lower stratosphere, especially over Antarctica where large modeled ozone losses give rise to a springtime Antarctic ozone hole, consistent with observations. As a result, a major focus is the projected evolution of polar lower stratospheric ozone during spring.

Figure 3-11 shows the evolution of the individual model and multi-model trend estimates of total column ozone (left panels) and lower stratospheric inorganic chlorine (Cl_y) (right panels), for March in the Arctic (60°N–90°N) and October in the Antarctic (60°S–90°S) from the 17 CCMs analyzed by Eyring et al. (2010a). In both polar regions, the long-term evolution of total column ozone is qualitatively the same as in other regions. There is a broad minimum around 2000 followed by a slow increase until the end of the 21st century. There are, however, as in the extrapolar regions, significant quantitative differences among the models, including a wide spread in minimum values over Antarctica around 2000. Austin et al. (2010a) and Chapter 9 of SPARC CCMVal (2010) indicate that the spread between the individual model simulations of Antarctic total column ozone increased from CCMVal-1 to CCMVal-2, while no change was seen for the Arctic. However, when adjusting the raw data to a common 1980 baseline by removing the individual offset values with the TSAM method (Section 3.3.2.2), the model spread is considerably reduced.

In the Antarctic, the strongest ozone depletion in the October mean multi-model trend is simulated in 2003 (see Table 3-3). The minimum in the October multi-model trend total column ozone is about 80 DU lower than the 1980 value. For the Arctic, the largest total column ozone depletion simulated in March 2002 is ~30% of the Antarctic depletion simulated in October 2003 (Figure 3-11, left panels). Arctic spring ozone returns earlier to historical values than Antarctic spring ozone. Arctic total column ozone is projected to regain 95% (75–115%)[1] of the amount lost between 1980 and 2002 by 2025. Arctic column ozone is simulated to increase to 46 DU above 1980 values by the end of the 21st century, which is equivalent to an increase in column ozone of twice the amount lost between 1980 and 2002 (see Table 3-3). In Antarctica, 45% (35–55%) of the ozone lost since 1980 is projected to be replenished by 2025, and 100% (85–110%) by 2050. By the end of the 21st century, Antarctic October ozone

[1] All quoted ranges are 95% confidence intervals.

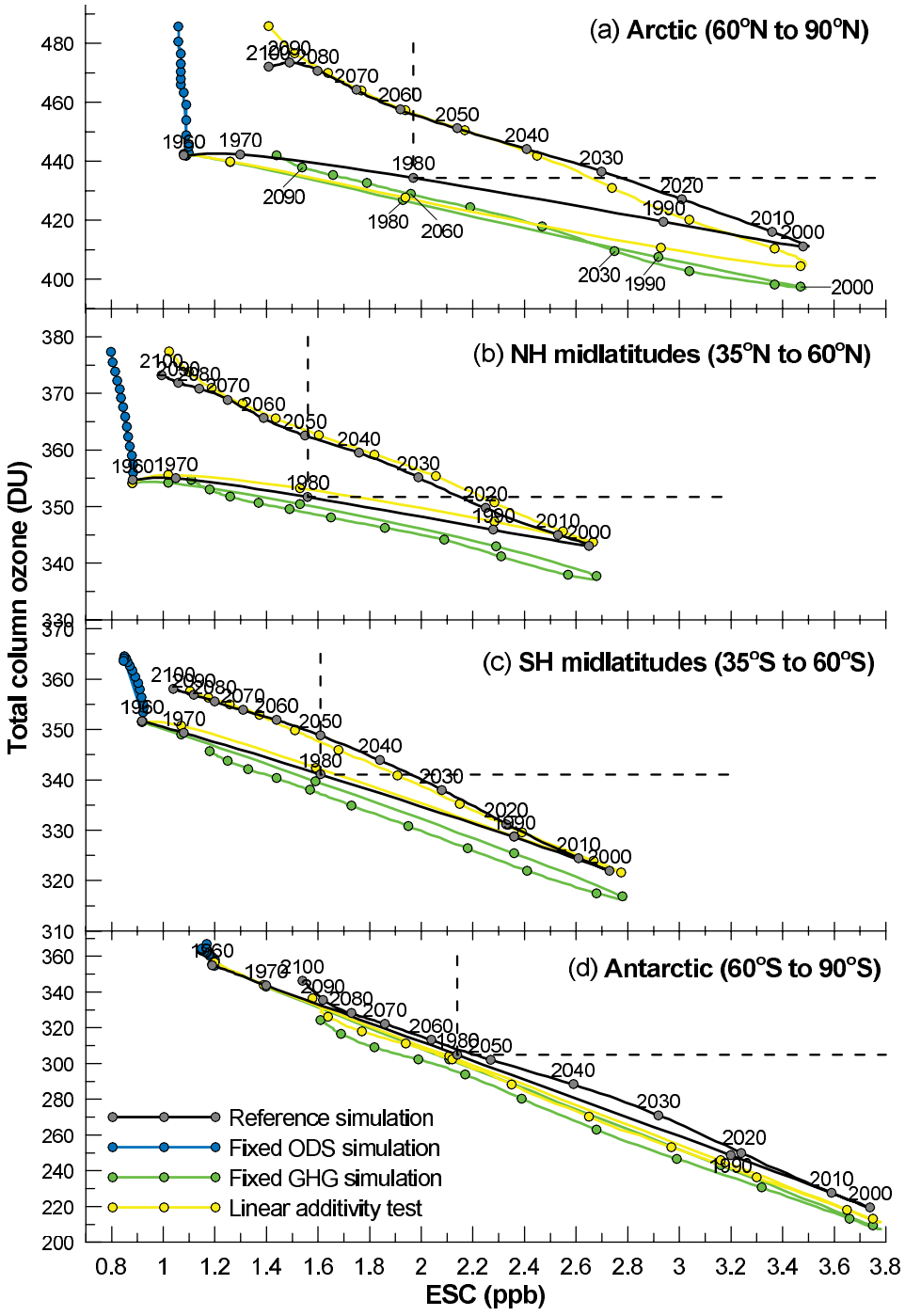

Figure 3-10. Correlative time series plots for total column ozone (Dobson units) averaged over different latitude ranges (Appendix 3A). (a) March means for the Arctic, (b) annual means for northern midlatitudes, (c) annual means for southern midlatitudes, and (d) October means for the Antarctic. ESC values are defined as ESC = $Cl_y + 60 \times Br_y$ at 50 hPa. The black trace shows the reference simulation with time-varying GHGs and ODSs with reference years shown every 10th data point. The blue trace shows results from a simulation where prescribed ODSs are fixed at 1960 values. The green trace shows results from a simulation where prescribed GHGs are fixed at 1960 values. The yellow traces show the additive effects of the fixed ODS and fixed GHG simulations (yellow = blue + green) as in Figure 3-8. Differences between the black and yellow traces indicate a lack of linear additivity in the system. The multi-model trend estimate is derived from five CCMs (CCSRNIES, CMAM, MRI, ULAQ, and WACCM; see Table 3-1). From Eyring et al. (2010a), their Figure 7.

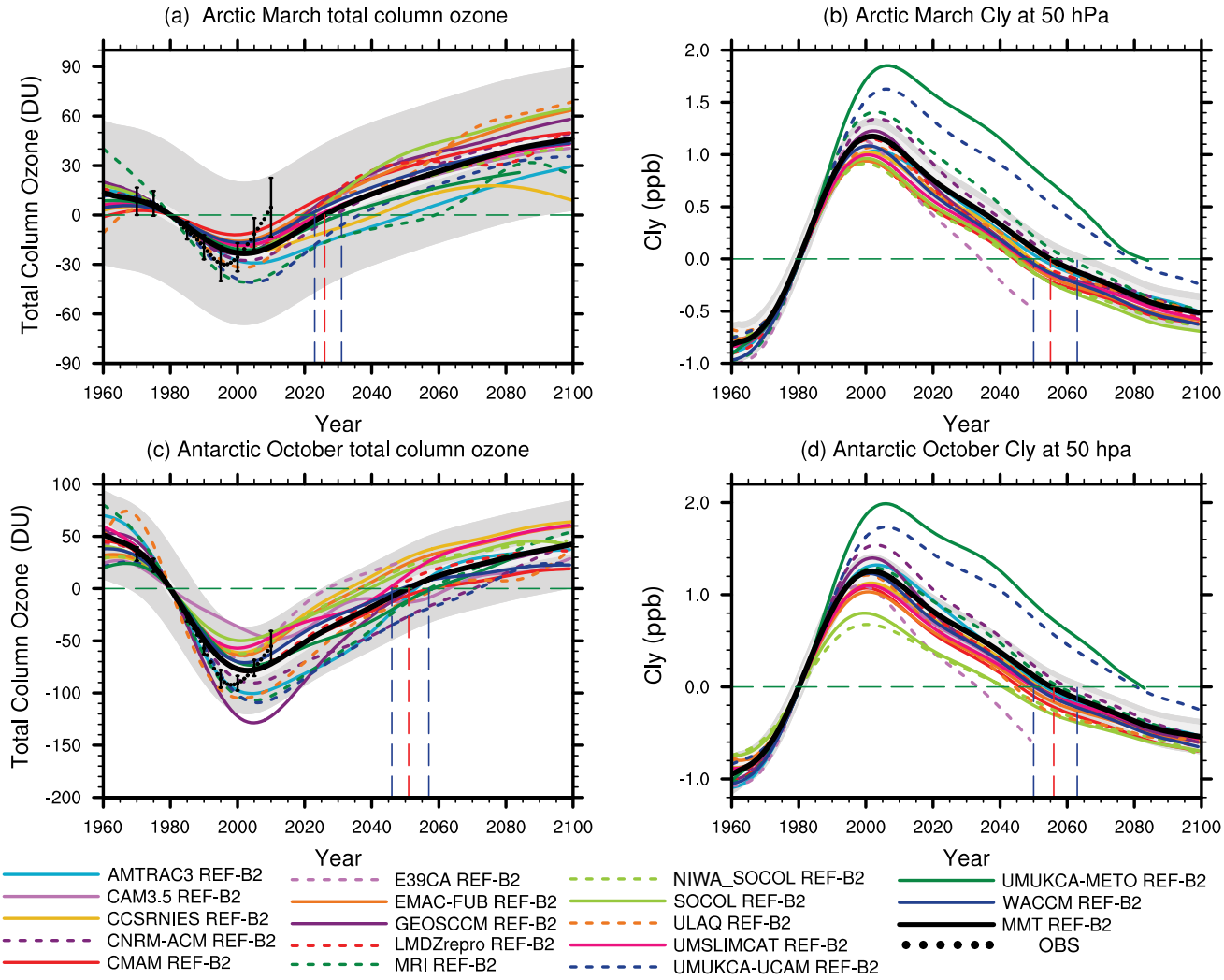

Figure 3-11. As in Figure 3-6, but for the latitude range 60°N–90°N in March (upper row) and the latitude range 60°S–90°S in October (lower row). The red vertical dashed line indicates the year when multi-model trend in total column ozone (DU; left) and Cl_y at 50 hPa (ppb; right) returns to 1980 values and the blue vertical dashed lines indicate the uncertainty in these return dates. Note the different vertical scale among the panels. Redrawn from Figures 9.11, 9.12, 9.13, and 9.14 of SPARC CCMVal (2010) and updated with two new CCM simulations.

is projected to be 43 DU above 1980 levels (compare to 78 DU decrease from 1980 to 2003). However, by 2100, October mean ozone is still projected to be 9 DU lower than in 1960 (95% of the 1960–2003 loss replenished) consistent with slightly enhanced ESC in 2100 compared to 1960.

Several different indices have been defined and applied in previous assessments to quantify variations in Antarctic ozone, in terms of the area of the ozone hole, the polar cap average ozone, the ozone mass deficit (Bodeker et al., 2005), or the daily minimum total column ozone in spring (WMO, 2007). Figure 3-12 (upper panel) shows the simulated and observed ozone hole areas, based on the size of the area with column ozone less than 220 DU, from 17 CCMVal-2 simulations (Austin et al., 2010b; Chapter 9 of SPARC CCMVal, 2010). While a few models capture the observed size of the Antarctic ozone hole reasonably well, the models on average underestimate the observed ozone hole area by about 20% (Austin et al., 2010b). This value is similar to that found for the CCMVal-1 simulations (Eyring et al., 2006). It reveals that, although some of the CCMs have been improved since CCMVal-1, others have become worse, and no fundamental improvement was achieved for the majority of the models. The projected date when the Antarctic ozone hole will disappear varies from the 2020s in models with small ozone holes to

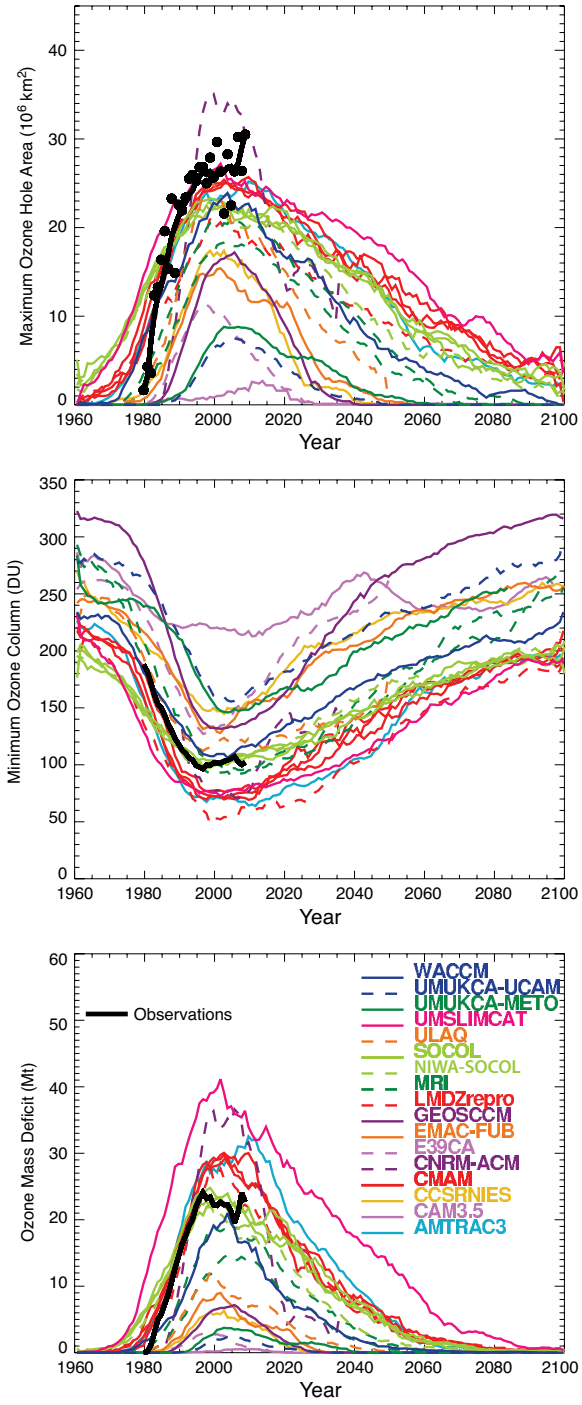

Figure 3-12. Simulated and observed ozone hole areas, based on a fixed 220 DU amount (upper panel), minimum Antarctic spring total ozone column (middle panel), and ozone mass deficit (lower panel) for the period 1960–2100, calculated from the CCMVal-2 REF-B2 simulations. The curves indicate 11-year running means of the data for individual years. See Table 3-1 for model descriptions. From Austin et al. (2010b), their Figures 4(a), 6, and 9.

the end of the simulation period in 2100 for those models that agree best with the observed ozone hole areas in the past. Even with some outliers removed, Antarctic spring ozone depletion below 220 DU is projected to still occur in a broad range between 2060 to 2100, or later. As discussed in Austin et al. (2010b), the representation of the ozone hole area in individual models depends on the definition used. For example, the use of an ozone isoline to define the ozone hole area (e.g., the 220 DU contour) in models that have a high or low ozone bias results in ozone hole areas that are systematically low or high, respectively, even if the models have realistic interannual and long-term variations. Calculating total column ozone changes relative to the 1960–1965 ozone mean leads to an improvement of the simulated ozone hole area in some models. These models have a general high ozone bias. Other models perform better when the steepest ozone gradient is used to define the edge of the ozone hole. This diagnostic identified some models where the simulated Antarctic polar vortices are too small in area compared to observations, which would also limit the size of their ozone holes (Bodeker et al., 2002). In general, most consistent results among the models are achieved when the steepest gradients are used. However, independent of the applied index for the ozone hole area, most CCMs have ozone holes that are significantly smaller than observed, by up to 30%. With the large spread between the individual CCM simulations of the Antarctic ozone hole and its likely dependence on the applied definition for the ozone hole, quantitative projections of the disappearance of the ozone hole remain uncertain.

The minimum spring ozone, calculated from Antarctic daily mean ozone from September to November (Figure 3-12, middle panel), shows a wide range of ozone values, from one model that does not fall below the 220 DU ozone hole threshold value to models with lower than observed ozone minima. Most models simulate the lowest ozone minima for the most recent years and suggest an increase of minimum ozone starting around 2010, which agrees well with projections in WMO (2007). Only models with a high ozone bias exceed the 220 DU limit by the end of the 21st century, while models that represent well or underestimate past ozone compared to observations, do not predict a return to minimum ozone values above 220 DU before 2100.

The ozone mass deficit, defined as the mass of ozone required to elevate column ozone everywhere over Antarctica to 220 DU, averaged over the months of September and October (Bodeker et al., 2005) (Figure 3-12, lower panel) is a sensitive diagnostic as it reflects how well the CCMs simulate the ozone hole area and the minimum ozone. Austin et al. (2010b) show that models that capture the observed size of the ozone hole area typically simulate lower than observed Antarctic ozone spring

minima, in contrast to models with smaller ozone holes that typically show higher than observed Antarctic ozone spring minima. Both errors contribute to a large spread in the ozone mass deficit of the models for the past and future. The models suggest that the ozone mass deficit should not increase any longer after about 2010; however, due to the sensitivity of this diagnostic, future projection of the ozone mass deficit is highly unreliable.

3.3.5.2 Processes Determining Future Polar Ozone

In both hemispheres, multi-model total column ozone in polar spring follows the evolution of Cl_y (Figure 3-11). Ozone starts to increase in the first decade of the 21st century at about the same time as the Cl_y abundances in the polar lower stratosphere have reached their maximum and begin to decline. Compared to CCMVal-1, the simulation of Cl_y, on average, has improved in the CCMVal-2 models due to improvements in individual CCMs (Austin et al., 2010a; Austin et al., 2010b; Chapter 9 of SPARC CCMVal, 2010); however, differences in Cl_y of up to 1 ppb in the polar lower stratosphere in October remain. These Cl_y differences, together with differences in the dynamical processes determining the strength of the stratospheric polar vortices and temperatures, cause the spread in simulated polar ozone.

The Cl_y concentrations in Figure 3-11 return to historical levels almost simultaneously in both hemispheres, while the ozone return dates show interhemispheric differences of more than two decades. As expected from the discussion in Section 3.2, this result implies that processes other than halogen chemistry affect the future evolution of polar ozone and that the relative impact of these processes varies with location. The relative contributions of ESC or increasing GHGs to the projected ozone change can be estimated by comparing the reference simulation with sensitivity simulations that use prescribed fixed historical abundances of GHGs or ODSs (Eyring et al., 2008). Waugh et al. (2009) compare a "climate change" simulation (i.e., using fixed ODS abundances for 1960) of the GEOSCCM with a reference simulation that accounts for GHG and ODS changes from 1960 to 2100. They find that in much of the stratosphere, the annual mean GHG-induced ozone increase from 1960–2100 is comparable to the ODS-induced ozone decrease for the period with highest ODS concentration (1995–2005). However, ozone in the Antarctic lower stratosphere is clearly dominated by ODS-induced destruction, and increases in GHG concentrations do not have a significant impact on Antarctic polar temperatures or ozone in their CCM. It should be noted that most studies of Antarctic ozone recovery focus on changes in October means. The effects of an extended polar vortex persistence, due to future GHG-induced cooling and an associated seasonal delay of ozone recovery to November, on UV exposure has not been thoroughly assessed in multi-model studies.

Eyring et al. (2010a) found similar results in a multi-model framework using additional CCMVal-2 sensitivity simulations. As illustrated in Figure 3-10(d), reference simulations in the Antarctic show multi-model total column ozone decreasing from 1960 to 2000 with an average 53 DU/ppb sensitivity to ESC, leading to a 38% decrease in total column ozone over this period. Unlike the midlatitudes and Arctic, the total column ozone evolution over Antarctica in October shows almost no sensitivity to changes in GHGs, with the return path (21st century) closely tracking the outbound path (20th century). This is corroborated by the fixed ODS simulation, which shows almost no change in Antarctic ozone in October in response to increasing GHGs. If anything, increasing GHGs have slightly elevated Antarctic total column ozone in the model simulations. This updates earlier studies that predicted that increasing radiative cooling generated by increasing levels of GHGs or by GHG-induced stratospheric water vapor enhancements would worsen polar ozone depletion by increasing the likelihood for PSC formation, and might even create an ozone hole in the Arctic (Austin et al., 1992; Shindell et al., 1998; Kirk-Davidoff et al., 1999; Waibel et al., 1999). More recent research suggests that in the Arctic, GHG-induced changes in dynamics are expected to dominate the effects of GHG-induced radiative cooling on the formation of PSCs (Eyring et al., 2010a). In comparison, in the Antarctic, where the wintertime polar temperatures typically fall below the threshold for PSC formation, stratospheric cooling due to increasing GHGs does not strongly enhance October total column ozone depletion.

The multi-model trend of the reference simulations in the Arctic (Figure 3-10(a)) shows total column ozone decreasing from 1960 to 2000 with a −14 DU/ppb sensitivity to ESC, somewhat smaller than the −20 DU/ppb reported in observations (Dhomse et al., 2006). The increase in ESC from 1.1 ppb in 1960 to 3.5 ppb in 2000 leads to a 7.4% decrease in total column ozone over this period. In contrast to the Antarctic, total column ozone over the Arctic is elevated above what would be expected from changes in ESC. This most likely does not result from the effects of GHG-induced upper stratospheric cooling as in the tropics (Figure 3-8(a)) since, as discussed in Butchart et al. (2010), in the models the extra radiative cooling from increasing GHGs is approximately balanced by a concomitant increase in the adiabatic warming through increased polar downwelling. The net effect is a near-zero temperature trend in the Arctic winter lower stratosphere (Butchart et al., 2010; Figure 4.4 of SPARC CCMVal, 2010). The more likely cause is the strengthening of the BDC (Section 3.2.4.1), which more effectively advects ozone into

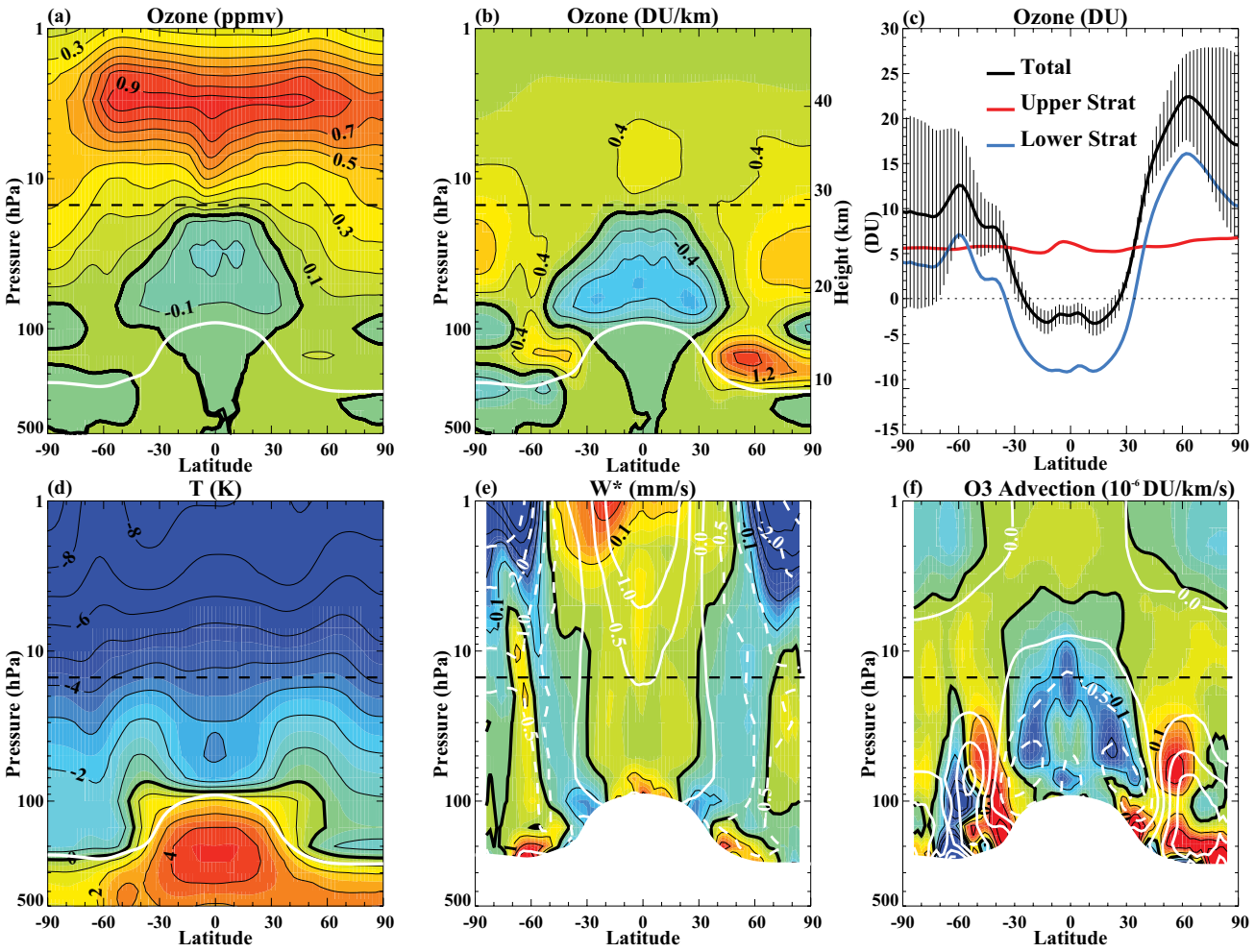

Figure 3-13. Annual mean, decadal differences between 2060–2069 and 1975–1984 from a simulation of the GEOS CCM with ODSs fixed at 1960 values. (a) Ozone concentrations in ppm, (b) ozone concentrations in DU/km, (c) total column ozone (DU) and contributions from the upper (above 15 hPa) and lower (below 15 hPa) stratosphere, (d) temperature (K) (e) Vertical residual velocity $\bar{w}^*$ in mm/s, and (f) mean ozone advection (10^{-6} DU/km/s). From Li et al. (2009), their Figure 2.

the Arctic than the Antarctic stratosphere (Austin and Wilson, 2006; Shepherd, 2008). The effects of ODSs and GHGs on Arctic total column ozone appear to be largely independent and therefore add linearly as evidenced by the close agreement of the black and yellow traces in Figure 3-10(a).

Li et al. (2009) analyzed in more detail the effects of climate change on annual mean ozone by comparing the post-CFC era (2060–2069) with the period 1975–1984 in two simulations with the GEOS CCM. They found a uniform increase in ozone mixing ratio in the upper stratosphere (Figure 3-13(a)) that they ascribe to a slowing of photochemical ozone loss rates due to GHG-induced cooling (Figure 3-13(d)). However, the simulated changes in ozone column and their latitudinal structure are controlled by changes in the lower stratosphere, where significant increases of column ozone are simulated at middle and high latitudes, specifically in the Northern Hemisphere (Figures 3-13(b) and (c)). They are associated with an acceleration of the Brewer-Dobson circulation in the model with increased tropical upwelling and extratropical downwelling (Figure 3-13(e)), leading to enhanced advective transport of ozone (Figure 3-13(f)). Although, in the annual mean, these dynamical effects are stronger at midlatitudes than at polar latitudes, the Li et al. (2009) study demonstrates that changes in ozone abundance and the mean advective transport have a qualitatively similar pattern in the lower stratosphere, and emphasizes the important role of changes in the mean advection for lower stratospheric ozone changes.

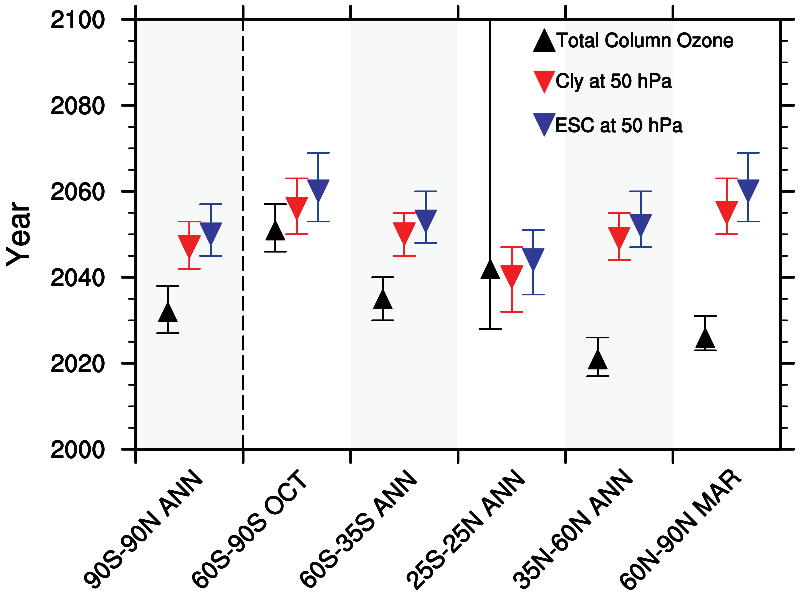

Figure 3-14. Date of return to 1980 total column ozone (black triangle and error bar), Cl_y at 50 hPa (red triangle and error bar), and ESC at 50 hPa (blue triangle and error bar) for the annual average (global, tropical, and midlatitude) and spring (polar) total ozone column derived from the multi-model trend of the CCMVal-2 reference simulations (17 CCMs) in each latitude band. The error bars on the multi-model trend estimate of return date are derived from the 95% confidence intervals. ESC is calculated as $Cl_y + 60 \times Br_y$ except for E39CA where Cl_y instead of ESC was used. While a few models project a return of tropical total column ozone to 1980 levels, most do not with the result that the 95% confidence interval extends from 2030 to beyond the end of the century which explains the large error bar in the tropical column ozone return dates. Redrawn from Figures 9.20 and 9.21 of SPARC CCMVal (2010) and updated with two new CCM simulations (from Eyring et al. (2010a), their Figure 10b).

3.3.6 Ozone Return Dates and Ozone Recovery

In this section, ozone return dates to levels typical of 1960 and 1980, derived from the CCM projections, are presented. These are complemented by quantitative statements about the expected date for full recovery of ozone from the effects of ODSs based on CCM simulations as described in Box 3-2. Specifically, a set of reference simulations and a set of fixed ODS simulations (as described in Section 3.3.1) are analyzed for the future date when the two sets of ozone projections are no longer statistically distinguishable within internal and inter-model variability (Eyring et al., 2010a). A Student *t*-test is applied to quantify the likelihood that, at some specified date, the ozone values taken from the two sets of simulations come from the same statistical population. The outcome of such tests is discussed using the terminology of the IPCC (see Box TS.1 of Solomon et al., 2007). For example a *t*-test result of >95% suggests that it is "extremely likely" that, within model variability, full ozone recovery from the effects of ODSs is projected to have occurred, if >90% it is "very likely" while if >66% it is "likely" that it is projected to have occurred. For values between 33% and 66% probability, it is "about as likely as not" and for values <33% it is "unlikely" that full recovery of ozone is projected to have occurred.

The response to the question of when stratospheric ozone will return to undisturbed levels depends on the selected target year. Figure 3-14 and Table 3-4 summarize 1960 and 1980 return dates of total column ozone in different latitude zones derived from the multi-model trend. Return dates generally occur later when referenced to 1960 and later at higher latitudes (Chapter 9 of SPARC CCMVal, 2010). However the increase is not symmetric about the equator, i.e., return dates are later in the Antarctic than in the Arctic.

CCM projections suggest that it is as likely as not that tropical total column ozone will return to 1980 values, since there is no consensus among the CCMs on a return to 1980 values by the end of the century (Austin et al., 2010a; Eyring et al., 2010a; Chapter 9 of SPARC CCMVal, 2010). Correspondingly, the uncertainty on tropical column ozone return dates derived from the 95% TSAM confidence interval extends from 2030 to beyond the end of the century in Figure 3-14. However, if instead of a return to 1980 values, a return to 1960 values is considered, models consistently predict that tropical total column ozone remains below values typical of 1960 due to the increase in tropical upwelling. In contrast, Cl_y and ESC (Table 3-5) in the tropics return to 1980 values faster than in all other regions with only minor differences between them. Full recovery of tropical column ozone from the effects of ODSs is not reached at the 95% confidence level by the end of the 21st century, while it is likely at the 65% level that total column ozone has fully recovered by ~2070 in the tropics (see Figure 3-15). In the tropical upper stratosphere, although ozone is influenced by ODSs throughout the 21st century, ozone returns to 1980 values

Table 3-4. Date of return to 1960 and 1980 total column ozone calculated from the multi-model trend estimate of the 17 CCMs' reference simulations.

Region	Date of Return	Year When Multi-Model Mean Total Column Ozone Returns	Year When Lower Bound of Error Bar Returns	Year When Upper Bound of Error Bar Returns
Global annual mean	1960	2053	2046	2064
	1980	2032	2027	2038
Tropics annual mean	1960	----	----	----
	1980	2042	2028	----
Northern midlatitude annual mean	1960	2029	2024	2036
	1980	2021	2017	2026
Southern midlatitude annual mean	1960	2055	2049	2064
	1980	2035	2030	2040
Antarctic October mean	1960	----	2100	---
	1980	2051	2046	2057
Arctic March mean	1960	2041	2036	2048
	1980	2026	2023	2031

in the late 2020s (Figure 3-8(a)), which is earlier than in other regions. Although ozone decreases continuously from 1960 to 2100 in the tropical lower stratosphere, together with the Arctic lower stratosphere, they are the only regions where ozone has very likely (i.e., more than 90% confidence level) fully recovered from the effects of ODSs by the end of the 21st century (Eyring et al., 2010a). However, in percentage terms, changes to the tropical ozone column over the 21st century are much smaller than those in other regions.

Of the five regions considered (see Table 3-4), total column ozone returns to 1980 values earliest over northern midlatitudes, around 2021 (2017–2026). While the total column ozone evolution is qualitatively similar

Table 3-5. Date of return to 1960 and 1980 ESC at 50 hPa calculated from the multi-model trend estimate of the 17 CCMs' reference simulations.

Region	Date of Return	Year When Multi-Model Mean ESC Returns	Year When Lower Bound of Error Bar Returns	Year When Upper Bound of Error Bar Returns
Global annual mean	1960	---	2092	---
	1980	2050	2045	2057
Tropics annual mean	1960	2087	2073	---
	1980	2044	2036	2051
Northern midlatitude annual mean	1960	---	---	---
	1980	2052	2047	2060
Southern midlatitude annual mean	1960	---	---	---
	1980	2053	2048	2060
Antarctic October mean	1960	---	---	---
	1980	2060	2053	2069
Arctic March mean	1960	---	---	---
	1980	2060	2053	2069

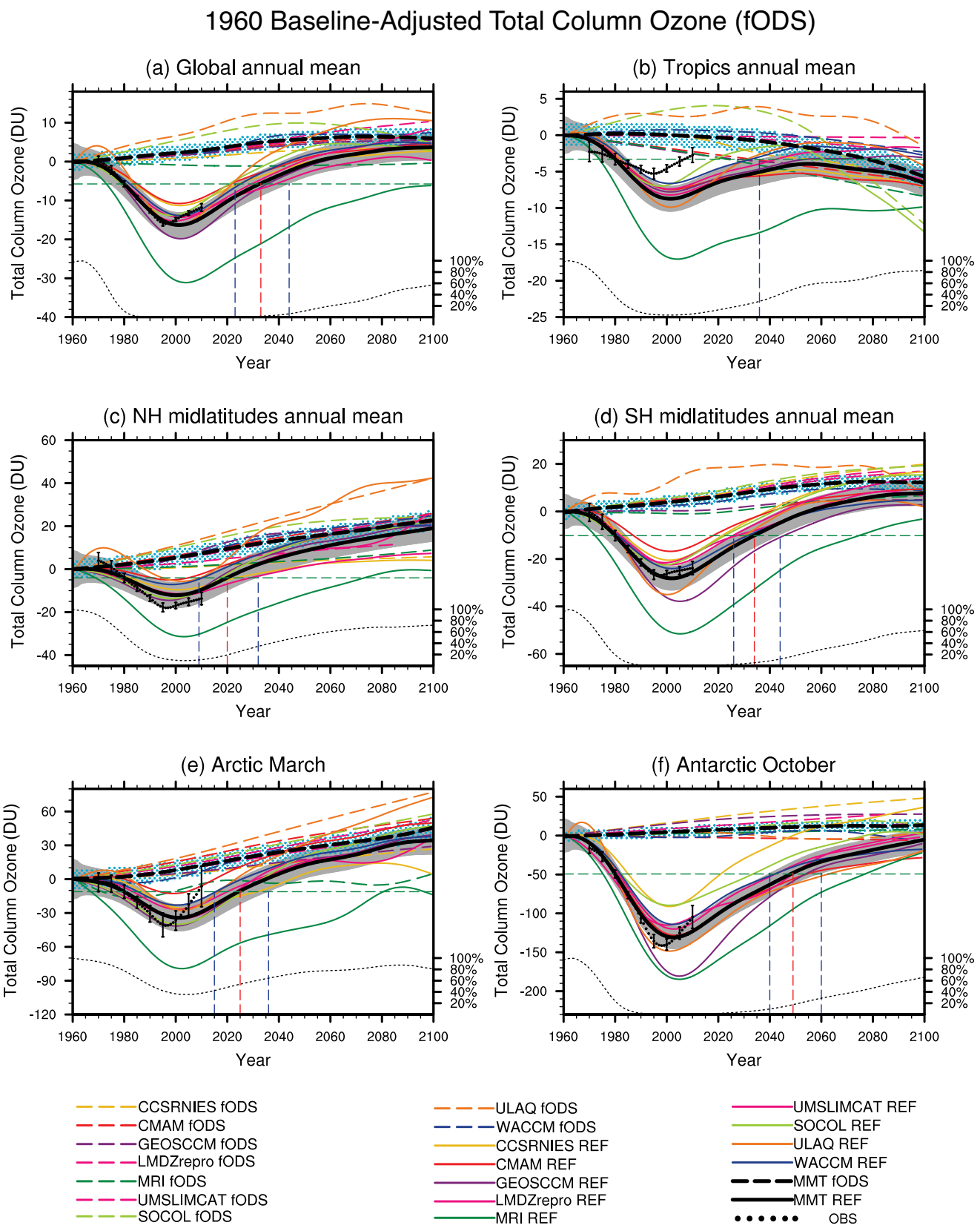
1960 Baseline-Adjusted Total Column Ozone (fODS)
(a) Global annual mean
(b) Tropics annual mean
(c) NH midlatitudes annual mean
(d) SH midlatitudes annual mean
(e) Arctic March
(f) Antarctic October
Total Column Ozone (DU)
Year
100%
80%
60%
40%
20%
CCSRNIES fODS
CMAM fODS
GEOSCCM fODS
LMDZrepro fODS
MRI fODS
UMSLIMCAT fODS
SOCOL fODS
ULAQ fODS
WACCM fODS
CCSRNIES REF
CMAM REF
GEOSCCM REF
LMDZrepro REF
MRI REF
UMSLIMCAT REF
SOCOL REF
ULAQ REF
WACCM REF
MMT fODS
MMT REF
OBS

over the midlatitudes of both hemispheres in the CCMs, southern midlatitude total column ozone returns to 1980 values later than over northern midlatitudes, i.e., around 2035 (2030–2040) (see Figure 3-14). The difference in the date of return to 1980 values appears to be due to interhemispheric differences in changes in transport. The increase in stratospheric circulation transports more ozone into the northern midlatitude lower stratosphere than into the southern midlatitudes (Shepherd, 2008). In addition, over southern midlatitudes, ozone is also influenced by ozone loss in the Antarctic, where the return to 1980 levels occurs much later. In all CCMs the return of ozone to 1980 values in the midlatitudes occurs 10 to 30 years earlier than that of Cl_y and ESC (around 2050 in both hemispheres). Nonetheless, by 2100 total column ozone over midlatitudes is still influenced by ODSs. Full recovery of total column ozone from ODSs has likely occurred in northern midlatitudes but not likely to have occurred over southern midlatitudes (Figure 3-15).

The Antarctic spring total column ozone evolution is dominated by the evolution of ODSs. Therefore, ozone, Cl_y, and ESC return dates are very similar in most models (Figure 3-14). The latest return of total column ozone to 1980 values is projected to occur over Antarctica which, for October means, occurs around 2051 (2046–2057), while 1960 values are not reached again before 2100 since Cl_y remains elevated above 1960 levels in 2100 (Figure 3-11(d)). In the Arctic, the sensitivity of the return date to the chosen baseline year (1960 or 1980) is small, with a return to 1980 ozone values around 2026 (2023–2031), and to 1960 values around 2041 (2036–2048). In contrast to the Antarctic, Arctic spring ozone returns earlier to 1980 values than Arctic chlorine, indicating that other effects such as changes in transport are more important for future ozone in the Arctic as is the case for northern midlatitudes (Section 3.3.4.2). A return of stratospheric chlorine to the low values of 1960 does not happen in the polar regions before the end of the 21st century. It is unlikely that full ozone recovery from ODSs will be reached by the end of the 21st century over Antarctica, while it is likely that it will occur in the Arctic by ~2035 (Waugh et al., 2009; Eyring et al., 2010a) (see also Figure 3-15).

Global total column ozone is projected to return to its 1980 value around 2032 (2027–2038), which is 15 years earlier than when global Cl_y at 50 hPa returns to its 1980 value and 18 years earlier than when global ESC returns to its 1980 value. CCM projections suggest that this early return is primarily a result of GHG-induced cooling of the upper stratosphere, because the effects of circulation changes on tropical and extratropical ozone largely cancel in the global mean. Figure 3-16 summarizes return dates as a function of latitude for annual mean total column ozone to a value appropriate to reference years between 1965 and 2000 (Austin et al., 2010a; Chapter 9 of SPARC CCMVal, 2010). The figure shows results for the partial ozone column above 20 hPa (upper panel), the partial column between 500 and 20 hPa (middle panel) and for the combined column above 500 hPa. Tropospheric ozone below 500 hPa is excluded. Above 20 hPa, where changes in halogens and temperature dominate the ozone evolution, the return of ozone to historical levels is projected to occur steadily. In the lower stratosphere (Figure 3-16, middle panel) a return date could not be determined for the tropics due to the strengthening BDC which systematically decreases tropical ozone as the simulations proceed (Waugh et al., 2009). The results also show a strong hemispheric asymmetry, with Antarctic ozone returning to historical levels much later than Arctic ozone. Again, this is largely due to the increased BDC, which for the models, on average, has much more influence in the Northern Hemisphere

Figure 3-15 (at left). 1960 baseline-adjusted total column ozone projections in the reference simulations (thick black solid line) compared to the fixed halogen simulation (fODS, thick black dashed line): (a) global (90°S–90°N annual mean), (b) tropics (25°S–25°N annual mean), (c) northern midlatitudes (35°N–60°N annual mean), (d) southern midlatitudes (35°S–60°S annual mean), (e) Arctic (60°N–90°N March mean), and (f) Antarctic (60°S–90°S October mean). The colored lines show individual models for the subset that submitted fODS (see Table 3-1 for model descriptions). The horizontal green line shows the level of the multi-model trend estimate in 1980. The red vertical dashed line indicates the year when the multi-model trend estimate in the reference simulation returns to 1980 values and the blue vertical dashed lines indicate the uncertainty in these return dates. The black solid circles with vertical bars show the observations and their 2σ errors processed as in Figures 3-6 and 3-11. Nine CCMs are included in the multi-model mean (CCSRNIES, CMAM, GEOSCCM, LMDZrepro, MRI, SOCOL, UMSLIMCAT, ULAQ, and WACCM). In all regions except the tropics, the milestone of full ozone recovery occurs significantly later than when ozone returns to its 1980 values. The milestone of full ozone recovery is derived from the period when the fixed halogen simulation is not statistically distinguishable from the reference simulation (black dotted line in the bottom of each panel plotted against the percentage scale at the bottom right). For clarity, only the 95% confidence intervals are shown. Adapted from Eyring et al. (2010a), their Figure SM12.

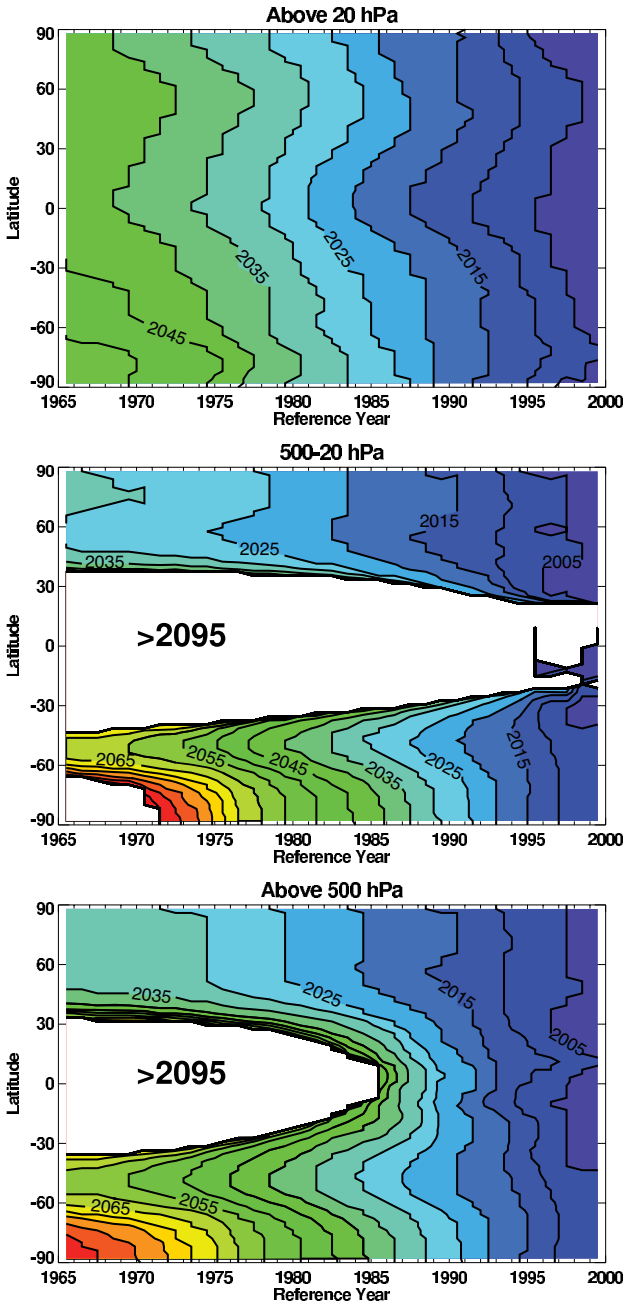

Figure 3-16. Date of return of the annual mean column ozone to the value appropriate to the reference year indicated on the abscissa. The mean model result was smoothed with an 11-year running mean filter. Contour interval is 5 years; red values indicate later dates and blue values indicate earlier dates. Data prior to 1965 (which limits the definition of the reference year data) or after 2094 (which limits the data for the return year) do not exist because of the need for an accurate time-smoothed field. The white region in the figure indicates where the mean model ozone has not recovered by the end of the simulations (nominally 2094). Results are shown for the total column above 500 hPa (bottom panel), for the range 500–20 hPa (middle panel), and for the column above 20 hPa (top panel). From Chapter 9 of SPARC CCMVal (2010), their Figure 9.25.

than in the Southern Hemisphere (Austin and Wilson, 2006; Shepherd, 2008). The combination of the lower and upper stratospheric columns (Figure 3-16, lower panel) shows that in the tropics the total ozone column increases until about 2050 due to decreasing halogen amounts and stratospheric cooling, but thereafter ozone decreases due to the increasing BDC and does not return to pre-1985 values before the end of the simulations.

The ozone return dates discussed above apply to a single GHG scenario, the SRES A1B scenario. However, this scenario represents only one plausible future and it is therefore important to also assess the ozone return dates under different GHG evolutions. Ideally, all models that performed the reference simulations would have also performed all sensitivity simulations. However, the various GHG scenarios were only performed by a small subset of models (see GHG-x simulations in Table 3-1). Differences in stratospheric column ozone among six GHG scenarios (SRES A1B, A2, and B1; RCP 2.6, 4.5, and 8.5; see also Section 3.3.1) assessed from four CCMs by Eyring et al. (2010b) are found to be largest over northern midlatitudes and in the Arctic with divergence mainly in the second half of the 21st century. In the midlatitudes, the return of stratospheric column ozone to 1980 values varies by up to 10 years among the GHG scenarios, while in polar regions differences of 15–20 years are found. Overall, the differences of ozone return dates among the GHG scenarios simulated by the four individual models is of the same order as the uncertainty in ozone return dates derived from the multi-model mean of the 17 CCMs in Eyring et al. (2010a) in the midlatitudes, while it is smaller in the tropics and larger in the Arctic and Antarctic. The results suggest that effects of GHG emissions on future stratospheric ozone should be considered in climate change mitigation policy, and ozone projections should be assessed under more than a single GHG scenario. However, more CCMs will need to perform the GHG sensitivity simulations to arrive at more robust conclusions. Furthermore, to assess full recovery of ozone from ODSs under different GHG scenarios, simulations with fixed ODSs under each scenario would be required.

3.3.7 Uncertainties in Model Projections and Open Questions

3.3.7.1 Uncertainty in Future Emissions Scenarios

Uncertainty in projections of stratospheric ozone can usefully be broken into four sources (Charlton-Perez et al. (2010) using an approach based on Hawkins and Sutton (2009)): (a) internal variability of the chemistry-climate system, (b) model uncertainty due to differences in the design and parameters of CCMs and missing or poorly represented processes in CCMs, (c) uncertainty in future emissions scenarios for GHGs, and (d) uncertainty in future emissions scenarios for ODSs, which is likely smaller than (a) to (c).

Figure 3-17 shows estimates of uncertainty in each of the three uncertainty components (a)–(c) for CCMVal-2 projections of total column ozone in six geographical regions of the globe. Note that the GHG scenario uncertainty was estimated using only a small subset of models. In total, four runs of three CCMs forced with SRES GHG scenarios (solid green lines) and three runs of a single CCM forced with RCP GHG scenarios (dashed green lines) provide the estimates shown (see Charlton-Perez et al. (2010) for more details).

In either case, it is clear that, for most geographical regions, model uncertainty is the dominant contributor to the total uncertainty in projections of future ozone column amount at least up to the mean estimate of ozone return to 1980 values. In the tropical band, internal variability is comparable in size to scenario uncertainty, but in other regions internal variability is generally a small contributor to total uncertainty in future ozone column amount. Charlton-Perez et al. (2010) therefore suggest that continued investment and development of CCMs could lead to a refinement of ozone projections for the period up to and including ozone return to 1980 values, assuming that CCM developments lead to a reduction in model uncertainty.

There remain other uncertainties associated with ozone prediction that are difficult to quantify, particularly the mean biases present in the ozone climatology of many of the CCMs (see Chapter 9 of SPARC CCMVal, 2010) and missing or poorly represented processes in the entire ensemble of CCMVal models (for example the quasi-biennial oscillation). The effects of solar variability were not considered in the CCM simulations assessed in this chapter. No CCM studies have yet assessed the effects of a long-term sustained change in solar output, such as the Maunder minimum, on stratospheric ozone. Other uncertainties, related to major changes in future human behavior

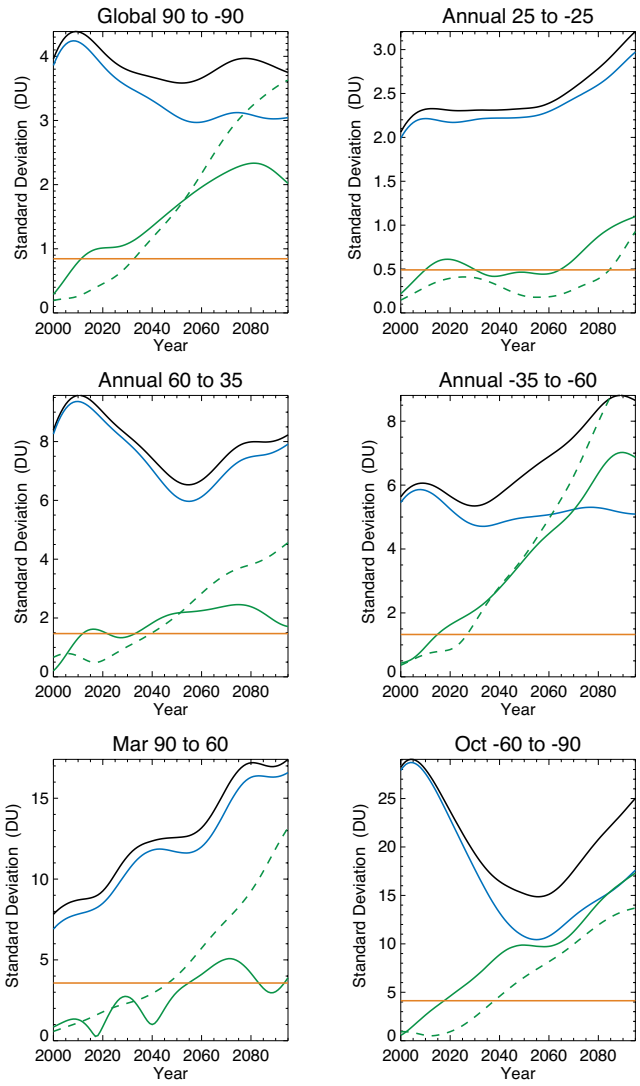

Figure 3-17. Uncertainty in the predicted total-column decadal-mean ozone amounts relative to 1980 values estimated for different geographic regions. Uncertainty is expressed as the one standard deviation estimate for internal variability (orange), model uncertainty (blue), and the total uncertainty (black) all shown in solid lines. Solid green lines show an estimate of the one standard deviation estimate for scenario uncertainty calculated from integrations of CCSRNIES, GEOSCCM, and WACCM forced with alternative SRES greenhouse gas scenarios. Dashed green lines show an alternative estimate of scenario uncertainty calculated using integrations of the CAM3.5 model forced with alternative RCP greenhouse gas scenarios. Total uncertainty estimates are derived from the SRES scenario integrations only. From Charlton-Perez et al. (2010), their Figure 3.

that are not considered in the scenarios used in this chapter, are discussed in Chapter 5 (Section 5.4) and include geoengineering of the climate system, increases in N_2O emissions from automotive biofuels, and enhanced emissions from aviation and rockets.

3.3.7.2 Future CCM Development

Following this Assessment, CCMs are likely to undergo significant further development that could have impacts on their projections of future ozone and could either increase or decrease the spread between models. The executive summary of SPARC CCMVal (2010) recommends that "Development should continue toward comprehensive troposphere-stratosphere CCMs, which include an interactive ocean, tropospheric chemistry, a naturally occurring QBO, spectrally resolved solar irradiance, and a fully resolved stratosphere." The impact of some of these processes on ozone projections was partially assessed in multiple CCMs by CCMVal.

Other than in CMAM, sea surface temperatures and sea ice concentrations were prescribed in all other CCM simulations used in this chapter. Important couplings between the atmosphere, the oceans, and the cryosphere are currently not represented in CCMs. Inclusion of these couplings in the CCMs will lead to a more complete representation of the climate system and climate feedbacks, which could be important for simulations of stratospheric ozone and its impact on tropospheric climate. Several recent studies have shown that changes in global mean climate will have a significant, regionally dependent influence on future ozone concentrations and the correspondence between the return of ozone to pre-1960 or 1980 levels and the return of ESC amounts to pre-1960 or 1980 levels (Waugh et al., 2009; Shepherd and Jonsson, 2008). The impact of coupling CCMs to interactive ocean models remains to be assessed since the number of CCMs able to perform this coupling remains small.

Future assessments should also consider brominated very short-lived species (VSLS, see Section 3.2.1), as well as the uncertainty in how the organic halogen lower boundary condition is prescribed in CCMs. Currently, projections of future organic halogen loadings are based on projected emission rates and an estimate of the global atmospheric lifetime of each organic halogen. These factors are used to create time-dependent volume mixing ratio lower boundary conditions that are then used to force the CCMs. However, the destruction of each halogen in the CCMs is dependent on the tropical upwelling and meridional mixing (both linked to the strength and structure of the BDC), and chemical loss rates (e.g., photolysis rates). The CCM-derived halogen lifetimes can be very different from the lifetimes assumed for the given projection scenario. Some studies (Douglass et al., 2008) suggest that the use of fixed mixing ratio lower boundary conditions provides an artificial constraint on model-derived ozone return dates. Furthermore, multi-model studies are necessary to fully evaluate the impact of ODS flux boundary conditions on ozone projections.

3.4 PROJECTIONS OF UV CHANGES RELATED TO OZONE CHANGES THROUGH THE 21ST CENTURY

Future changes in stratospheric ozone will cause changes of opposite sign in solar UV radiation received at the surface. However, UV radiation is also affected by a number of other factors (see Section 3.2.8), which are likely to change in the future. In this section only changes due to ozone are addressed. Simulations of future UV are based on ozone projections by CCMs, which take into account the effects of climate change on ozone (see Section 3.3). The effect of changes in ozone on erythemal irradiance can be quantified either with empirical relationships, such as the radiation amplification factor (RAF) concept (Booth and Madronich, 1994; Madronich, 2007), or, more accurately, with radiative transfer models.

3.4.1 Midlatitude and Tropical UV

Calculations with a radiative transfer model were used by Tourpali et al. (2009) to simulate the noontime erythemal solar irradiance received at the Earth's surface under cloud-free conditions. These simulations were based only on total ozone columns, and vertical profiles of ozone and temperature, derived from 11 CCMs (CCMVal-1 models) simulating the evolution of stratospheric ozone (Eyring et al., 2006; Eyring et al., 2007). Following a peak between the late 1990s and early 2000s, erythemal irradiance was projected to decrease at all latitudes and in all seasons during the 21st century. Since erythemal irradiance changes were mostly driven by changes in total ozone, they tended to follow the pattern of the stratospheric ozone changes. The weakest changes, of the order of a few percent, were found in the tropics. At midlatitudes, the decreases ranged from 5–15% between 2000 and 2100, while at southern high latitudes the decrease was a factor two stronger because of the projected recovery of Antarctic ozone layer there.

A follow-up study (Kazantzidis et al., 2010) provided quantitative estimates for the effect of the projected ozone changes on different biological weightings of UV irradiance (doses), such as DNA damage and vitamin D production, which have different sensitivities to ozone changes. For example, in some cases, changes in doses relevant to DNA damage can exceed those for erythema by a factor of two.

Ozone recovery will be affected by climate change (see also Section 3.2) and this will in turn affect the levels of UV radiation at the surface. Hegglin and Shepherd (2009) reported that the effects of a strengthened BDC on stratospheric ozone, which they entirely attributed to changes in GHG concentrations (assuming that the effect of ODSs on ozone were negligible in 1965 and 2095 in their simulations), would result in decreases in erythemal irradiance from 1965 to 2095 by about 9% at northern high latitudes. This change was found to be about three times larger than the change attributed to stratospheric ozone recovery from ODSs only, as estimated from the change in erythemal irradiance from 1965 to 2000.

More robust ozone projections can improve the accuracy of the estimated changes in surface UV irradiance. A new subset of simulations from 15 CCMs has become recently available through the CCMVal-2 activity of SPARC (see SPARC CCMVal (2010) and Section 3.3), and are used to repeat the erythemal irradiance calculations reported by Tourpali et al. (2009). More realistic and spatially varying climatological values for aerosols (Kinne et al., 2006) and surface reflectivity (Herman et al., 2001) are prescribed in the present calculations. Although cloud and aerosol fields are expected to change in the future (IPCC, 2007), they are kept constant here. For the period covered by the CCM simulations (1965–2100) and over a global grid of 10° × 15° respectively, solar UV irradiance spectra (280–400 nm) at the surface are calculated with the radiative transfer model package libRadtran (Mayer and Kylling, 2005) for the 15th of each month.

These new simulations, shown in Figure 3-18, result in lower inter-model spread compared to the results of Tourpali et al. (2009), allowing a more robust estimation of the dates when erythemal irradiance is projected to return to 1980 values. At midlatitudes, erythemal irradiance is projected to decrease for all models throughout the 21st century. The return of the multi-model mean to

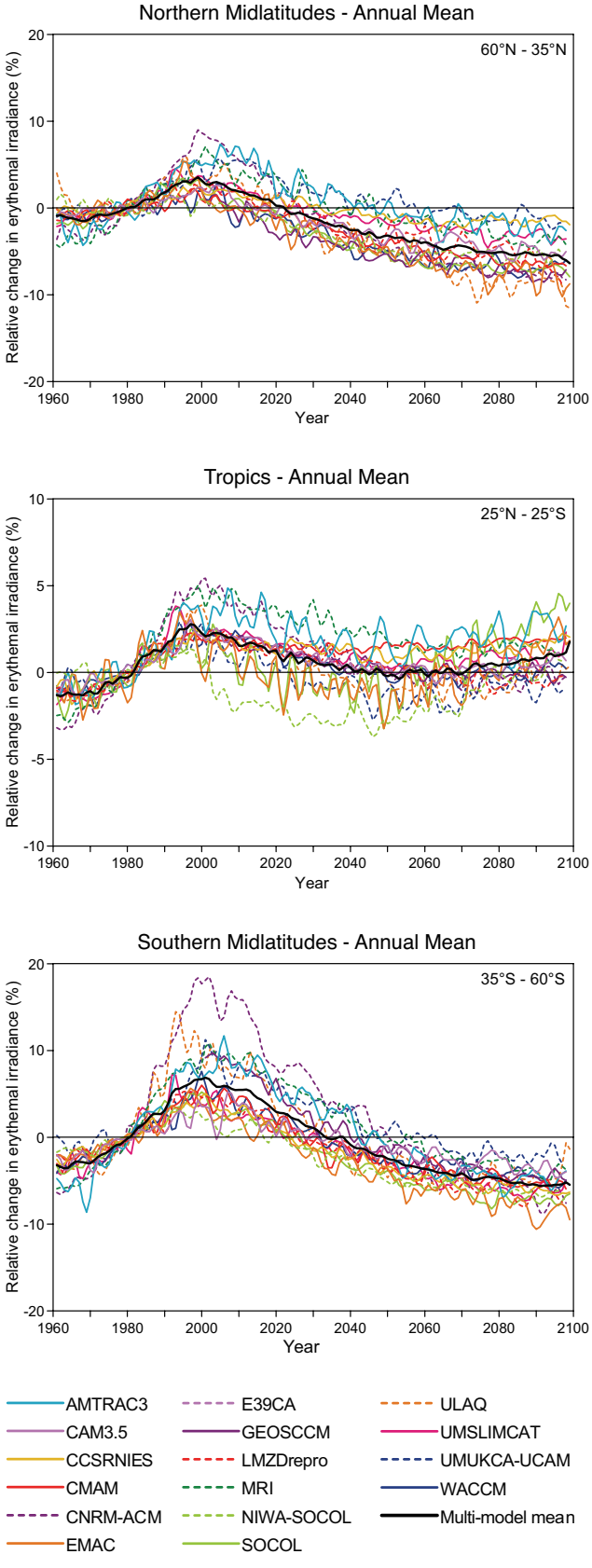

Figure 3-18. Annual means of surface erythemal irradiance changes (in %, relative to 1975–1985) under cloud-free conditions for three latitude belts representative for Northern Hemisphere midlatitudes (upper panel), tropics (middle panel), and Southern Hemisphere midlatitudes (lower panel), calculated with a radiative transfer model using projections of ozone and temperature from 15 CCMs. See Table 3-1 for model descriptions. For the models providing multiple runs, the average change of irradiance is shown. The black thick line represents the multi-model mean. All lines have been smoothed with a 1:2:1 filter. Note the different scale for the tropical belt. Updated from Tourpali et al. (2009) using projections from 15 CCMVal-2 models.

1980 values is projected to occur in 2023 for the Northern Hemisphere and in 2035 for the Southern Hemisphere; for individual models, the return date ranges from 2016 to 2055 and from 2038 to 2055, respectively. The large range on the erythemal irradiance return date reflects the large inter-model differences in total column ozone used as inputs in the surface UV calculations. The projected increases in column ozone above its levels in 1980 after the mid-21st century, especially in the Northern Hemisphere, result in decreases in erythemal irradiance of up to 5% below its levels in 1980 (Figure 3-18, upper panel), with important implications for ecosystems at high latitudes (UNEP, 2010). For example, such decreases may contribute to further deficiency in the vitamin D levels of humans (Edvardsen et al., 2007; Kazantzidis et al., 2009; Kimlin et al., 2007; Webb and Engelsen, 2006), unless other factors, such as a possible decrease in cloudiness, would counteract these changes. In the event of increasing cloudiness due to climate change, or increasing aerosol load (likely over inhabited areas), the adverse effects concerning vitamin D production would be even larger.

The simulations for the tropics (Figure 3-18, middle panel) show a steady increase in surface erythemal irradiance up to the late 1990s and then a slow decrease until ~2050, when it reaches a minimum that is still higher than 1980 levels for most models. Thereafter, surface UV is projected to slowly increase toward the end of the 21st century, in response to the projected decreases in tropical column ozone due to the acceleration of the BDC. The tropical changes are small (at most 5% with respect to 1980 values) in comparison to the changes projected for the higher latitudes. This temporal behavior of tropical erythemal irradiance is common to most models and agrees with the simple estimates of Hegglin and Shepherd (2009). UV-B radiation in the tropics is high due to naturally occurring low total ozone columns and high solar elevation angles. Assuming no variations from other factors, if UV-B radiation remains above its values in 1980, the adverse effects on ecosystems from UV exposure might be enhanced in this region during the 21st century.

The uncertainty of the surface UV projections presented here could be much larger than the model range indicates. Indeed, more realistic projections of future UV radiation should include not only ozone, but also clouds, aerosols, and surface reflectivity. All these will likely be affected by climate change. In addition, anthropogenic tropospheric ozone and aerosols in the lower troposphere are likely to change as well (see Section 3.2.8). Clouds are the main modulator of UV radiation and current work shows that they may introduce considerable variability to the future UV time series and modify, or even reverse, the ozone-related trends in UV radiation. The evolution of these factors in the future, with patterns exhibiting strong spatial variations (e.g., Trenberth and Fasullo, 2009), may modify accordingly the projected return date of UV irradiance to its 1980 levels.

3.4.2 Polar UV

In polar regions, the UV signatures of ozone reductions have been more pronounced compared to midlatitudes (see Chapter 2), resulting in measurable changes and, in some cases (e.g., in Antarctica), detectable increases in surface UV radiation (Bernhard et al., 2006).

In Tourpali et al. (2009), the ozone recovery projected by CCMs for the southern polar latitudes resulted in large reductions in erythemal irradiance under cloudless conditions of more than 30% between 2000 and 2095. When, instead of the annual mean, monthly means are considered, reductions of ~50% are found in the austral spring. The sign of the erythemal irradiance changes is reversed for polar regions, when its levels in the 1960s are taken as reference. Hegglin and Shepherd (2009) estimated increases in erythemal irradiance of up to 20% between 1965 and 2095 over the same region in late spring and early summer. This increase is nearly half of that generated by the Antarctic ozone hole from the increase in ODS levels since the 1960s. The increase is not so large in the new calculations, with the multi-model mean in 2100 being just above the 1960 level, though the range in the model estimates is large (see Figure 3-19). Some CCMs even report small decreases in erythemal irradiance for the same period.

The new UV simulations show that increases in clear-sky erythemal irradiance reach a rather broad maximum centered over the 2000s (Figure 3-19). The magnitude of this maximum varies between models, ranging, for the spring months, from ~5 to 15% in the Arctic, and from ~30 to 110% in Antarctica. This spread in the model estimates is a measure of the uncertainty of the simulations, which, together with their large year-to-year variability, makes it difficult to assess more accurately the magnitude and timing of the UV maximum. After the 2000–2010 decade, erythemal irradiance is projected to decrease at different rates for the two regions. In the Arctic, it is projected to return to its 1980 value between 2020 and 2030, while in Antarctica the return occurs only in the 2nd half of the 21st century. The rather slow decline in UV levels over Antarctica may have important biological consequences for Antarctic ecosystems, which will continue to be exposed to excess UV for most of the 21st century.

The expected increase in stratospheric ozone levels at southern polar latitudes is projected to accelerate surface warming over Antarctica (Son et al., 2009). This may accelerate ice and/or snow melting and, ultimately, may lead to exposure of organisms under the ice to UV

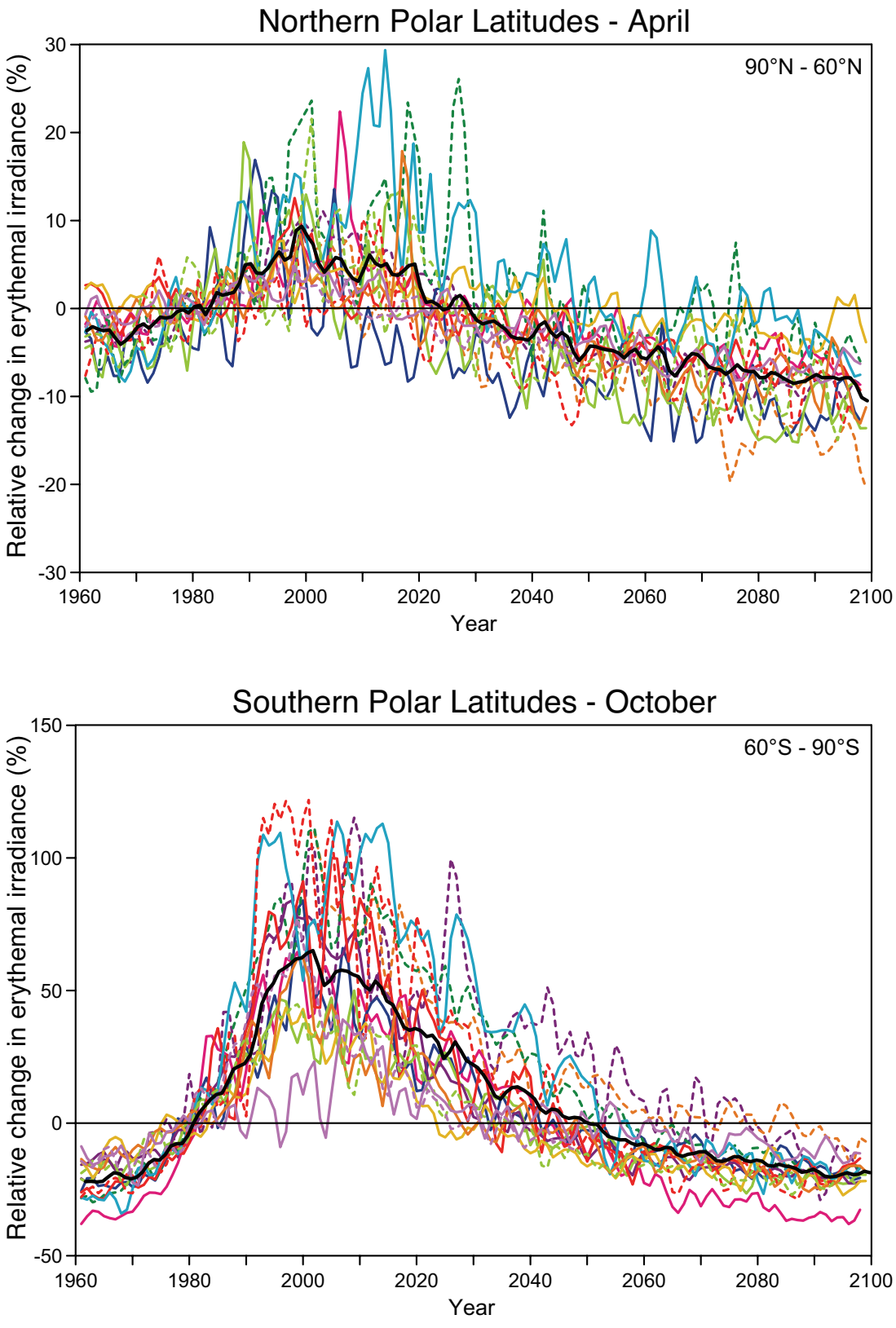

Figure 3-19. As in Figure 3-18 but for April in the Arctic (upper) and October in Antarctica (lower). The legend of Figure 3-18 applies also here. Note the different scales in the two panels. Updated from Tourpali et al. (2009) using projections from 15 CCMVal-2 models.

radiation and to a decrease of surface reflectivity. The reduction in surface reflectivity would reinforce the effect of rising stratospheric ozone levels by decreasing further surface UV irradiance over this region.

3.4.3 Link to UNEP Environmental Effects Panel Assessment

Changes in solar UV radiation at the surface are important due to the biological consequences—both negative and positive—for humans and for different ecosystems. The adverse effects of UV radiation on human health have dominated the public awareness during the last three decades because of ozone depletion. In recent years, though, much attention has been drawn to the benefits of solar UV radiation with respect to its involvement in the production of vitamin D, an important agent for human health (Edvardsen et al., 2007; Kazantzidis et al., 2009; McKenzie et al., 2009; Webb et al., 1988). As the spectral characteristics of solar UV radiation at the surface depend on the changes in ozone, the recovery of the stratospheric ozone layer will reduce the harmful biological doses received by humans, but will reduce also the rate of production of vitamin D, especially in the winter months at high latitudes. Ozone depletion has also influenced other communities, terrestrial and marine, as well as biological and chemical processes in the environment (UNEP, 2007). Therefore, the recovery of stratospheric ozone and the timing of this recovery are important for both. The impacts of ozone depletion and recovery, and of the resulting changes in UV radiation on the environment and the ecosystems, will be focal points for discussion in the forthcoming assessment report of the Environmental Effects Assessment Panel (EEAP) of UNEP (UNEP, 2010).

Ozone depletion has shown seasonal and latitudinal variations. The projections of surface UV irradiance in the 21st century based on ozone changes projected by CCMs (as described in Section 3.4.1) reveal the importance of ozone variations in different regions. This can be seen in Figure 3-20, which shows the average change in daily erythemal irradiance between 1975–1985 and 2089–2099 for different seasons. Evidently there is a strong meridional gradient in the UV changes, which are small and positive in the tropics (up to 4%) and become negative with increasing magnitude at the middle and high latitudes. Although small in percentage, this increase in the tropics may be important for ecosystems living in this region, where irradiance levels are already high. As discussed above, the changes over Antarctica exceed −30% and are rather zonally symmetric. Such large decreases will have implications for the Antarctic ecosystems. Overall, the changes in UV radiation are fairly zonal over the middle and tropical latitudes and for all seasons, with longitudinal variations of a few percent. In the winter/spring period of the Northern Hemisphere these longitudinal variations are slightly larger due to more regional changes in column ozone.

In the present report, the future UV radiation has been simulated only in terms of ozone variations. However, climate change may significantly impact surface UV levels either directly through changes in clouds, albedo, and aerosols, or indirectly through interaction with ozone, as discussed in Section 3.2.8. Clear-sky UV simulations, calculated from changes in ozone and changes in cloudiness and surface reflectivity taken from climate models, will be discussed in more detail in the forthcoming assessment report of the EEAP/UNEP (UNEP, 2010).

Because ozone depletion has been most severe in the southern high and polar latitudes, the effects on the ecosystems would likely be most pronounced and detectable over these regions. Antarctic communities have been exposed to alterations in the surface conditions of temperature, moisture, and ultraviolet radiation resulting from climate change and stratospheric ozone depletion (Solomon et al., 2005). After three decades of ozone depletion and enhanced UV exposure, communities may already be undergoing adaptation, species selection, and changes in species assemblages, communities, and distributions, with effects on ecosystem function (Wall, 2007). For the Antarctic terrestrial communities, the timing of exposure in early spring might be more important than the magnitude of UV-B exposure, since, in early spring, organisms may be in a physiologically inactive state and unaccustomed to these levels (Wall, 2007). Terrestrial organisms are also living under the snow cover that may provide protection from UV radiation (Cockell and Cordoba-Jabonero, 2004). Climate changes may result either in prolongation (through cooling) or in shrinking (through increases in sublimation and strengthening of katabatic winds) of periods with snow cover (Wall, 2007).

3.5 CONCLUSIONS

The focus of this chapter has been to assess and discuss projections of future ozone and its impact on surface UV. Future ozone will be mostly determined by changes in stratospheric halogen loading (ESC) and changes in climate parameters. Thus, the chronology of the third and last stage of ozone recovery from ODSs as defined in WMO (2007), and employed here, depends critically on the combination of these two factors. Separately evaluating the role of halogens in ozone depletion is of great interest because it is the primary concern of the Parties to the Montreal Protocol. Section 3.2 describes the primary factors controlling future ozone and surface UV. Stratospheric halogen loading has been the strongest influence on ozone in the last decades since the onset of the Antarctic ozone hole and midlatitude depletion. Stratospheric

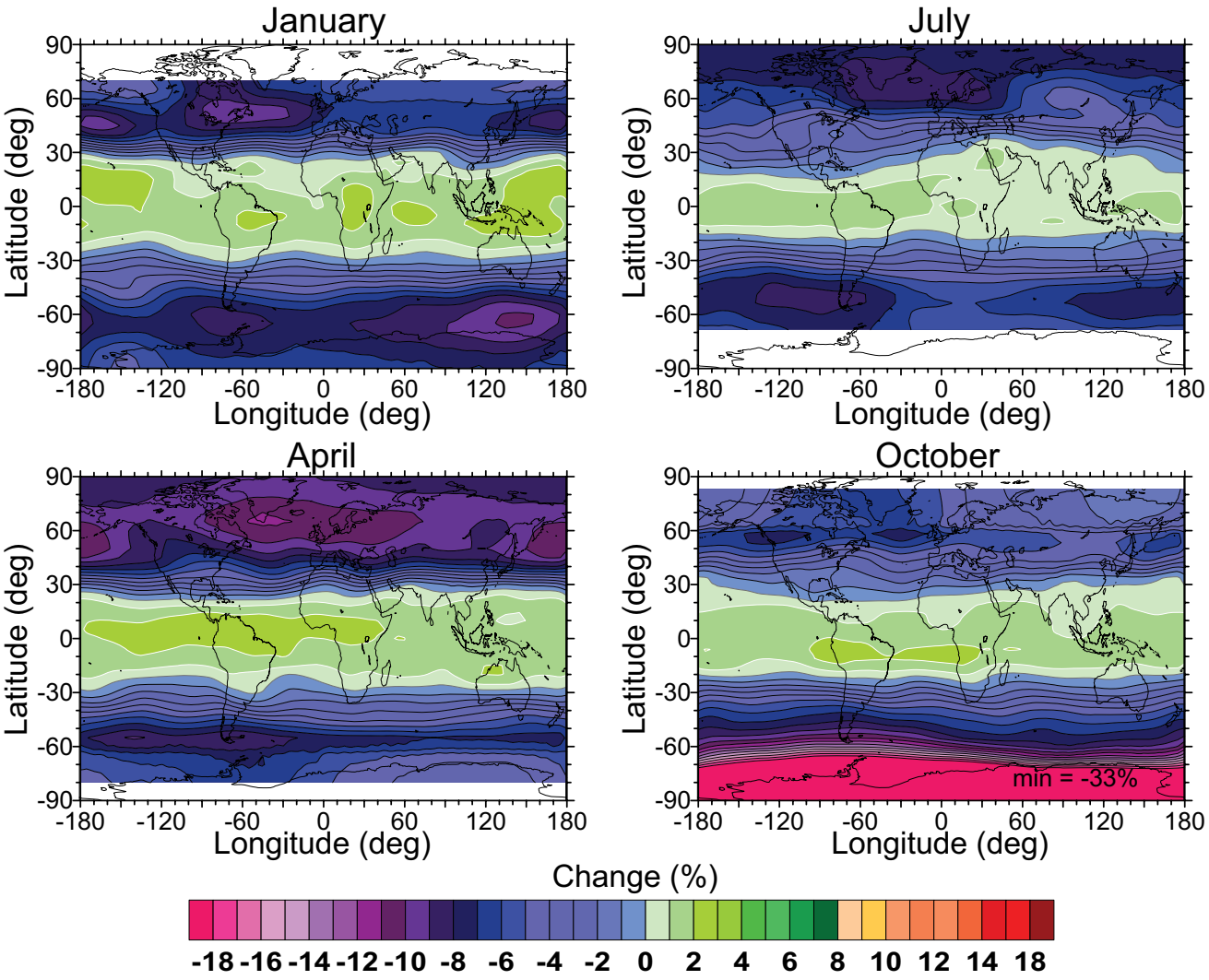

Figure 3-20. Multi-model average changes in surface erythemal irradiance between 2089–2099 and 1975–1985 under cloud-free conditions for four months, calculated with a radiative transfer model using projections of ozone and temperature from 15 CCMs. Updated from Tourpali et al. (2009) using projections from 15 CCMVal-2 models.

halogen loading has peaked in all regions of the stratosphere in the last two decades and is now diminishing at a rate primarily controlled by the atmospheric lifetimes of individual chlorine and bromine gases. Global and regional projections for the removal of halogens have very similar time dependences as shown in Figure 3-21 and indicate that the return of halogen amounts to 1960 values will not be achieved before 2100, except in the tropical lower stratosphere. A prominent feature of the halogen time series is that regional peak values are quite different. Because of the long average lifetimes of ODSs, the highest values are found in polar regions, where the average age of stratospheric air is greatest.

Other leading factors discussed in Section 3.2 are stratospheric levels of key ozone-destroying hydrogen and nitrogen species, stratospheric temperatures, the Brewer-Dobson circulation, dynamics of the polar vortex, and stratospheric aerosols. Many of these factors, which already influence ozone to some degree, are coupled such that the effects of an initial perturbation may be amplified to result in a larger effect on ozone than would have been the case otherwise. Links between components of the chemistry-climate system are indicated in Figure 3-22 with arrows representing chemistry, radiation, transport and other mechanisms. Many of these factors are influenced by anthropogenic emissions of GHGs and ODSs.

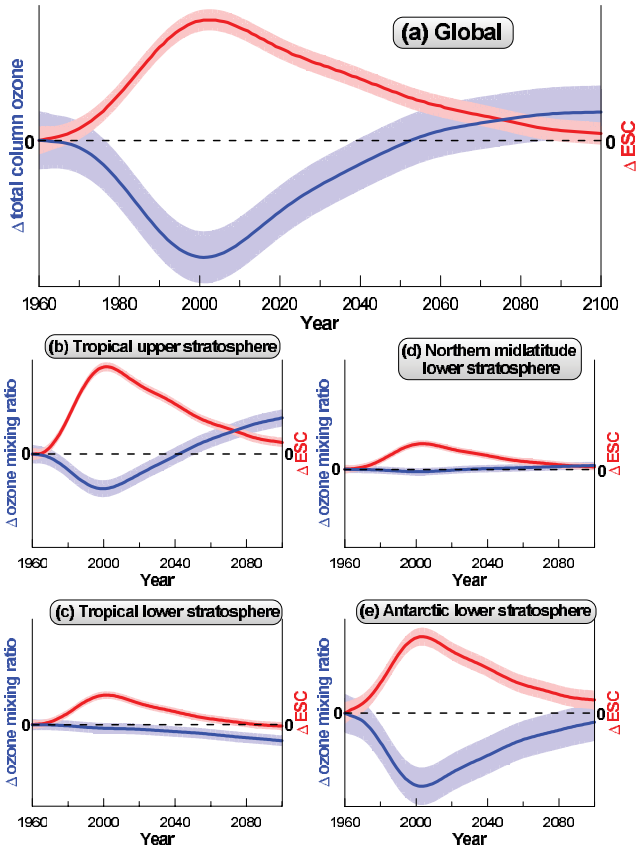

Figure 3-21. A schematic contrasting global and vertically resolved changes in ozone (blue) and ESC (red). In all cases changes with respect to the 1960 value are shown. Panel (a) shows the most common framework in which future projections of ozone are considered (compare to Figure 6-1 of WMO, 2007) while the other panels show the greater variety of responses of ozone to ESC in different regions of the atmosphere resulting from non-ESC drivers of ozone changes and their feedbacks and interactions (see Figure 3-22). The schematic is generated from multi-model means (solid lines) and 95% prediction intervals (shading) of REF-B2 simulations (Table 3-2) from the suite of CCMs used in this chapter.

For example, the increase in stratospheric CO_2 abundances is the main cause of the cooling trend in the stratosphere (see Section 4.2).

These multiple drivers of ozone changes and their interactions will create more diverse regional behavior in stratospheric ozone than would be expected from average global behavior or from the evolution of ODSs alone. This point is illustrated schematically in the time series shown in Figure 3-21, where an anticorrelation between the evolutions of ESC and total column ozone can be seen for the global average, for the Antarctic lower stratosphere, and for the tropical upper stratosphere. However, the influence of other drivers, in particular GHGs, is manifest in the global and tropical upper stratosphere, where ozone amounts return to 1960 levels in the middle of 21st century, although ODSs are still enhanced during this period. It is only in the Antarctic lower stratosphere, where the sensitivity of ozone to ESC maximizes, that ESC appears to remain the dominant driver until the end of the 21st century. In other regions, ozone changes are not well correlated with ESC. For example, in the tropical lower stratosphere, ozone amounts decrease steadily from 1960 to 2100 whereas in the northern midlatitude lower stratosphere, ozone shows a small negative response to ESC until 2020 before increasing throughout the 21st century. In these regions, GHG changes are the dominant driver of ozone changes.

The multiple interactions between the components of the chemistry-climate system (Figure 3-22) complicate a clean attribution of changes in ozone to changes in ODSs and other factors as required by the definition of full ozone recovery employed in this Assessment. For example, decreases in polar stratospheric ozone, resulting from increases in ESC, cool the stratosphere since heating from UV absorption by ozone is also reduced. This cooling in turn enhances the effectiveness of ESC by promoting the formation of polar stratospheric clouds. Increases in GHG concentrations drive additional radiative stratospheric cooling, but at the same time strengthen the BDC, which adiabatically warms the polar stratosphere and enhances mixing with lower latitudes. Sensitivity simulations using CCMs can be used to disentangle the effects of different drivers to ozone changes. Model results indicate that changes in ODSs and GHGs appear to affect ozone nearly independently.

The primary drivers of ozone changes, and their interactions, are largely described in the CCMs that have been used to make the ozone and UV projections presented in this chapter. To identify the causes of simulated future ozone changes, CCMs were also used to conduct sensitivity simulations in which one particular driver of ozone changes (e.g., ODSs or GHGs) was held constant. There are, however, processes that are not yet fully realized in models, such as potential changes in the quasi-biennial oscillation and coupling to the ocean. There are additional processes and associated potential feedbacks in the ocean-climate-stratosphere system (e.g., changes in marine biogenic emissions of halocarbons induced by changes in climate and surface UV) and in the terrestrial biosphere-climate-stratosphere system (e.g., emissions of ozone precursors) that are also currently absent in CCMs. Therefore, as progress is made toward the development of full Earth Systems Models that include a wider variety of processes and feedbacks, more comprehensive and robust future projections of ozone will become possible.

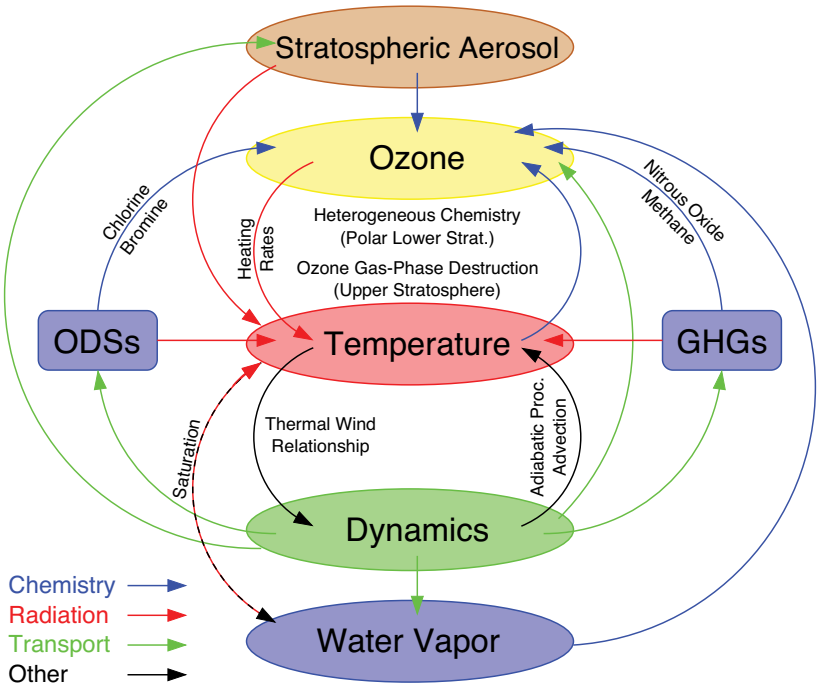

Figure 3-22. Schematic of ozone-focused stratospheric chemistry-climate interactions. Links between elements of the chemistry-climate system are indicated with arrows representing chemistry (blue), radiation (red), transport (green), and other mechanisms (black). Simple and more complex feedback cycles can be constructed following the linking mechanisms. A simple example is ozone depletion in the upper stratosphere leading to lower temperatures. Lower temperatures slow the gas-phase destruction of ozone, thereby reducing the amount of ozone depletion. The feedback loops involving stratospheric aerosol are currently not important, but they might become important again after a large volcanic eruption or in the context of some geoengineering proposals.

REFERENCES

Akiyoshi, H., L.B. Zhou, Y. Yamashita, K. Sakamoto, M. Yoshiki, T. Nagashima, M. Takahashi, J. Kurokawa, M. Takigawa, and T. Imamura, A CCM simulation of the breakup of the Antarctic polar vortex in the years 1980-2004 under the CCMVal scenarios, *J. Geophys. Res.*, *114*, D03103, doi: 10.1029/2007JD009261, 2009.

Austin, J., and R.J. Wilson, Ensemble simulations of the decline and recovery of stratospheric ozone, *J. Geophys. Res.*, *111*, D16314, doi: 10.1029/2005JD006907, 2006.

Austin, J., and R.J. Wilson, Sensitivity of polar ozone to sea surface temperatures and halogen amounts, *J. Geophys. Res.*, *115*, D18303, doi: 10.1029/2009JD013292, 2010.

Austin, J., N. Butchart, and K.P. Shine, Possibility of an Arctic ozone hole in a doubled-CO_2 climate, *Nature*, *360*, 221-225, doi: 10.1038/360221a0, 1992.

Austin, J., J. Wilson, F. Li, and H. Vömel, Evolution of water vapor concentrations and stratospheric age of air in coupled chemistry-climate model simulations, *J. Atmos. Sci.*, *64*, 905-921, doi: 10.1175/JAS3866.1, 2007.

Austin, J., K. Tourpali, E. Rozanov, H. Akiyoshi, S. Bekki, G. Bodeker, C. Brühl, N. Butchart, M. Chipperfield, M. Deushi, V. Fomichev, M. Giorgetta, L. Gray, K. Kodera, F. Lott, E. Manzini, D. Marsh, K. Matthes, T. Nagashima, K. Shibata, R.S. Stolarski, H. Struthers, and W. Tian, Coupled chemistry climate model simulations of the solar cycle in ozone and temperature, *J. Geophys. Res.*, *113*, D11306, doi: 10.1029/2007JD009391, 2008.

Austin, J., J. Scinocca, D. Plummer, L. Oman, D. Waugh, H. Akiyoshi, S. Bekki, P. Braesicke, N. Butchart, M. Chipperfield, D. Cugnet, M. Dameris, S. Dhomse, V. Eyring, S. Frith, R.R. Garcia, H. Garny, A. Gettelman, S.C. Hardiman, D. Kinnison, J.F. Lamarque, E. Mancini, M. Marchand, M. Michou, O. Morgenstern, T. Nakamura, S. Pawson, G. Pitari, J. Pyle, E. Rozanov, T.G. Shepherd, K. Shibata, H. Teyssèdre, R.J. Wilson, and Y. Yamashita, Decline and recovery of total column ozone using a multimodel time series analysis, *J. Geophys. Res.*, *115*, D00M10, doi: 10.1029/2010JD013857, 2010a.

Austin, J., H. Struthers, J. Scinocca, D.A. Plummer, H. Akiyoshi, A.J.G. Baumgaertner, S. Bekki, G.E. Bodeker, P. Braesicke, C. Brühl, N. Butchart, M.P. Chipperfield, D. Cugnet, M. Dameris, S. Dhomse, S. Frith, H. Garny, A. Gettelman, S.C. Hardiman, P. Jöckel, D. Kinnison, A. Kubin, J.F. Lamarque, U. Langematz, E. Mancini, M. Marchand, M. Michou, O. Morgenstern, T. Nakamura, J.E. Nielsen, G. Pitari, J. Pyle, E. Rozanov, T.G. Shepherd, K. Shibata, D. Smale, H. Teyssèdre, and Y.Yamashita, Chemistry-climate model simulations of spring Antarctic ozone, *J. Geophys. Res.*, *115*, D00M11,

doi: 10.1029/2009JD013577, 2010b.

Avallone, L.M., and M.J. Prather, Photochemical evolution of ozone in the lower tropical stratosphere, *J. Geophys. Res.*, *101* (D1), 1457-1461, 1996.

Badosa, J., R.L. McKenzie, M. Kotkamp, J. Calbó, J.A. González, P.V. Johnston, M. O'Neill, and D.J. Anderson, Towards closure between measured and modelled UV under clear skies at four diverse sites, *Atmos. Chem. Phys*., *7*, 2817-2837, 2007.

Bais, A.F., and D. Lubin (Lead Authors), A. Arola, G. Bernhard, M. Blumthaler, N. Chubarova, C. Erlick, H.P. Gies, N. Krotkov, K. Lantz, B. Mayer, R.L. McKenzie, R.D. Piacentini, G. Seckmeyer, J.R. Slusser, and C.S. Zerefos, Surface ultraviolet radiation: Past, Present, and Future, Chapter 7 in *Scientifictt Assessment of Ozone Depletion: 2006*, Global Ozone Research and Monitoring Project–Report No. 50, 572 pp., World Meteorological Organization, Geneva, Switzerland, 2007.

Baldwin, M., and M. Dameris (Lead Authors), J. Austin, S. Bekki, B. Bregman, N. Butchart, E. Cordero, N. Gillett, H.-F. Graf, C. Granier, D. Kinnison, S. Lal, T. Peter, W. Randel, J. Scinocca, D. Shindell, H. Struthers, M. Takahashi, and D. Thompson, Climate-ozone connections, Chapter 5 in *Scientific Assessment of Ozone Depletion: 2006*, Global Ozone Research and Monitoring Project–Report No. 50, 572 pp., World Meteorological Organization, Geneva, Switzerland, 2007.

Bell, C.J., L.J. Gray, and J.E. Kettleborough, Changes in Northern Hemisphere stratospheric variability under increased CO_2 concentrations, *Quart. J. Roy. Meteorol. Soc.*, *136*, 1181-1190, doi: 10.1002/qj.633, 2010.

Bernhard, G., C.R. Booth, J.C. Ehramjian, and S.E. Nichol, UV climatology at McMurdo Station, Antarctica, based on version 2 data of the National Science Foundation's Ultraviolet Radiation Monitoring Network, *J. Geophys. Res.*, *111*, D11201, doi: 10.1029/2005JD005857, 2006.

Bodeker, G.E., and D.W. Waugh (Lead Authors), H. Akiyoshi, P. Braesicke, V. Eyring, D.W. Fahey, E. Manzini, M.J. Newchurch, R.W. Portmann, A. Robock, K.P. Shine, W. Steinbrecht, and E.C. Weatherhead, The ozone layer in the 21st century, Chapter 6 in *Scientific Assessment of Ozone Depletion: 2006*, Global Ozone Research and Monitoring Project–Report No. 50, 572 pp., World Meteorological Organization, Geneva, Switzerland, 2007.

Bodeker, G.E., H. Struthers, and B.J. Connor, Dynamical containment of Antarctic ozone depletion, *Geophys. Res. Lett.*, *29* (7), 1098, doi: 10.1029/2001GL014206, 2002.

Bodeker, G.E., H. Shiona, and H. Eskes, Indicators of Antarctic ozone depletion, *Atmos. Chem. Phys*., *5*, 2603-2615, 2005.

Booth, C.R., and S. Madronich, Radiation amplification factors: Improved formulations accounts for large increases in ultraviolet radiation associated with Antarctic ozone depletion, in *Ultraviolet Radiation in Antarctica: Measurements and Biological Effects*, AGU Antarctic Research Series, edited by C.S. Weiler and P.A. Penhale, 39-42, Washington, D.C., 1994.

Bradley, R.S., F.T. Keimig, and H.F. Diaz, Projected temperature changes along the American cordillera and the planned GCOS network, *Geophys. Res. Lett.*, *31*, L16210, doi: 10.1029/2004GL020229, 2004.

Braesicke, P., and J.A. Pyle, Changing ozone and changing circulation in northern mid-latitudes: Possible feedbacks?, *Geophys. Res. Lett. 30* (2), 1059, doi: 10.1029/2002GL015973, 2003.

Brühl, C., and P.J. Crutzen, On the disproportionate role of tropospheric ozone as a filter against solar UV-B radiation, *Geophys. Res. Lett.*, *16* (7), 703-706, 1989.

Butchart, N., and A.A. Scaife, Removal of chlorofluorocarbons by increased mass exchange between the stratosphere and troposphere in a changing climate, *Nature*, *410* (6830), 799-802, 2001.

Butchart, N., I. Cionni, V. Eyring, T.G. Shepherd, D.W. Waugh, H. Akiyoshi, J. Austin, C. Brühl, M.P. Chipperfield, E. Cordero, M. Dameris, R. Deckert, S. Dhomse, S.M. Frith, R.R. Garcia, A. Gettelman, M.A. Giorgetta, D.E. Kinnison, F. Li, E. Mancini, C. McLandress, S. Pawson, G. Pitari, D.A. Plummer, E. Rozanov, F. Sassi, J.F. Scinocca, K. Shibata, B. Steil, and W. Tian, Chemistry-climate model simulations of 21st century stratospheric climate and circulation changes, *J. Clim*., *23* (20), 5349-5374, doi: 10.1175/2010JCLI3404.1, 2010.

Caldeira, K., and L. Wood, Global and Arctic climate engineering: Numerical model studies, *Phil. Trans. Roy. Soc. A*, *366* (1882), 4039-4056, 2008.

Charlton-Perez, A.J., L.M. Polvani, J. Austin, and F. Li, The frequency and dynamics of stratospheric sudden warmings in the 21st century, *J. Geophys. Res.*, *113*, D16116, doi: 10.1029/2007JD009571, 2008.

Charlton-Perez, A.J., E. Hawkins, V. Eyring, I. Cionni, G.E. Bodeker, D.E. Kinnison, H. Akiyoshi, S.M. Frith, R. Garcia, A. Gettelman, J.F. Lamarque, T. Nakamura, S. Pawson, Y. Yamashita, S. Bekki, P. Braesicke, M.P. Chipperfield, S. Dhomse, M. Marchand, E. Mancini, O. Morgenstern, G. Pitari, D. Plummer, J.A. Pyle, E. Rozanov, J. Scinocca, K. Shibata, T.G. Shepherd, W. Tian, and D.W. Waugh, The potential to narrow uncertainty in projections of stratospheric ozone over the 21st century, *Atmos. Chem. Phys.*, *10*, 9473-9486, doi: 10.5194/acp-10-

9473-2010, 2010.

Chipperfield, M.P., New version of the TOMCAT/SLIMCAT off-line chemical transport model: Intercomparison of stratospheric tracer experiments, *Quart. J. Roy. Meteorol. Soc.*, *132* (617), 1179-1203, doi: 10.1256/qj.05.51, 2006.

Chipperfield, M.P., and W. Feng, Comment on: Stratospheric ozone depletion at northern mid-latitudes in the 21st century: The importance of future concentrations of greenhouse gases nitrous oxide and methane, *Geophys. Res. Lett.*, *30* (7), 1389, doi: 10.1029/2002GL016353, 2003.

Chipperfield, M.P., and V.E. Fioletov (Lead Authors), B. Bregman, J. Burrows, B.J. Connor, J.D. Haigh, N.R.P. Harris, A. Hauchecorne, L.L. Hood, S.R. Kawa, J.W. Krzyścin, J.A. Logan, N.J. Muthama, L. Polvani, W.J. Randel, T. Sasaki, J. Stähelin, R.S. Stolarski, L.W. Thomason, and J.M. Zawodny, Global ozone: Past and Present, Chapter 3 in *Scientific Assessment of Ozone Depletion: 2006*, Global Ozone Research and Monitoring Project–Report No. 50, 572 pp., World Meteorological Organization, Geneva, Switzerland, 2007.

Chubarova, N.Y., UV variability in Moscow according to long-term UV measurements and reconstruction model, *Atmos. Chem. Phys.*, *8*, 3025-3031, 2008.

Chubarova, N.Y., Seasonal distribution of aerosol properties over Europe and their impact on UV irradiance, *Atmos. Meas. Tech.*, *2*, 593-608, doi: 10.5194/amt-2-593-2009, 2009.

Chubarova, N.Y., N.G. Prilepsky, A.N. Rublev, and A.R. Riebau, A mega-fire event in central Russia: Fire weather, radiative, and optical properties of the atmosphere, and consequences for subboreal forest plants, in *Developments in Environmental Science*, Volume 8, edited by A. Bytnerowicz, M. Arbaugh, A. Riebau, and C. Andersen, 247-264, Elsevier B.V., Amsterdam, The Netherlands, available: http://www.fs.fed.us/psw/publications/4451/psw_2009_4451-001_247-264.pdf, 2009.

CIE (Commission Internationale de l'Éclairage), Reference Action spectra for ultraviolet induced erythema and pigmentation of different human skin types, in *Technical Collection 103/3*, p.15-21, 1993.

Clarke, L., J. Edmonds, H. Jacoby, H. Pitcher, J. Reilly, and R. Richels, *Scenarios of Greenhouse Gas Emissions and Atmospheric Concentrations*. Subreport 2.1A of Synthesis and Assessment Product 2.1 by the U.S. Climate Change Science Program and the Subcommittee on Global Change Research. Department of Energy, Office of Biological & Environmental Research, Washington, D.C., U.S.A., 154 pp., 2007.

Clement, A.C., R. Burgman, and J.R. Norris, Observational and model evidence for positive low-level cloud feedback, *Science*, *325* (5939), 460-464, doi: 10.1126/science.1171255, 2009.

Cockell, C.S., and C. Córdoba-Jabonero, Coupling of climate change and biotic UV exposure through changing snow-ice covers in terrestrial habitats, *Photochem. Photobiol.*, *79* (1), 26-31, 2004.

Comiso, J.C., C.L. Parkinson, R. Gersten, and L. Stock, Accelerated decline in the Arctic sea ice cover, *Geophys. Res. Lett.*, *35*, L01703, doi: 10.1029/2007GL0319, 2008.

Crutzen, P.J., Albedo enhancement by stratospheric sulfur injections: A contribution to resolve a policy dilemma?, *Clim. Change*, *77* (3-4), 211-219, doi: 10.1007/s10584-006-9101-y, 2006.

de Grandpré, J., S.R. Beagley, V.I. Fomichev, E. Griffioen, J.C. McConnell, A.S. Medvedev, and T.G. Shepherd, Ozone climatology using interactive chemistry: Results from the Canadian Middle Atmosphere Model, *J. Geophys. Res.*, *105* (D21), 26475-26491, 2000.

Déqué, M., Frequency of precipitation and temperature extremes over France in an anthropogenic scenario: Model results and statistical correction according to observed values, *Global Planet. Change*, *57* (1-2), 16-26, doi: 10.1016/j.gloplacha.2006.11.030, 2007.

Dhomse, S., M. Weber, I. Wohltmann, M. Rex, and J.P. Burrows, On the possible causes of recent increases in northern hemispheric total ozone from a statistical analysis of satellite data from 1979 to 2003, *Atmos. Chem. Phys.*, *6*, 1165-1180, 2006.

Douglass, A.R., R.S. Stolarski, M.R. Schoeberl, C.H. Jackman, M.L. Gupta, P.A. Newman, J.E. Nielsen, and E.L. Fleming, Relationship of loss, mean age of air and the distribution of CFCs to stratospheric circulation and implications for atmospheric lifetimes, *J. Geophys. Res.*, *113*, D14309, doi: 10.1029/2007JD009575, 2008.

Dufresne, J.L., and S. Bony, An assessment of the primary sources of spread of global warming estimates from coupled atmosphere–ocean models, *J. Clim.*, *21* (19), 5135-5144, doi: 10.1175/2008JCLI2239.1, 2008.

Edvardsen, K., M. Brustad, O. Engelsen, and L. Aksnes, The solar UV radiation level needed for cutaneous production of vitamin D3 in the face. A study conducted among subjects living at a high latitude (68°N), *Photochem. Photobiol. Sci.*, *6*, 57-62, doi: 10.1039/b613263d, 2007.

Egorova, T., E. Rozanov, V. Zubov, E. Manzini, W. Schmutz, and T. Peter, Chemistry-climate model SOCOL: A validation of the present-day climatology, *Atmos. Chem. Phys.*, *5*, 1557-1576, 2005.

Engel, A., T. Möbius, H. Bönisch, U. Schmidt, R. Heinz, I. Levin, E. Atlas, S. Aoki, T. Nakazawa, S. Sug-

awara, F. Moore, D. Hurst, J. Elkins, S. Schauffler, A. Andrews, and K. Boering, Age of stratospheric air unchanged within uncertainties over the past 30 years, *Nature Geoscience*, *2*, 28-31, doi: 10.1038/ngeo388, 2009.

Eyring, V., N.R.P. Harris, M. Rex, T.G. Shepherd, D.W. Fahey, G.T. Amanatidis, J. Austin, M.P. Chipperfield, M. Dameris, P.M. De F. Forster, A. Gettelman, H.F. Graf, T. Nagashima, P.A. Newman, S. Pawson, M.J. Prather, J.A. Pyle, R.J. Salawitch, B.D. Santer, and D.W. Waugh, A strategy for process-oriented validation of coupled chemistry-climate models, *Bull. Amer. Meteorol. Soc.*, *86* (8), 1117-1133, doi: 10.1175/BAMS-86-8-1117, 2005.

Eyring, V., N. Butchart, D.W. Waugh, H. Akiyoshi, J. Austin, S. Bekki, G.E. Bodeker, B.A. Boville, C. Brühl, M.P. Chipperfield, E. Cordero, M. Dameris, M. Deushi, V.E. Fioletov, S.M. Frith, R.R. Garcia, A. Gettelman, M.A. Giorgetta, V. Grewe, L. Jourdain, D.E. Kinnison, E. Mancini, E. Manzini, M. Marchand, D.R. Marsh, T. Nagashima, P.A. Newman, J.E. Nielsen, S. Pawson, G. Pitari, D.A. Plummer, E. Rozanov, M. Schraner, T.G. Shepherd, K. Shibata, R.S. Stolarski, H. Struthers, W. Tian, and M. Yoshiki, Assessment of temperature, trace species, and ozone in chemistry-climate model simulations of the recent past, *J. Geophys. Res.*, *111*, D22308, doi: 10.1029/2006JD007327, 2006.

Eyring, V., D.W. Waugh, G.E. Bodeker, E. Cordero, H. Akiyoshi, J. Austin, S.R. Beagley, B.A. Boville, P. Braesicke, C. Brühl, N. Butchart, M.P. Chipperfield, M. Dameris, R. Deckert, M. Deushi, S.M. Frith, R.R. Garcia, A. Gettelman, M.A. Giorgetta, D.E. Kinnison, E. Mancini, E. Manzini, D.R. Marsh, S. Matthes, T. Nagashima, P.A. Newman, J.E. Nielsen, S. Pawson, G. Pitari, D.A. Plummer, E. Rozanov, M. Schraner, J.F. Scinocca, K. Semeniuk, T.G. Shepherd, K. Shibata, B. Steil, R.S. Stolarski, W. Tian, and M. Yoshiki, Multimodel projections of stratospheric ozone in the 21st century, *J. Geophys. Res.*, *112*, D16303, doi: 10.1029/2006JD008332, 2007.

Eyring, V., M.P. Chipperfield, M.A. Giorgetta, D.E. Kinnison, E. Manzini, K. Matthes, P.A. Newman, S. Pawson, T.G. Shepherd, and D.W. Waugh, Overview of the new CCMVal reference and sensitivity simulations in support of upcoming ozone and climate assessments and the planned SPARC CCMVal Report, *SPARC Newsletter No. 30*, 20-26, 2008.

Eyring, V., I. Cionni, G.E. Bodeker, A.J. Charlton-Perez, D.E. Kinnison, J.F. Scinocca, D.W. Waugh, H. Akiyoshi, S. Bekki, M.P. Chipperfield, M. Dameris, S. Dhomse, S.M. Frith, H. Garny, A. Gettelman, A. Kubin, U. Langematz, E. Mancini, M. Marchand, T. Nakamura, L.D. Oman, S. Pawson, G. Pitari, D.A. Plummer, E. Rozanov, T.G. Shepherd, K. Shibata, W. Tian, P. Braesicke, S.C. Hardiman, J.F. Lamarque, O. Morgenstern, J.A. Pyle, D. Smale, and Y. Yamashita, Multi-model assessment of stratospheric ozone return dates and ozone recovery in CCMVal-2 models, *Atmos. Chem. Phys.*, *10*, 9451-9472, doi: 10.5194/acp-10-9451-2010, 2010a.

Eyring, V., I. Cionni, J.-F. Lamarque, H. Akiyoshi, G.E. Bodeker, A.J. Charlton-Perez, S.M. Frith, A. Gettelman, D.E. Kinnison, T. Nakamura, L.D. Oman, S. Pawson, and Y. Yamashita, Sensitivity of 21st century stratospheric ozone to greenhouse gas scenarios, *Geophys. Res. Lett.*, *37*, L16807, doi: 10.1029/2010GL044443, 2010b.

Fleming, E.L., C.H. Jackman, D.K. Weisenstein, and M.K.W. Ko, The impact of interannual variability on multidecadal total ozone simulations, *J. Geophys. Res.*, *112*, D10310, doi: 10.1029/2006JD007953, 2007.

Fioletov, V.E., G.E. Bodeker, A.J. Miller, R.D. McPeters, and R. Stolarski, Global and zonal total ozone variations estimated from ground-based and satellite measurements: 1964-2000, *J. Geophys. Res.*, *107* (D22), 4647 doi: 10.1029/2001JD001350, 2002.

Fomichev, V.I., W.E. Ward, S.R. Beagley, C. McLandress, J.C. McConnell, N.A. McFarlane, and T.G. Shepherd, Extended Canadian Middle Atmosphere Model: Zonal-mean climatology and physical parameterizations, *J. Geophys. Res.*, *107* (D10), 4087, doi: 10.1029/2001JD000479, 2002.

Garcia, R.R., D.R. Marsh, D.E. Kinnison, B.A. Boville, and F. Sassi, Simulation of secular trends in the middle atmosphere, 1950–2003, *J. Geophys. Res.*, *112*, D09301, doi: 10.1029/2006JD007485, 2007.

Garny, H., G.E. Bodeker, and M. Dameris, Trends and variability in stratospheric mixing: 1979-2005, *Atmos. Chem. Phys.*, *7*, 5611-5624, 2007.

Garny, H., M. Dameris, and A. Stenke, Impact of prescribed SSTs on climatologies and long-term trends in CCM simulations, *Atmos. Chem. Phys.*, *9*, 6017-6031, 2009.

Gauss, M., G. Myhre, G. Pitari, M.J. Prather, I.S.A. Isaksen, T.K. Berntsen, G.P. Brasseur, F.J. Dentener, R.G. Derwent, D.A. Hauglustaine, L.W. Horowitz, D.J. Jacob, M. Johnson, K.S. Law, L.J. Mickley, J.-F. Müller, P.-H. Plantevin, J.A. Pyle, H.L. Rogers, D.S. Stevenson, J.K. Sundet, M. van Weele, and O. Wild, Radiative forcing in the 21st century due to ozone changes in the troposphere and the lower stratosphere, *J. Geophys. Res.*, *108* (D9), 4292, doi: 10.1029/2002JD002624, 2003.

Gillett, N.P., H. Akiyoshi, S. Bekki, V. Eyring, R. Garcia, C.A. McLinden, A. Yu. Karpechko, D.A. Plummer, E. Rozanov, J. Scinocca, and K. Shibata, Attribution of observed changes in stratospheric ozone and tem-

perature, *Atmos. Chem. Phys. Discuss.*, *10*, 17341-17367, doi: 10.5194/acpd-10-17341-2010, 2010.

Guillas, S., M.L. Stein, D.J. Wuebbles, and J. Xia, Using chemistry transport modeling in statistical analysis of stratospheric ozone trends from observations, *J. Geophys. Res.*, *109*, D22303, doi: 10.1029/2004JD005049, 2004.

Hadjinicolaou, P., and J.A. Pyle, The impact of Arctic ozone depletion on northern middle latitudes: Interannual variability and dynamical control, *J. Atmos. Chem*., *47* (1), 25-43, 2004.

Hadjinicolaou, P., J.A. Pyle, M.P. Chipperfield, and J.A. Kettleborough, Effect of interannual meteorological variability on mid-latitude O_3, *Geophys. Res. Lett*., *24* (23), 2993-2996, 1997.

Hawkins, E., and R. Sutton, The potential to narrow uncertainty in regional climate predictions, *Bull. Amer. Meteorol. Soc.*, *90* (8), 1095-1107, doi: 10.1175/2009BAMS2607, 2009.

Heckendorn, P., D. Weisenstein, S. Fueglistaler, B.P. Luo, E. Rozanov, M. Schraner, L.W. Thomason, and T. Peter, Impact of geoengineering aerosols on stratospheric temperature and ozone, *Env. Res. Lett.*, *4* (4), 045108, doi: 10.1088/1748-9326/4/4/045108, 2009.

Hegglin, M.I., and T.G. Shepherd, Large climate-induced changes in ultraviolet index and stratosphere-to-troposphere ozone flux, *Nature Geoscience*, *2*, 687-691 doi: 10.1038/ngeo604, 2009.

Herman, J.R., D. Larko, E. Celarier, and J. Ziemke, Changes in the Earth's UV reflectivity from the surface, clouds and aerosols, *J. Geophys. Res.*, *106* (D6), 5353-5368, doi: 10.1029/2000JD900435, 2001.

IPCC (Intergovernmental Panel on Climate Change), *Emissions Scenarios. A Special Report of Working Group III of the Intergovernmental Panel on Climate Change*, edited by N. Nakicenovic and R. Swart, 570 pp., Cambridge University Press, Cambridge, U.K., and New York, NY, U.S.A., 2000.

IPCC (Intergovernmental Panel on Climate Change), *Climate Change 2007: The Physical Science Basis: Contribution of Working Group I to the Fourth Assessment Report of the Intergovernmental Panel on Climate Change*, edited by Solomon, S., D. Qin, M. Manning, Z. Chen, M. Marquis, K.B. Averyt, M. Tignor, and H.L. Miller, 996 pp., Cambridge University Press, Cambridge, U.K., and New York, NY, U.S.A., 2007.

Jacobson, M.Z., and D.G. Streets, Influence of future anthropogenic emissions on climate, natural emissions, and air quality, *J. Geophys. Res.*, *114*, D08118, doi: 10.1029/2008JD011476, 2009.

Jöckel, P., H. Tost, A. Pozzer, C. Brühl, J. Buchholz, L. Ganzeveld, P. Hoor, A. Kerkweg, M.G. Lawrence, R. Sander, B. Steil, G. Stiller, M. Tanarhte, D. Taraborrelli, J. van Aardenne, and J. Lelieveld, The atmospheric chemistry general circulation model ECHAM5/MESSy1: Consistent simulation of ozone from the surface to the mesosphere, *Atmos. Chem. Phys.*, *6*, 5067-5104, doi: 10.5194/acp-6-5067-2006, 2006.

Jonsson, A.I., V.I. Fomichev, and T.G. Shepherd, The effect of nonlinearity in CO_2 heating rates on the attribution of stratospheric ozone and temperature changes. *Atmos. Chem. Phys.*, *9*, 8447-8452, doi: 10.5194/acp-9-8447-2009, 2009.

Jourdain, L., S. Bekki, F. Lott, and F. Lefèvre, The coupled chemistry-climate model LMDz-REPROBUS: Description and evaluation of a transient simulation of the period 1980–1999, *Ann. Geophys.*, *26*, 1391-1413, doi: 10.5194/angeo-26-1391-2008, 2008.

Kazadzis, S., A. Bais, V. Amiridis, D. Balis, C. Meleti, N. Kouremeti, C.S. Zerefos, S. Rapsomanikis, M. Petrakakis, A. Kelesis, P. Tzoumaka, and K. Kelektsoglou, Nine years of UV aerosol optical depth measurements at Thessaloniki, Greece, *Atmos. Chem. Phys.*, *7*, 2091-2101, doi: 10.5194/acp-7-2091-2007, 2007.

Kazantzidis, A., A.F. Bais, D.S. Balis, E. Kosmidis, and C.S. Zerefos, Sensitivity of solar UV radiation to ozone and temperature profiles at Thessaloniki (40.5°N, 23°E), Greece, *J. Atmos. Sol.-Terr. Phys.*, *67* (14), 1321-1330, doi: 10.1016/j.jastp.2005.05.003, 2005.

Kazantzidis, A., A.F. Bais, M.M. Zempila, S. Kazadzis, P.N. den Outer, T. Koskela, and H. Slaper, Calculations of the human vitamin D exposure from UV spectral measurements at three European stations, *Photochem. Photobiol. Sci.*, *8*, 45-51, doi: 10.1039/b811216a, 2009.

Kazantzidis, A., K. Tourpali, and A.F. Bais, Variability of cloud-free ultraviolet dose rates on global scale due to modeled scenarios of future ozone recovery, *Photochem. Photobiol.*, *86*, 117-122, doi: 10.1111/j.1751-1097.2009.00645.x, 2010.

Kimlin, M.G, W.J. Olds, and M.R. Moore, Location and vitamin D synthesis: Is the hypothesis validated by geophysical data?, *J. Photochem. Photobiol. B: Biol.*, *86* (3), 234-239, doi: 10.1016/j.jphotobiol.2006.10.004, 2007.

Kinne, S., M. Schulz, C. Textor, S. Guibert, Y. Balkanski, S.E. Bauer, T. Berntsen, T.F. Berglen, O. Boucher, M. Chin, W. Collins, F. Dentener, T. Diehl, R. Easter, J. Feichter, D. Fillmore, S. Ghan, P. Ginoux, S. Gong, A. Grini, J. Hendricks, M. Herzog, L. Horowitz, I. Isaksen, T. Iversen, A. Kirkavag, S. Kloster, D. Koch, J.E. Kristjansson, M. Krol, A. Lauer, J.-F. Lamarque, G. Lesins, X. Liu, U. Lohmann, V. Montanaro, G. Myhre, J. Penner, G. Pitari,

S. Reddy, O. Seland, P. Stier, T. Takemura, and X. Tie, An AeroCom initial assessment – optical properties in aerosol component modules of global models, *Atmos. Chem. Phys.*, *6*, 1815-1834, doi: 10.5194/acp-6-1815-2006, 2006.

Kinnison, D.E., K.E. Grant, P.S. Connell, D.A. Rotman, and D.J. Wuebbles, The chemical and radiative effects of the Mount Pinatubo eruption, *J. Geophys. Res.*, *99* (D12), 25705-25731, 1994.

Kirk-Davidoff, D.B., E.J. Hintsa, J.G. Anderson, and D.W. Keith, The effect of climate change on ozone depletion through changes in stratospheric water vapour, *Nature*, *402*, 399-401, doi: 10.1038/46521, 1999.

Konopka, P., J.-U. Grooß, K.W. Hoppel, H.-M. Steinhorst, and R. Müller, Mixing and chemical ozone loss during and after the Antarctic polar vortex major warming in September 2002, *J. Atmos. Sci.*, *62* (3), 848-859, 2005.

Lamarque, J.-F., D.E. Kinnison, P.G. Hess, and F.M. Vitt, Simulated lower stratospheric trends between 1970 and 2005: Identifying the role of climate and composition changes, *J. Geophys. Res*., *113*, D12301, doi: 10.1029/2007JD009277, 2008.

Lamarque, J.-F., T.C. Bond, V. Eyring, C. Granier, A. Heil, Z. Klimont, D. Lee, C. Liousse, A. Mieville, B. Owen, M.G. Schultz, D. Shindell, S.J. Smith, E. Stehfest, J. Van Aardenne, O.R. Cooper, M. Kainuma, N. Mahowald, J.R. McConnell, V. Naik, K. Riahi, and D.P. van Vuuren, Historical (1850–2000) gridded anthropogenic and biomass burning emissions of reactive gases and aerosols: Methodology and application, *Atmos. Chem. Phys.*, *10*, 7017-7039, doi: 10.5194/acp-10-7017-2010, 2010.

Lapeta, B., O. Engelsen, Z. Litynska, B. Kois, and A. Kylling, Sensitivity of surface UV radiation and ozone column retrieval to ozone and temperature profiles, *J. Geophys. Res.*, *105* (D4), 5001-5007, 2000.

Li, F., R.S. Stolarski, and P.A. Newman, Stratospheric ozone in the post-CFC era, *Atmos. Chem. Phys.*, *9*, 2207-2213, doi: 10.5194/acp-9-2207-2009, 2009.

Lindfors, A., and A. Arola, On the wavelength-dependent attenuation of UV radiation by clouds, *Geophys. Res. Lett.*, *35*, L05806, doi: 10.1029/2007GL032571, 2008.

Madronich, S., Analytic formula for the clear-sky UV index, *Photochem. Photobiol.*, *83* (6), 1537-1538, doi: 10.1111/j.1751-1097.2007.00200.x, 2007.

Madronich, S., and S. Flocke: The role of solar radiation in atmospheric chemistry, in *The Handbook of Environmental Chemistry*, edited by P. Boule, 1-26, Springer-Verlag, Berlin Heidelberg, 1999.

Madronich S., R.L. McKenzie, L.O. Björn, and M.M. Caldwell, Changes in biologically active ultraviolet radiation reaching the Earth's surface, *Photochem. Photobiol. B: Biology*, *46* (1-3), 5-19, doi: 10.1016/S1011-1344(98)00182-1, 1998.

Matthews, H.D., and K. Caldeira, Transient climate-carbon simulations of planetary geoengineering, *Proc. Nat. Acad. Sci.*, *104* (24), 9949-9954, doi: 10.1073/pnas.0700419104, 2007.

Mayer, B., and A. Kylling, Technical note: The libRadtran software package for radiative transfer calculations – description and examples of use, *Atmos. Chem. Phys.*, *5*, 1855-1877, doi: 10.5194/acp-5-1855-2005, 2005.

McKenzie, R., D. Smale, G. Bodeker, and H. Claude, Ozone profile differences between Europe and New Zealand: Effects on surface UV irradiance and its estimation from satellite sensors, *J. Geophys. Res.*, *108* (D6), 4179, doi: 10.1029/2002JD002770, 2003.

McKenzie, R.L., C. Weinreis, P.V. Johnston, B. Liley, H. Shiona, M. Kotkamp, D. Smale, N. Takegawa, and Y. Kondo, Effects of urban pollution on UV spectral irradiances, *Atmos*. *Chem. Phys.*, *8*, 5683-5697, doi: 10.5194/acp-8-5683-2008, 2008.

McKenzie, R.L., J.B. Liley, and L.O. Björn, UV radiation: Balancing risks and benefits, *Photochem. Photobiol.*, *85* (1), 88-98, doi: 10.1111/j.1751-1097.2008.00400.x, 2009.

McLandress, C., and T.G. Shepherd, Simulated anthropogenic changes in the Brewer-Dobson circulation, including its extension to high latitudes, *J. Clim.*, *22* (6), 1516-1540, doi: 10.1175/2008JCLI2679.1, 2009a.

McLandress, C., and T.G. Shepherd, Impact of climate change on stratospheric sudden warmings as simulated by the Canadian Middle Atmosphere Model, *J. Clim.*, *22* (20), 5449-5463, 2009b.

McLandress, C., A.I. Jonsson, D.A. Plummer, M.C. Reader, J.F. Scinocca, and T.G. Shepherd, Separating the dynamical effects of climate change and ozone depletion: Part 1. Southern Hemisphere stratosphere, *J. Clim*., *23* (18), 5002-5020, doi: 10.1175/2010JCLI3586.1, 2010.

Meehl, G.A., T.F. Stocker, W.D. Collins, P. Friedlingstein, A.T. Gaye, J.M. Gregory, A. Kitoh, R. Knutti, J.M. Murphy, A. Noda, S.C.B. Raper, I.G. Watterson, A.J. Weaver, and Z.-C. Zhao, Global climate projections, in *Climate Change 2007: The Physical Science Basis. Contribution of Working Group I to the Fourth Assessment Report of the Intergovernmental Panel on Climate Change*, edited by S. Solomon, D. Qin, M. Manning, Z. Chen, M. Marquis, K.B. Averyt, M. Tignor and H.L. Miller, 996 pp., Cambridge University Press, Cambridge, U.K., and New York, NY, U.S.A., 2007.

Millard, G.A., T.A. Mather, D.M. Pyle, W.I. Rose, and B. Thornton, Halogen emissions from a small volcanic eruption: Modeling the peak concentrations,

dispersion, and volcanically induced ozone loss in the stratosphere, *Geophys. Res. Lett.*, *33*, L19815, doi: 10.1029/2006GL026959, 2006.

Miller, A.J., R.M. Nagatani, L.E. Flynn, S. Kondragunta, E. Beach, R. Stolarski, R.D. McPeters, P.K. Bhartia, M.T. DeLand, C.H. Jackman, D.J. Wuebbles, K.O. Patten, and R.P. Cebula, A cohesive total ozone data set from SBUV(/2) satellite system, *J. Geophys. Res.*, *107(D23)*, 4701, doi: 10.1029/2001JD000853, 2002.

Morgenstern, O., P. Braesicke, M.M. Hurwitz, F.M. O'Connor, A.C. Bushell, C.E. Johnson, and J.A. Pyle, The world avoided by the Montreal Protocol, *Geophys. Res. Lett.*, *35*, L16811, doi: 10.1029/2008GL034590, 2008.

Morgenstern, O., P. Braesicke, F.M. O'Connor, A.C. Bushell, C.E. Johnson, S.M. Osprey, and J.A. Pyle, Evaluation of the new UKCA climate-composition model - Part 1: The stratosphere, *Geosci. Model Dev.*, *2*, 43-57, doi: 10.5194/gmd-2-43-2009, 2009.

Morgenstern, O., M.A. Giorgetta, K. Shibata, V. Eyring, D.W. Waugh, T.G. Shepherd, H. Akiyoshi, J. Austin, A.J.G. Baumgaertner, S. Bekki, P. Braesicke, C. Brühl, M.P. Chipperfield, D. Cugnet, M. Dameris, S. Dhomse, S.M. Frith, H. Garny, A. Gettelman, S.C. Hardiman, M.I. Hegglin, P. Jöckel, D.E. Kinnison, J.-F. Lamarque, E. Mancini, E. Manzini, M. Marchand, M. Michou, T. Nakamura, J.E. Nielsen, D. Olivié, G. Pitari, D.A. Plummer, E. Rozanov, J.F. Scinocca, D. Smale, H. Teyssèdre, M. Toohey, W. Tian, and Y. Yamashita, Review of the formulation of present-generation stratospheric chemistry-climate models and associated external forcings, *J. Geophys. Res.*, *115*, D00M02, doi: 10.1029/2009JD013728, 2010.

Moss, R., M. Babiker, S. Brinkman, E. Calvo, T. Carter, J. Edmonds, I. Elgizouli, S. Emori, L. Erda, K. Hibbard, R. Jones, M. Kainuma, J. Kelleher, J.-F. Lamarque, M. Manning, B. Matthews, J. Meehl, L. Meyer, J. Mitchell, N. Nakicenovic, B. O'Neill, R. Pichs, K. Riahi, S. Rose, P. Runci, R. Stouffer, D. van Vuuren, J. Weyant, T. Wilbanks, J.P. van Ypersele, and M. Zurek, *Towards New Scenarios for Analysis of Emissions, Climate Change, Impacts, and Response Strategies*, IPCC Expert Meeting Report, Intergovernmental Panel on Climate Change, Geneva, 132 pp., available: http://www.aimes.ucar.edu/docs/IPCC.meetingreport.final.pdf, 2008.

Newman, P.A., J.S. Daniel, D.W. Waugh, and E.R. Nash, A new formulation of equivalent effective stratospheric chlorine (EESC), *Atmos. Chem. Phys.*, *7*, 4537-4552, doi: 10.5194/acp-7-4537-2007, 2007.

Nissen, K.M., K. Matthes, U. Langematz, and B. Mayer, Towards a better representation of the solar cycle in general circulation models, *Atmos. Chem. Phys.*, *7*, 5391-5400, doi: 10.5194/acp-7-5391-2007, 2007.

Oman, L., D.W. Waugh, S. Pawson, R.S. Stolarski, and J.E. Neilsen, Understanding the changes of stratospheric water vapor in coupled chemistry-climate model simulations, *J. Atmos. Sci.*, *65* (10), 3278-3291, doi: 10.1175/2008JAS2696, 2008.

Oman, L.D., D.W. Waugh, S.R. Kawa, R.S. Stolarski, A.R. Douglass, and P.A. Newman, Mechanisms and feedbacks causing changes in upper stratospheric ozone in the 21st century, *J. Geophys. Res.*, *115*, D05303, doi: 10.1029/2009JD012397, 2010.

Overland, J.E., and M. Wang, Future regional Arctic sea ice declines, *Geophys. Res. Lett.*, *34*, L17705, doi: 10.1029/2007GL030808, 2007.

Pawson, S., R.S. Stolarski, A.R. Douglass, P.A. Newman, J.E. Nielsen, S.M. Frith, and M.L. Gupta, Goddard Earth Observing System chemistry-climate model simulations of stratospheric ozone-temperature coupling between 1950 and 2005, *J. Geophys. Res.*, *113*, D12103, doi: 10.1029/2007JD009511, 2008.

Pitari, G., E. Mancini, V. Rizi, and D.T. Shindell, Impact of future climate and emission changes on stratospheric aerosols and ozone, *J. Atmos. Sci.*, *59* (3), 414-440, 2002.

Portmann, R.W., and S. Solomon, Indirect radiative forcing of the ozone layer during the 21st century, *Geophys. Res. Lett.*, *34*, L02813, doi: 10.1029/2006GL028252, 2007.

Portmann, R.W., S. Solomon, R.R. Garcia, L.W. Thomason, L.R. Poole, and M.P. McCormick, Role of aerosol variations in anthropogenic ozone depletion in the polar regions, *J. Geophys. Res.*, *101* (D17), 22991-23006, 1996.

Portmann, R.W., S.S. Brown, T. Gierczak, R.K. Talukdar, J.B. Burkholder, and A.R. Ravishankara, Role of nitrogen oxides in the stratosphere: A reevaluation based on laboratory studies, *Geophys. Res. Lett.*, *26* (15), 2387-2390, 1999.

Randel, W.J., F. Wu, H. Vömel, G.E. Nedoluha, and P. Forster, Decreases in stratospheric water vapor after 2001: Links to changes in the tropical tropopause and the Brewer-Dobson circulation, *J. Geophys. Res.*, *111*, D12312, doi: 10.1029/2005JD006744, 2006.

Randel, W.J., K.P. Shine, J. Austin, J. Barnett, C. Claud, N.P. Gillett, P. Keckhut, U. Langematz, R. Lin, C. Long, C. Mears, A. Miller, J. Nash, D.J. Seidel, D.W.J. Thompson, F. Wu, and S. Yoden, An update of observed stratospheric temperature trends, *J. Geophys. Res.*, *114*, D02107, doi: 10.1029/2008JD010421, 2009.

Randeniya, L.K., P.F. Vohralik, and I.C. Plumb, Stratospheric ozone depletion at northern mid latitudes in the 21st century: The importance of future concentrations of greenhouse gases nitrous oxide and

methane, *Geophys. Res. Lett.*, *29* (4), 1051, doi: 10.1029/2001GL014295, 2002.

Rasch, P.J., S. Tilmes, R.P. Turco, A. Robock, L. Oman, C.-C. Chen, G.L. Stenchikov, and R.R. Garcia, An overview of geoengineering of climate using stratospheric sulphate aerosols, *Phil. Trans. R. Soc. A*, *366* (1882), 4007-4037, doi: 10.1098/rsta.2008.0131, 2008.

Ravishankara, A.R., J.S. Daniel, and R.W. Portmann, Nitrous oxide (N_2O): The dominant ozone-depleting substance emitted in the 21st century, *Science*, *326* (5949), 123-125, doi: 10.1126/science.1176985, 2009.

Riahi, K., A. Grübler, and N. Nakicenovic, Scenarios of long-term socio-economic and environmental development under climate stabilization, *Technological Forecasting and Social Change*, *74* (7), 887-935, doi: 10.1016/j.techfore.2006.05.026, 2007.

Rieder, H.E., F. Holawe, S. Simic, M. Blumthaler, J.W. Krzyścin, J.E. Wagner, A.W. Schmalwieser, and P. Weihs, Reconstruction of erythemal UV-doses for two stations in Austria: A comparison between alpine and urban regions, *Atmos. Chem. Phys.*, *8*, 6309-6323, doi: 10.5194/acp-8-6309-2008, 2008.

Rind, D., J. Lerner, J. Jonas, and C. McLinden, Effects of resolution and model physics on tracer transports in the NASA Goddard Institute for Space Studies general circulation models, *J. Geophys Res.*, *112*, D09315, doi: 10.1029/2006JD007476, 2007.

Robock, A., A. Marquardt, B. Kravitz, and G. Stenchikov, Benefits, risks, and costs of stratospheric geoengineering, *Geophys. Res. Lett.*, *36*, L19703, doi: 10.1029/2009GL039209, 2009.

Rohs, S., C. Schiller, M. Riese, A. Engel, U. Schmidt, T. Wetter, I. Levin, T. Nakazawa, and S. Aoki, Long-term changes of methane and hydrogen in the stratosphere in the period 1978–2003 and their impact on the abundance of stratospheric water vapor, *J. Geophys. Res.*, *111*, D14315, doi: 10.1029/2005JD006877, 2006.

Rosenfield, J.E., and A.R. Douglass, Doubled CO_2 effects on NO_y in a coupled 2D model, *Geophys. Res. Lett.*, *25* (23), 4381-4384, 1998.

Royal Society, *Geoengineering the Climate: Science, Governance and Uncertainty*, Report 10/09, 98 pp., London GB, Royal Society, available: http://royalsociety.org/geoengineering-the-climate/, 2009.

Schraner, M., E. Rozanov, C. Schnadt Poberaj, P. Kenzelmann, A.M. Fischer, V. Zubov, B.P. Luo, C.R. Hoyle, T. Egorova, S. Fueglistaler, S. Brönnimann, W. Schmutz, and T. Peter, Technical Note: Chemistry-climate model SOCOL: Version 2.0 with improved transport and chemistry/microphysics schemes, *Atmos. Chem. Phys.*, *8*, 5957-5974, doi: 10.5194/acp-8-5957-2008, 2008.

Schulz, M., C. Textor, S. Kinne, Y. Balkanski, S. Bauer, T. Berntsen, T. Berglen, O. Boucher, F. Dentener, S. Guibert, I.S.A. Isaksen, T. Iversen, D. Koch, A. Kirkevåg, X. Liu, V. Montanaro, G. Myhre, J.E. Penner, G. Pitari, S. Reddy, Ø. Seland, P. Stier, and T. Takemura, Radiative forcing by aerosols as derived from the AeroCom present-day and pre-industrial simulations, *Atmos. Chem. Phys.*, *6*, 5225-5246, doi: 10.5194/acp-6-5225-2006, 2006.

Schwander, H., P. Koepke, and A. Ruggaber, Uncertainties in modeled UV irradiances due to limited accuracy and availability of input data, *J. Geophys. Res.*, *102* (D8), 9419-9429, doi: 10.1029/97JD00244, 1997.

Scinocca, J.F., N.A. McFarlane, M. Lazare, J. Li, and D. Plummer, Technical Note: The CCCma third generation AGCM and its extension into the middle atmosphere, *Atmos. Chem. Phys.*, *8*, 7055-7074, doi: 10.5194/acp-8-7055-2008, 2008.

Shepherd, T.G., Dynamics, stratospheric ozone, and climate change, *Atmos.-Ocean*, *46* (1), 117-138, doi: 10.3137/ao.460106, 2008.

Shepherd, T.G., and A.I. Jonsson, On the attribution of stratospheric ozone and temperature changes to changes in ozone-depleting substances and well-mixed greenhouse gases, *Atmos. Chem. Phys.*, *8*, 1435-1444, doi: 10.5194/acp-8-1435-2008, 2008.

Shindell, D.T., D. Rind, and P. Lonergan, Increased polar stratospheric ozone losses and delayed eventual recovery owing to increasing greenhouse-gas concentrations, *Nature*, *392*, 589-592, doi: 10.1038/33385, 1998.

Shibata, K., and M. Deushi, Long-term variations and trends in the simulation of the middle atmosphere 1980-2004 by the chemistry-climate model of the Meteorological Research Institute, *Ann. Geophys.*, *26*, 1299-1326, doi: 10.5194/angeo-26-1299-2008, 2008a.

Shibata, K., and M. Deushi, Simulations of the stratospheric circulation and ozone during the recent past (1980-2004) with the MRI chemistry-climate model, *CGER's Supercomputer Monograph Report Vol.13*, Center for Global Environmental Research, National Institute for Environmental Studies, Japan, 154 pp., 2008b.

Sinnhuber, B.-M., and I. Folkins, Estimating the contribution of bromoform to stratospheric bromine and its relation to dehydration in the tropical tropopause layer, *Atmos. Chem. Phys.*, *6*, 4755-4761, doi: 10.5194/acp-6-4755-2006, 2006.

Sinnhuber, B.-M., N. Sheode, M. Sinnhuber, M.P. Chipperfield, and W. Feng, The contribution of anthropogenic bromine emissions to past stratospheric ozone trends: A modeling study, *Atmos. Chem. Phys.*, *9*, 2863-2871, doi: 10.5194/acp-9-2863-2009, 2009.

Solomon, S., R.W. Portmann, R.R. Garcia, L.W. Thomason, L.R. Poole, and M.P. McCormick, The role of aerosol variations in anthropogenic ozone depletion at northern midlatitudes, *J. Geophys. Res.*, *101 (D3)*, 6713-6727, doi: 10.1029/95JD03353, 1996.

Solomon, S., R.W. Portmann, T. Sasaki, D.J. Hofmann, and D.W.J. Thompson, Four decades of ozonesonde measurements over Antarctica, *J. Geophys. Res.*, *110*, D21311, doi: 10.1029/2005JD005917, 2005.

Solomon, S., D. Qin, M. Manning, R.B. Alley, T. Berntsen, N.L. Bindoff, Z. Chen, A. Chidthaisong, J.M. Gregory, G.C. Hegerl, M. Heimann, B. Hewitson, B.J. Hoskins, F. Joos, J. Jouzel, V. Kattsov, U. Lohmann, T. Matsuno, M. Molina, N. Nicholls, J. Overpeck, G. Raga, V. Ramaswamy, J. Ren, M. Rusticucci, R. Somerville, T.F. Stocker, P. Whetton, R.A. Wood, and D. Wratt, Technical Summary. In: *Climate Change 2007: The Physical Science Basis. Contribution of Working Group I to the Fourth Assessment Report of the Intergovernmental Panel on Climate Change*, edited by S. Solomon, D. Qin, M. Manning, Z. Chen, M. Marquis, K.B. Averyt, M. Tignor and H.L. Miller, 996 pp., Cambridge University Press, Cambridge, U.K., and New York, NY, U.S.A., 2007.

Son, S.-W., N.F. Tandon, L.M. Polvani, and D.W. Waugh, Ozone hole and Southern Hemisphere climate change, *Geophys. Res. Lett.*, *36*, L15705, doi: 10.1029/2009GL038671, 2009.

SPARC (Stratospheric Processes And their Role in Climate), *Assessment of Stratospheric Aerosols Properties*, edited by L. Thomason and Th. Peter, SPARC Report No. 4, WCRP-124, WMO/TD- No. 1295, 2006.

SPARC CCMVal, *SPARC CCMVal Report on the Evaluation of Chemistry-Climate Models*, edited by V. Eyring, T.G. Shepherd, D.W. Waugh, SPARC Report No. 5, WCRP-132, WMO/TD-No. 1526, available: http://www.atmosp.physics.utoronto.ca/SPARC/ccmval_final/index.php, 2010.

Staiger, H., P.N. den Outer, A.F. Bais, U. Feister, B. Johnsen, and L. Vuilleumier, Hourly resolved cloud modification factors in the ultraviolet, *Atmos. Chem. Phys.*, *8*, 2493-2508, doi: 10.5194/acp-8-2493-2008, 2008.

Stenke, A., V. Grewe, and M. Ponater, Lagrangian transport of water vapor and cloud water in the ECHAM4 GCM and its impact on the cold bias, *Clim. Dyn.*, *31* (5), 491-506, doi: 10.1007/s00382-007-0347-5, 2008.

Stenke, A., M. Dameris, V. Grewe, and H. Garny, Implications of Lagrangian transport for simulations with a coupled chemistry-climate model, *Atmos. Chem. Phys.*, *9*, 5489-5504, doi: 10.5194/acp-9-5489-2009, 2009.

Stolarski, R.S., and S. Frith, Search for evidence of trend slow-down in the long-term TOMS/SBUV total ozone data record: The importance of instrument drift uncertainty, *Atmos. Chem. Phys.*, *6*, 4057-4065, doi: 10.5194/acp-6-4057-2006, 2006.

Strahan, S.E., and B.C. Polansky, Meteorological implementation issues in chemistry and transport models, *Atmos. Chem. Phys.*, *6*, 2895-2910, doi: 10.5194/acp-6-2895-2006, 2006.

Stroeve, J., M.M. Holland, W. Meier, T. Scambos, and M. Serreze, Arctic sea ice decline: Faster than forecast, *Geophys. Res. Lett.*, *34*, L09501, doi: 10.1029/2007GL029703, 2007.

Tanskanen, A., and T. Manninen, Effective UV surface albedo of seasonally snow-covered lands, *Atmos. Chem. Phys.*, *7*, 2759-2764, doi: 10.5194/acp-7-2759-2007, 2007.

Taylor, K.E., R.J. Stouffer, and G.A. Meehl, A Summary of the CMIP5 Experiment Design, https://cmip.llnl.gov/cmip5/docs/Taylor_CMIP5_design.pdf, 2009.

Tegen, I., M. Werner, S.P. Harrison, and K.E. Kohfeld, Relative importance of climate and land use in determining present and future global soil dust emission, *Geophys. Res. Lett.*, *31*, L05105, doi: 10.1029/2003GL019216, 2004.

Telford, P., P. Braesicke, O. Morgenstern, and J. Pyle, Reassessment of causes of ozone column variability following the eruption of Mount Pinatubo using a nudged CCM, *Atmos. Chem. Phys.*, *9*, 4251-4260, doi: 10.5194/acp-9-4251-2009, 2009.

Teyssèdre, H., M. Michou, H.L. Clark, B. Josse, F. Karcher, D. Olivié, V.-H. Peuch, D. Saint-Martin, D. Cariolle, J.-L. Attié, P. Nédélec, P. Ricaud, V. Thouret, R.J. van der A, A. Volz-Thomas, and F. Chéroux, A new tropospheric and stratospheric Chemistry and Transport Model MOCAGE-Climat for multi-year studies: Evaluation of the present-day climatology and sensitivity to surface processes, *Atmos. Chem. Phys.*, *7*, 5815-5860, doi: 10.5194/acp-7-5815-2007, 2007.

Tian, W., and M.P. Chipperfield, A new coupled chemistry-climate model for the stratosphere: The importance of coupling for future O_3-climate predictions, *Quart. J. Roy. Meteorol. Soc.*, *131* (605), 281-303, 2005.

Tian, W., M.P. Chipperfield, L.J. Gray, and J.M. Zawodny, Quasi-biennial oscillation and tracer distributions in a coupled chemistry-climate model, *J. Geophys. Res.*, *111*, D20301, doi: 10.1029/2005JD006871, 2006.

Tian, W., M.P. Chipperfield, and D. Lu, Impact of increasing stratospheric water vapor on ozone depletion and temperature change, *Adv. Atm. Sci.*, *26* (3), 423-437, doi: 10.1007/s00376-009-0423-3, 2009.

Tie, X., and G. Brasseur, The response of stratospheric ozone to volcanic eruptions: Sensitivity to atmospheric chlorine loading, *Geophys. Res. Lett.*, *22* (22), 3035-3038, doi: 10.1029/95GL03057, 1995.

Tilmes, S., R. Müller, and R. Salawitch, The sensitivity of polar ozone depletion to proposed geoengineering schemes, *Science*, *320* (5880), 1201-1204, doi: 10.1126/science.1153966, 2008a.

Tilmes S., R. Müller, R.J. Salawitch, U. Schmidt, C.R. Webster, H. Oelhaf, C.C. Camy-Peyret, and J.M. Russell III, Chemical ozone loss in the Arctic winter 1991-1992, *Atmos. Chem. Phys.*, *8*, 1897-1910, doi: 10.5194/acp-8-1897-2008, 2008b.

Tilmes, S., R.R. Garcia, D.E. Kinnison, A. Gettelman, and P.J. Rasch, Impact of geoengineered aerosols on the troposphere and stratosphere, *J. Geophys. Res.*, *114*, D12305, doi: 10.1029/2008JD011420, 2009.

Tourpali K., A.F. Bais, A. Kazantzidis, C.S. Zerefos, H. Akiyoshi, J. Austin, C. Brühl, N. Butchart, M.P. Chipperfield, M. Dameris, M. Deushi, V. Eyring, M.A. Giorgetta, D.E. Kinnison, E. Mancini, D.R. Marsh, T. Nagashima, G. Pitari, D.A. Plummer, E. Rozanov, K. Shibata, and W. Tian, Clear sky UV simulations for the 21st century based on ozone and temperature projections from Chemistry-Climate Models, *Atmos. Chem. Phys.*, *9*, 1165-1172, doi: 10.5194/acp-9-1165-2009, 2009.

Trenberth, K.E., and J.T. Fasullo, Global warming due to increasing absorbed solar radiation, *Geophys. Res. Lett.*, *36*, L07706, doi: 10.1029/2009GL037527, 2009.

Tsay, S.-C., and K. Stamnes, Ultraviolet radiation in the Arctic: The impact of potential ozone depletions and cloud effects, *J. Geophys. Res.*, *97* (D8), 7829-7840, 1992.

UNEP (United Nations Environment Programme), *Environmental Effects of Ozone Depletion and Its Interaction with Climate Change: 2006 Assessment*, Nairobi, 206 pp., 2007.

UNEP (United Nations Environment Programme), *Environmental Effects of Ozone Depletion and Its Interactions with Climate Change: 2010 Assessment*, Nairobi, in preparation, 2010.

van Vuuren, D.P., M.G.J. den Elzen, P.L. Lucas, B. Eickhout, B.J. Strengers, B. van Ruijven, S. Wonink, and R. van Houdt, Stabilizing greenhouse gas concentrations at low levels: An assessment of reduction strategies and costs, *Clim. Change*, *81*, 119-159, doi: 10.1007/s/10584-006-9172-9, 2007.

Waibel, A.E., Th. Peter, K.S. Carslaw, H. Oelhaf, G. Wetzel, P.J. Crutzen, U. Pöschl, A. Tsias, E. Reimer, and H. Fischer, Arctic ozone loss due to dentrification, *Science*, *283* (5410), 2064-2069, doi: 10.1126/science.283.5410.2064, 1999.

Wall, D.H., Global change tipping points: Above- and below-ground biotic interactions in a low diversity ecosystem, *Phil. Trans. Roy. Soc. B*, *362* (1488), 2291-2306, doi: 10.1098/rstb.2006.1950, 2007.

Waugh, D.W., and V. Eyring, Quantitative performance metrics for stratospheric-resolving chemistry-climate models, *Atmos. Chem. Phys.*, *8*, 5699-5713, doi: 10.5194/acp-8-5699-2008, 2008.

Waugh, D.W., L. Oman, S.R. Kawa, R.S. Stolarski, S. Pawson, A.R. Douglass, P.A. Newman, and J.E. Nielsen, Impacts of climate change on stratospheric ozone recovery, *Geophys. Res. Lett.*, *36*, L03805, doi: 10.1029/2008GL036223, 2009.

Webb, A.R., and O. Engelsen, Calculated ultraviolet exposure levels for a healthy vitamin D status, *Photochem. Photobiol.*, *82*, 1697-1703, 2006.

Webb, A.R., L. Kline, and M.F. Holick, Influence of season and latitude on the cutaneous synthesis of vitamin D3: Exposure to winter sunlight in Boston and Edmonton will not promote vitamin D3 synthesis in human skin, *J. Clinic. Endocrin. Metabol.*, *67* (2), 373-378, doi: 10.1210/jcem-67-2-373, 1988.

Wigley, T.M.L., A combined mitigation/geoengineering approach to climate stabilization, *Science*, *314* (5798), 452- 454, doi: 10.1126/science.1131728, 2006.

Wohltmann, I., R. Lehmann, M. Rex, D. Brunner, and J.A. Mäder, A process-oriented regression model for column ozone, *J. Geophys. Res.*, *112*, D12304, 1-18, doi: 10.1029/2006JD007573, 2007.

WMO (World Meteorological Organization), *Scientific Assessment of Ozone Depletion: 1998*, Global Ozone Research and Monitoring Project–Report No. 44, Geneva, Switzerland, 1999.

WMO (World Meteorological Organization), *Scientific Assessment of Ozone Depletion: 2002*, Global Ozone Research and Monitoring Project–Report No. 47, 498 pp., Geneva, Switzerland, 2003.

WMO (World Meteorological Organization), *Scientific Assessment of Ozone Depletion: 2006*, Global Ozone Research Monitoring Project–Report No. 50, 572 pp., Geneva, Switzerland, 2007.

Zhang, X., and J.E. Walsh, Toward a seasonally ice-covered Arctic Ocean: Scenarios from the IPCC AR4 model simulations, *J. Clim.*, *19* (9), 1730-1747, doi: 10.1175/JCLI3767.1, 2006.

APPENDIX 3A
Constructing Correlative Time Series Plots

The correlative time series plots shown in Figures 3-8 and 3-10 were constructed to illustrate how the rise and fall of ESC correlates with stratospheric ozone changes over multi-decadal time periods in scenarios that include and exclude the effects of GHGs and ODSs. This appendix describes how these plots are constructed and evaluated.

Calculated global or regional stratospheric ozone values typically are shown as time series and qualified by the corresponding time series of temperature and ESC because of the strong influence these parameters have in controlling ozone amounts. As an example, Figure 3A-1(a) shows multi-model area weighted ozone mixing ratios from 25°S to 25°N at 5 hPa from 1960 to 2100 for the reference (black), ODSs fixed at 1960 values (blue), and GHGs fixed at 1960 values (green) simulations (Table 3-2). The combination of the fixed ODS and fixed GHG simulations (detailed below), used to test for linear additivity, is shown in yellow. The CCSRNIES, MRI, and WACCM chemistry-climate models were used to form the multi-model trend and all time series were subjected to the TSAM smoothing described in Section 3.3.2.2. The results for temperature and ESC in the same model runs are shown in Figure 3A-1(b) and (c).

To test the linear additivity of the ozone responses to changes in ODSs and GHGs, the sum of the individual ozone responses in the fixed ODS and fixed GHG simulations was evaluated as a function of time (t) as

$$\mathrm{Ozone}_{\mathrm{sum}}(t) = \mathrm{fGHG}_{\mathrm{ozone}}(t) + \mathrm{fODS}_{\mathrm{ozone}}(t) - \mathrm{fODS}_{\mathrm{ozone}}(1960)$$

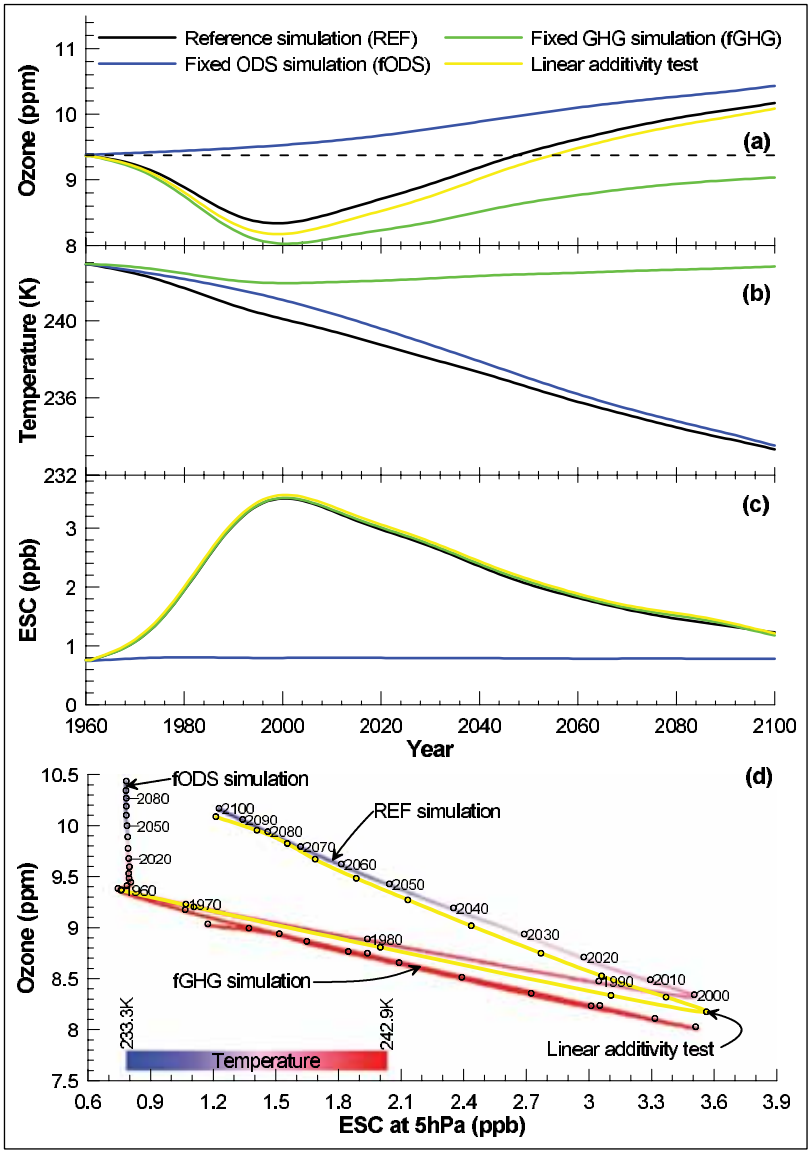

where $\mathrm{fODS}_{\mathrm{ozone}}(1960)$ is the ozone value in 1960 in all simulations (dashed line in Figure 3A-1(a)). This $\mathrm{Ozone}_{\mathrm{sum}}$ time series is shown as a yellow trace in Figure 3A-1(a) and (d). As for ozone, the linear additivity of the effects of changes in ODSs and GHGs on ESC is tested by calculating

$$\mathrm{ESC}_{\mathrm{sum}}(t) = \mathrm{fGHG}_{\mathrm{ESC}}(t) + \mathrm{fODS}_{\mathrm{ESC}}(t) - \mathrm{fODS}_{\mathrm{ESC}}(1960)$$

where the ESC terms correspond to those defined above for ozone and $\mathrm{fODS}_{\mathrm{ESC}}(1960)$ is the ESC value in 1960 in all simulations. The $\mathrm{ESC}_{\mathrm{sum}}$ time series is shown as a yellow trace in Figure 3A-1(c) and (d). In the interests of clarity, the linear additivity of the effects of changes in ODSs and GHGs on temperature were not investigated and are therefore not shown in panel (b).

A correlative time series plot corresponding to the ozone, temperature,

Figure 3A-1. Time series for (a) ozone (ppm), (b) temperature (K), and (c) ESC (ppb) from CCM simulation results for 5 hPa between 25°S and 25°N (area-weighted) and corresponding correlative time series plot (d). The traces in (d) are color-coded by temperature, and decade year markers are shown with symbols and labels.

and ESC time series is shown in Figure 3A-1(d) with a separate line for each of the scenarios discussed above. Ozone is plotted on the ordinate and ESC on the abscissa because ESC is the expected main driver in the long-term ozone evolution. Symbols are used to mark decade years along each time series line and temperature is indicated with a color scale. A correlative time-series plot is of value because it highlights in a single panel the sensitivity and response of ozone to ESC and other variables in the CCMs over a multi-decadal period in a specific region or globally.

There are several important features of this plot type. For example, in this case, the fODS simulation appears in Figure 3A-1(d) as a nearly vertical line, the length of which indicates the overall effect of non-ODS factors on ozone. The fODS line may also deviate from the vertical indicating that non-ODS factors affect the conversion of ODSs to ESC. If the non-ODS factors had no influence on ozone and ESC, the fODS result would appear as a point on the plot. The temperature gradient along the line indicates a systematic change in this controlling factor. Apart from the fODS simulation, all simulations trace a broad path along the ESC axis from very low concentrations of ESC in 1960, through the peak in ESC around 2000 on the far right of the plot, and back to lower ESC concentrations by the end of the 21st century. In these cases, if ozone was controlled solely by ESC, the increasing and decreasing legs of this time series would trace the same path. Any deviation between the increasing and decreasing legs is indicative of a systematic influence of non-ODS factors. Finally, the separation at each point between the reference and linear additivity test traces indicates the degree to which the influence of ODS and GHG changes on ozone do not act independently, assuming that the uncertainties in these projections are small compared to this separation (McLandress et al., 2010). Thus, the time series displays and the correlative time series plot offer complementary views and insights into the evaluation of the CCM results.